Design and Development of a Three-degree-of-freedom Parallel Manipulator to Track the Sun for Concentrated Solar Power Towers

A Thesis

Submitted for the Degree of

Doctor of Philosophy

in the **Faculty of Engineering**

by

Ashith Shyam R Babu

Mechanical Engineering
Indian Institute of Science
Bangalore – 560 012 (INDIA)

October 2017

DEDICATED TO

My parents, B. Rajendra Babu and N.R. Beena,
My grandmothers Padmini and Ambujakshi,
My brother Baban Shyam and my wife Simna

And to all my teachers, friends and well wishers

CERTIFICATE

I hereby certify that the content embodied in this thesis titled **Design and Development of a Three-degree-of-freedom Parallel Manipulator to Track the Sun for Concentrated Solar Power Towers** has been carried out by Mr. Ashith Shyam R Babu at the Indian Institute of Science, Bangalore under my supervision and that it has not been submitted elsewhere for the award of any degree or diploma.

Signature of the Thesis Supervisor: .....

Professor Ashitava Ghosal
Dept. of Mechanical Engineering
Indian Institute of Science, Bangalore

DECLARATION

I hereby declare that the content embodied in this thesis titled **Design and Development of a Three-degree-of-freedom Parallel Manipulator to Track the Sun for Concentrated Solar Power Towers** is the research carried out by me at the Department of Mechanical Engineering, Indian Institute of Science, Bangalore under the supervision Prof. Ashitava Ghosal, Department of Mechanical Engineering, IISc. In keeping with the general practice in reporting scientific observations, due acknowledgment has been made wherever the work described is based on the findings of other investigations.

Signature of the Author: .....

Ashith Shyam R Babu
Dept. of Mechanical Engineering
Indian Institute of Science, Bangalore

Acknowledgements

I take this opportunity to thank my advisor *Prof. Ashitava Ghosal* who has motivated and encouraged me all through the course of this thesis work. I appreciate his patience in explaining things to me particularly when I made mistakes. I have learned many things from him and without his valuable guidance, I would not have come this far.

I would also like to thank the Department of Mechanical Engineering, Indian Institute of Science for all the facilities given to me and made my stay in the campus pleasant and fruitful. A sincere thanks goes to all the professors and staff members in IISc. for motivating, guiding and helping me during my stay in IISc.

A special thanks goes to all my labmates especially to *Midhun S. Menon, Ashwin Prabhakaran, Ashwin Bose, Arka, Shounak, Mohit Acharya, Puneet Singh, Ravi Teja Chanamolu* and my team mates *Vikram Chaturvedi, Debajit Sarma, Dibyendu Mallik, Ravi Teja Upadrashta, Lalit Patnaik, Kiran KG, Varun Raturi, Raghav Nallani, Syam Venugopal, Manish Mandloi, Pranesh P, Salil Kashyap, Naga raju M, Mayank, Arjun Chiluka, Prof. Arindam Ghosh, Anirudha Datta Roy, Sounik Saha, Gogo, Harshan J, Sreedhara* etc . My other friends in the campus like *Akhil G, Bau, Midhun Ben Thomas, Naveen Yeshu James, Naresh N, Koshychayan, 'My american driver' Chintoo, Nippo, Paara, Habeeb Rehman, Mahind Jayan, Varghese Mathai (our adima), Jahfer daivam Sharif, Ambi, U block teams, Sandy hari, Aman P.V.* were of immense help to make my life in IISc. fun filled.

Thanks to SIMA for organizing various events, both cultural and sporting and gave me an opportunity to be a part of it.

Technical guidance from *Jude Baby George* and *Vineeth Muralidharan* helped me a lot in understanding the electronics parts of my project. I also extend my gratitude to Solar Energy Research Institute for India and the United States (SERIIUS) for funding my project.

Thanks to IISc. Gymkhana and sports officer *Mr. C.P. Poonacha* for helping me in various ways while I was the convener and captain of IISc. Gymkhana Cricket Team.

A special mention goes to my wife *Simna Manoharan* without whose efforts this would not have been possible.

Finally I extend my gratitude to my parents, *B. Rajendra Babu* and *Beena N.R.*, my brother *Baban Shyam* and grandmothers *Padmini* and *Ambujakshi* and my in-laws *Manoharan C.* and all energetic *Prasanna Manoharan, Surya chechi, Saumi* and our little gift *Malutty* and all other family members who have always been there by my side as pillars of support.

Ashith Shyam R Babu
Department of Mechanical Engineering
Indian Institute of Science
Bangalore.

Abstract

In concentrated solar power (CSP) stations, large arrays of mirrors which are capable of changing its orientation are used to reflect the incident solar energy to a stationary receiver kept at a distance. Such mirrors are often called as heliostats. The receiver contains a heat absorbing medium like molten salt. By absorbing the thermal energy reflected from thousands of heliostats, the temperature would reach around 600 ^{0}C and the heat can be used in thermal power plants to generate steam and thus run a turbine to produce electricity. One of the biggest advantages of CSP over conventional energy harvesting from Sun is that it can generate electricity during night for long hours of time from the thermal energy stored during daytime. This eliminates the usage of batteries or any other energy storing methods. The conversion efficiency is also high in CSP due to the high temperature achieved.

With prior knowledge of the station coordinates, viz., the latitude and longitude, the day of the year and time, the direction or the path of Sun can be fully determined. Typically, the Sun's motion is tracked by the azimuth-elevation (Az-El) or the target-aligned configuration heliostats. In both these approaches, the mirror needs to be moved about two axes independently using two actuators in series with the mirror effectively mounted at a single point at the centre. This arrangement causes the mirror to deform in presence of gusty winds in a solar field which results in loss of pointing accuracy. Typically a beam error of less than 2-3 mrad is desirable in a large solar field and this value also includes other sources of loss of pointing accuracy like gravity and wind loading. In order to prevent this, a rigid support frame is required for each of the heliostats.

In this work, two three degree-of-freedom parallel manipulators, viz., the 3-UPU wrist and 3-RPS, have been proposed to track the Sun in central receiver systems. The main reasons for choosing a parallel manipulator as heliostat are its desirable characteristics like large load carrying capacity, high accuracy in positioning the mirror and easy to obtain the inverse kinematics and convenient for real time control. The proposed parallel manipulators support the load of the mirror, structure and wind loading at three points resulting in less deflection and thus a much larger mirror can be moved with the required tracking accuracy and without increasing

the weight of the support structure. The algorithm for Sun tracking is developed, extensive simulation study with respect to actuations required, variation of joint angles, spillage loss and leg intersection has been carried out. Using FEA, it is shown that for same sized mirror, wind loading of 22 m/s and maximum deflection requirement (2 mrad), the weight of the support structure is between 15% and 60% less with the parallel manipulators when compared to azimuth-elevation or the target-aligned configurations. A comprehensive study on stroke minimization of prismatic joints is carried out. It is found that a stroke of 700 mm is required for a 2 m x 2 m heliostat at Bangalore when the farthest heliostat is at a distance of 300 m from the tower. Although, there is an extra motor required to track the Sun, the 3-RPS manipulator is better than the conventional methods if the mirror area per actuator criteria is taken into consideration.

Prototypes of the Az-El and 3-RPS heliostats were made with a mirror size of 1 m x 1 m. A PID controller implemented using MATLAB-Simulink and a low cost, custom made motor driver circuit is used to control the motion of the 3-RPS heliostat. The algorithm developed is tested on the prototype by tracking a point marked on the wall of the lab space and is found to have a tracking error of only 7.1 mrad. Finally, the actual Sun tracking is carried out on the roof of a building reflecting the sunlight to a wall situated 6.72 m above and a distance of 15.87 m from the heliostats. The images are captured at various instances of time from 11:15 a.m. to 3:30 p.m. on October 15th and November 10th, 2016, tracking errors are quantified and it is demonstrated that the proposed 3-RPS parallel manipulator can indeed work as a heliostat in concentrated solar power plants.

Publications from the Thesis

- **Journals**

  1. R.B. Ashith Shyam and A Ghosal. *Path Planning of a 3-UPU Wrist Manipulator for Sun Tracking in Central Receiver Tower Systems*, **Mechanism and Machine Theory**, 119:130-141, 2017
  2. R.B. Ashith Shyam, Mohit Acharya and A Ghosal. *A Heliostat Based on a Three Degree-of-Freedom Parallel Manipulator*. **Solar Energy**, 157: 672-686, 2017
  3. R.B. Ashith Shyam and A Ghosal. *Three-degree-of-freedom parallel manipulator to track the sun for concentrated solar power systems*. **Chinese Journal of Mechanical Engineering**, 28(4): 793-800, 2015.

- **Conferences**

  1. R.B. Ashith Shyam, Mohit Acharya and A Ghosal. *Experiments in Sun Tracking with a Novel Three-Degree-Of-Freedom Parallel Manipulator*, In **SOLARPACES**, 2017 (accepted)
  2. R.B. Ashith Shyam, A. Ghosal , *A three-degree-of-freedom parallel manipulator for concentrated solar power towers: Modeling, simulation and design.* In **SOLARPACES**, 2015: International Conference on Concentrating Solar Power and Chemical Energy Systems 2016 May 31 (Vol. 1734, No. 1, p. 160006). AIP Publishing.
  3. R.B. Ashith Shyam, Mohit Acharya and A. Ghosal. *A comparative study on conventional sun tracking mechanism and a novel 3-RPS heliostat.* 9th **National Symposium on Aerospace and Related Mechanisms**, ISRO satellite centre, India, Jan 30-31, 2015.
  4. R.B. Ashith Shyam, A. Ghosal, *A Parallel Mechanism for Tracking the Sun*, proceedings of 2014 **IFToMM Asian Conference on Mechanism and Machine Science**, July 9-10, 2014, Tianjin, China

Contents

List of Figures

List of Tables

Nomenclature

Acronyms

Az-El	Azimuth Elevation
CR	Central Receiver
CCD	Charge Coupled Devices
CAD	Computer Aided Design
CSP	Concentrating Solar Power
DOF	Degree-of-Freedom
D-H	Denavit-Hartenberg
DNI	Direct Normal Irradiance
FoS	Factor of Safety
FEA	Finite Element Analysis
PCM	Phase Change Material
PV	Photo Voltaic
P	Prismatic or sliding joint
PID	Proportional Integral Derivative
PWM	Pulse Width Modulation
R	Revolute joint
S	Spherical or ball joint
Sun vector	A unit vector pointing towards Sun
T-A	Target Aligned
TES	Thermal Energy Storage
U	Universal of Hooke's joint

Greek Symbols

ρ	Density of air
γ	Orientation of the base platform with respect to global co-ordinate system, Rotation about Z axis.
ψ	The angle which the line joining the global origin and the centre of the heliostat makes with the East axis

User Defined Symbols

r_b	Circum-radius of the base equilateral triangle
r_p	Circum-radius of the top equilateral triangle
C_d	Coefficient of drag

Chapter 1

Introduction

1.1 Motivation

Availability of low cost and reliable energy is essential for development and especially so in emerging economies. A major part of the energy requirement are now met from non-renewable fossil fuels which are abundant and affordable. However, extraction and burning of fossil fuels to meet the energy requirements for development has resulted in extensive environmental destruction and pollution and, in addition, release of green house gases to the atmosphere which is now widely accepted to be a leading cause of global warming and climate change. There is thus an increasing awareness and urgency to use renewable sources of energy often referred to as clean or green energy. Solar energy is perhaps the most abundant, renewable and non-polluting form of clean energy. It is available throughout the year and in many parts of the world and is believed to have the highest potential as a source of clean energy. Various governments and other organizations across the globe are pushing for a solar revolution and is considered to be the energy for the future. India gets around 300 days of sunshine a year of which the annual average of Direct Normal Irradiance (DNI) varies from 3 to 7 KWh/m^2 [1]. The amount of solar power that can be generated is more than 500,000 TWh per year of electricity, assuming 10 % conversion efficiency [2]. There are two main ways to harvest solar energy – one can use photo-voltaic (PV) panels to convert incident sunlight to electrical energy or one can convert the incident solar energy first to thermal energy at a higher temperature which is then converted to electricity. The efficiency of conversion in current PV is around 20 % whereas in the route of thermal and conversion to electricity, such as in concentrating solar power (CSP) systems, efficiencies can be as high as 30 % [3] due to the high operating temperatures. In a solar PV system, energy must be stored, typically in expensive batteries, to match demand and generation and to provide electricity at night. In a CSP system, the energy can be more easily stored

thermally in molten salts and other medium and electricity can be generated during night or to match demand. Due to higher efficiency and ease of storage, CSP systems can compete with solar PV systems and several CSP systems are being developed around the world. One of the obstacle hindering large scale deployment of CSP plant is the high initial investment required [4]. In order to bring down the levelised cost of solar electricity, the Sunshot initiative was launched by the US DoE in 2011. The main goals set for 2020 are to bring solar electricity cost to $ 0.06 per kWh [5]. Kolb et al. [6], in his work, presents a detailed study of how to improve technology for reducing the cost. The CSP technology is yet to reach its maturity and it has a huge potential to be cost effective [7].

In any CSP system, a key task is to concentrate the incident solar energy on to a receiver in an efficient manner. Typically several mirrors or reflectors are used which reflect the incoming solar radiation on to a stationary receiver – the mirrors with its support structure, actuators and controllers is also known as a heliostat. From a large number of heliostats, a large amount of incident solar energy is concentrated in a small receiver volume resulting in high temperatures ($>$ 500 °C [8]) and this gives rise to higher conversion efficiencies in CSP systems. A typical solar field could have several thousand such heliostats (for example, at Ivanpah [8] there are three central receivers and 173500 heliostats) and it is estimated that the heliostats contribute up to 50 % [9] of the total cost of the CSP system. It is thus an area of research to develop low cost heliostats.

Generally the Sun moves across the sky daily in an East-West direction and in a North-South direction with the progress of seasons, a mechanism is needed to track the Sun and reflect the incident solar energy on to the stationary receiver. Due to the East-West and North-South motion of the Sun a two axis or a two degree-of-freedom (DOF) mechanism is required for Sun tracking and reflecting the energy on to the receiver. There exists several two DOF mechanisms for tracking the Sun (see section 1.4), each having its own advantages and disadvantages. In this thesis, we propose two parallel manipulators which can be used to track the Sun and thus can be used as heliostats. We demonstrate that these parallel manipulators have several inherent advantages over the existing designs and they have the potential to reduce cost and increase efficiency in CSP systems.

Before we discuss relevant literature on CSP systems and existing Sun tracking system, in the next section we describe the geometry, the terms and the parameters involved in Sun tracking.

1.2 Sun tracking and geometry

Sun tracking refers to the calculation of Sun's azimuth and elevation angles from any location on the earth's surface at every instant of time. There are various sources in the literature [10, 11, 12, 13] which show how to calculate the azimuth and elevation angles of Sun. For completeness, some terminologies and the equations are reproduced here from reference [12].

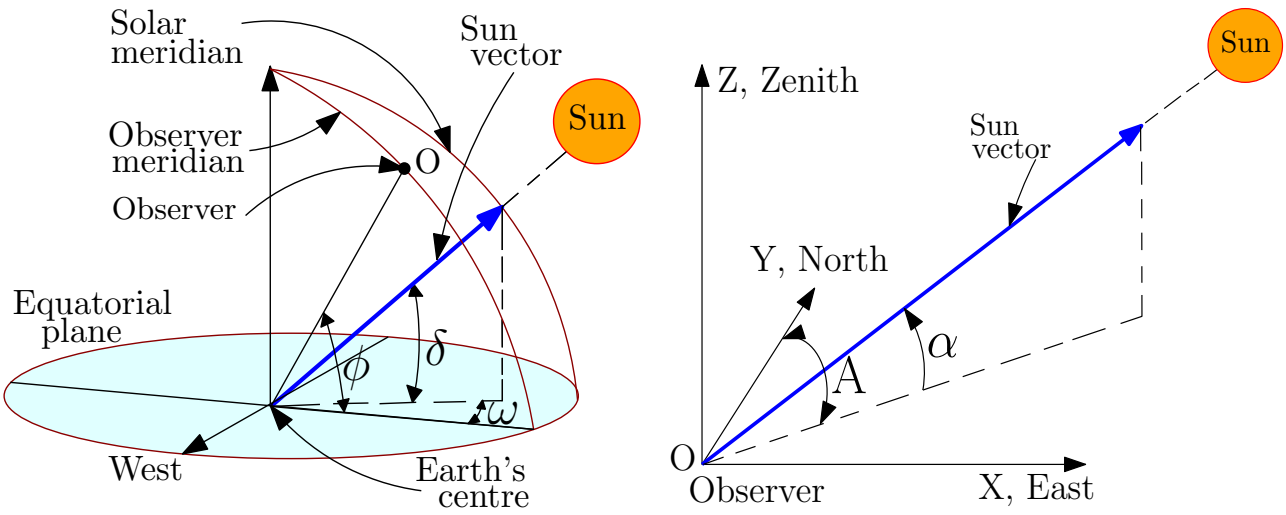

(a) Earth centre co-ordinate system

(b) Earth surface co-ordinate system

Figure 1.1: Co-ordinate system for defining various angles

The Earth surface and Earth centre co-ordinate systems shown in figure 1.1 has X, Y and Z axes pointing towards East, North and Zenith, respectively. These are related by a rotation about the East-West axis by the latitude angle and a translation along the radius of Earth. Since the radius is very small compared to the distance between Sun and Earth, this translation is neglected. Referring to figure 1.1, the definition of various angles are as follows:

- **Hour angle** (ω) is the angle between the meridian of the observer and the meridian whose plane contains the Sun in Earth centre co-ordinate system. The hour angle is zero at solar noon or in other words, the meridian of the observer and the Sun coincides when the Sun reaches the highest point in the sky. It varies from -180° to +180° having negative values in the morning and positive values after noon

- **Declination angle** (δ) is the angle between the line drawn from the centre of the Earth towards the Sun and the Earth's equatorial plane in Earth centre co-ordinate system. The value of δ varies $\pm$ 23.45° annually. The declination angle is zero at the equinoxes

where the day and night are of equal lengths. The declination angle is positive when the northern part of the earth's rotational axis is inclined towards the Sun.

- **Latitude angle** (ϕ) is the angle between a line drawn from a point on the Earth's surface to the center of the Earth and the Earth's equatorial plane in Earth centre co-ordinate system. Latitude angle is zero at the equatorial plane and varies between +90° at the North pole to -90° at the South pole.

- **Azimuth angle** (A) is the angle between the local North axis in Earth surface co-ordinate system and the projection of Sun vector on to the horizontal plane. The azimuth angle is measured from the local North axis and is positive clockwise. It varies from 0-360°.

- **Elevation angle** (α) is the angle the Sun vector makes with the X-Y plane described in Earth surface co-ordinate system. The elevation angle is zero when the Sun is at the horizon and varies from 0-90°

The Sun vector described in Earth surface co-ordinate system has the direction cosines $[\cos\alpha \sin A \quad \cos\alpha \cos A \quad \sin\alpha]^T$. Similarly, in Earth centre co-ordinate system, the Sun vector is $[\cos\delta \sin\omega \quad \cos\delta \cos\omega \quad \sin\delta]^T$. The azimuth and elevation angles are function of the declination, latitude and hour angle as follows:

$$\alpha = \sin^{-1}\left(\sin\delta \sin\phi + \cos\delta \cos\omega \cos\phi\right) \tag{1.1}$$

if $\cos\omega \geq \left(\frac{\tan\delta}{\tan\phi}\right)$,

$$A = 180 - \sin^{-1}\left(\frac{-\cos\delta \sin\omega}{\cos\alpha}\right) \tag{1.2}$$

else if $\cos\omega < \left(\frac{\tan\delta}{\tan\phi}\right)$,

$$A = 360 + \sin^{-1}\left(\frac{-\cos\delta \sin\omega}{\cos\alpha}\right) \tag{1.3}$$

Using these equations, the azimuth and elevation angles of the Sun for Bangalore, India on the two solstices and the two equinoxes are found out and is shown in figure 1.2. The MATLAB® [14] code for finding the Sun's azimuth and elevation angles are given in Appendix and can be used for any location on the Earth's surface and for any day in the year.

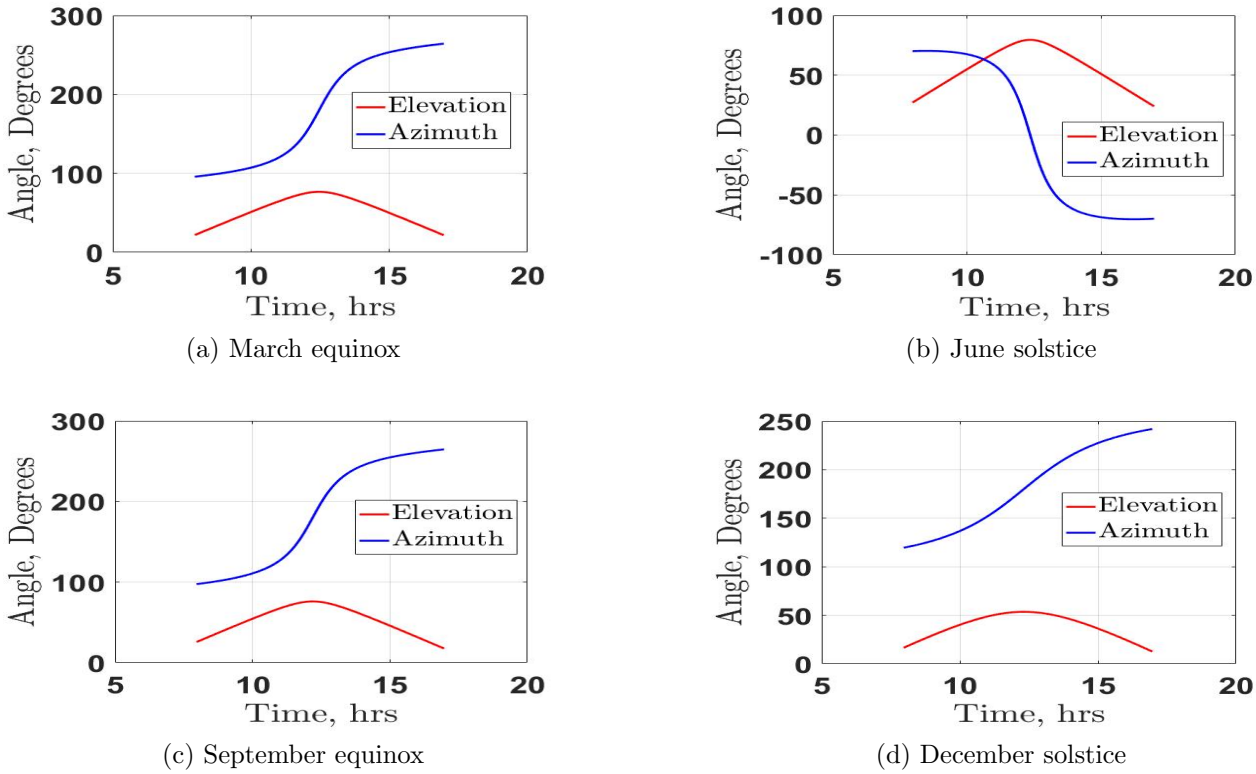

(a) March equinox

(b) June solstice

(c) September equinox

(d) December solstice

Figure 1.2: Azimuth and Elevation angles of the Sun for equinoxes and solstices, Bangalore

1.3 Methods for concentrating solar power (CSP)

Solar energy has two parts, namely the direct and diffuse radiations and CSP can only use the direct radiations. The US Department of Energy (US DoE) gives a comprehensive history of the solar technology [15]. Energy harvesting from the Sun is classified mainly into two main categories, viz., concentrating and non-concentrating type. The concentrating type includes parabolic troughs, paraboloid dishes, central receiver towers, linear Fresnel and Fresnel lenses (for concentrating photo-voltaic). The non-concentrating type includes flat plate collectors, evacuated tube and solar ponds. Our primary interest is on concentrating type and in this category, the three popular methods are parabolic troughs, paraboloid dishes and central receiver tower.

1.3.1 Parabolic trough

One of the first persons in the recent history to understand the importance of solar power was Frank Schuman. He had successfully built a parabolic trough powered water pumping system in Egypt in 1913 [16]. These troughs track the Sun on one axis and focus the incident solar

energy to a receiver tube kept along the focal line of the parabola as shown in figure 1.3a. A heat transfer fluid (like oil) is pumped through the tube which would absorb the thermal energy. This thermal energy is used for the generation of steam which is in turn used in power plants or as process steam. A detailed study on the various working fluids, viz., pressurized water, therminol VP-1, nitrate molten salt, sodium liquid, air, carbon dioxide and helium in the temperature range 300 - 1300 K is given by Bellos et al. [17]. A review article on the thermal performance of trough collectors in terms of heat loss, environmental conditions, temperature, heat flux, report cost and economic strategy is given by Conrado et al. [18].

Moya [19] discusses the design of the parabolic trough collectors. Initially researchers used a torque box design and later on shifted to a torque tube. Other innovative design concepts to improve concentration ratio [20], the effect of gravity load on mirror shape based on finite element analysis [21] etc. are also available in the literature. Since Sun tracking is done only in one axis, some amount of already diluted Sun's energy is lost and if coupled with cloudy days, the energy output is greatly reduced.

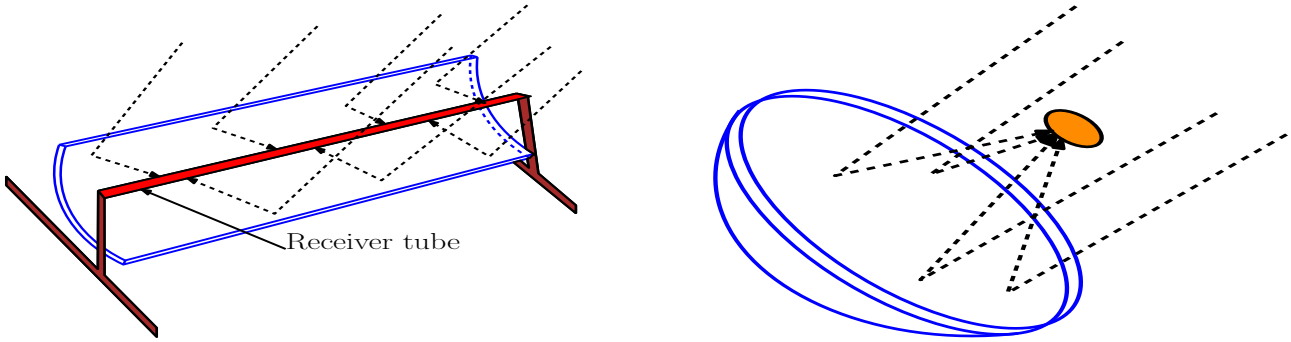

(a) Parabolic trough (b) Paraboloid dish

Figure 1.3: Solar concentrators

1.3.2 Paraboloid dish

Parabolic dishes concentrate solar radiations to a point focus (see figure 1.3b). They track the Sun along two axes and hence always look directly at the Sun producing temperatures of about 1000 °C [22] which results in high solar conversion efficiencies. India's Mega Kitchens [23] which are capable of producing around 40,000 meals per day use parabolic dishes to concentrate heat and produce about 2800 kg of steam. Among the solar concentrators, parabolic dishes have the highest conversion efficiency from sunlight to electricity of around 30 % [24]. Efforts are being made to increase the efficiency further by coupling the dish with an air micro gas turbine [25] thus initiating the development of a hybrid version.

Andraka [26] has proposed a thermal energy storage system for the dishes combining latent energy transport and latent energy storage. In this work, the author investigates the technical feasibility of the system. Another interesting study by Lertsatitthanakorn et al. [27] attempt to use a parabolic dish to concentrate Sun's radiations to a thermoelectric module to generate electricity.

For both parabolic troughs and paraboloid dishes, precise manufacturing is of utmost important to achieve the high concentration ratios. Between the two, currently only the parabolic trough has thermal storage capability of 6 hours [28].

1.3.3 Central receiver tower

Figure 1.4 shows the Ivanpah central receiver (CR) system in California, USA. It consists of a central receiver tower several meters high (70-195 m), surrounded by an array of movable mirrors which could be as far as 1.4 km away from the tower. These mirrors, also called heliostats, can be of various sizes – in Ivanpah, the areas of each mirror is 15 m^2. The motion of the heliostats are programmable and also calibrated periodically to ensure that the incident rays are always reflected to the receiver tower at all instants of time during a day and throughout the year. The receiver has a heat absorbing medium to absorb the thermal energy and is stored in an

Figure 1.4: Ivanpah in California, USA (Google images)

insulated chamber. Thermal energy storage (TES) enables large amount of energy to be stored without any hazards. It has small daily self-discharge loss, high energy density, high specific energy and is economically viable [29, 30]. Hence TES is considered to be the best method to

store energy in CSP plants. TES using phase change materials (PCMs) have been a very active topic of research in the last two decades or so and several PCMs both organic and inorganic have been developed. A detailed study of various PCMs are given by Zalba et al. [31] and Lane [32]. This heat can be used to boil water and generate steam which in turn can be used to drive a turbine for producing electricity or any other applications which require heat. The thermal energy stored can also be used for generating process steam for industrial applications [33]. Latest trends in energy storage may be found in the report published by Sandia National Laboratories [34].

The first CR demonstration project was carried out in the USA in 1982. This was named *Solar One* and had a capacity of 10 MW [15]. The Andasol 1 solar thermal power plant in Andalucia, Spain, [35] claims that they can produce electricity from heat stored in molten salts (28500 tons) for seven and a half hours after sunset. The receiver outlet temperature achieved in CR systems is very high (about 565 ^{0}C in Ivanpah, USA) and hence this heat could be used at night to drive a steam turbine. The high temperature achieved also helps in achieving higher conversion efficiencies as per the Carnot's theorem [36].

1.4 Overview of existing Sun tracking methods

There are various algorithms used for Sun tracking (see Lipps and Vant-Hull [37]) – the main ones are the azimuth-elevation, radial-pitch-roll, azimuthal-pitch-roll, polar and the target-aligned. Mousazadeh et al. [38] and Lee et al. [39] present a review of the Sun-tracking methods employed currently by various researchers across the globe using passive, single-axis and dual axis tracking. This paper also gives the energy gain obtained while using various types of trackers, close-loop and open-loop types of tracking employed currently. The most popular method for tracking the Sun in central receiver systems is the Azimuth-Elevation (Az-El) . The Target-Aligned (T-A) or also called as the spinning-elevation method is also developed as an alternate tracking methodology but almost not used at all. In both the above methods, there are two actuators which track the Sun and orient the heliostats in such a way that the incident ray from the Sun is always reflected onto a fixed central receiver.

As mentioned in section 1.2, the relative motion of the Sun in the sky with respect to Earth is known completely from the knowledge of date, time and location. Referring to figure 1.5, let O represents the origin of the global co-ordinate system (which is also the base of the receiver tower) and the OX, OY and OZ axes pointing towards the East, North and Zenith directions respectively. Let the mirror centre be at G and $\overrightarrow{GN}$, $\overrightarrow{GR}$ and $\overrightarrow{GS}$ denote the unit vectors representing the normal to the mirror, reflected ray and Sun-vector, respectively. From the laws of reflection, a) the incident ray, reflected ray and the normal should lie on the same plane,

and b) the angle of incidence equals the angle of reflection. The unit normal to the mirror can be found out as given in Shyam and Ghosal [40] as

$$\overrightarrow{GN} = \frac{\overrightarrow{GS} + \overrightarrow{GR}}{||\overrightarrow{GS} + \overrightarrow{GR}||} \tag{1.4}$$

where || represents the modulus function. Both Az-El and T-A heliostats use this information for the calculation of the actuations required and are explained further in detail.

1.4.1 The Azimuth-Elevation method

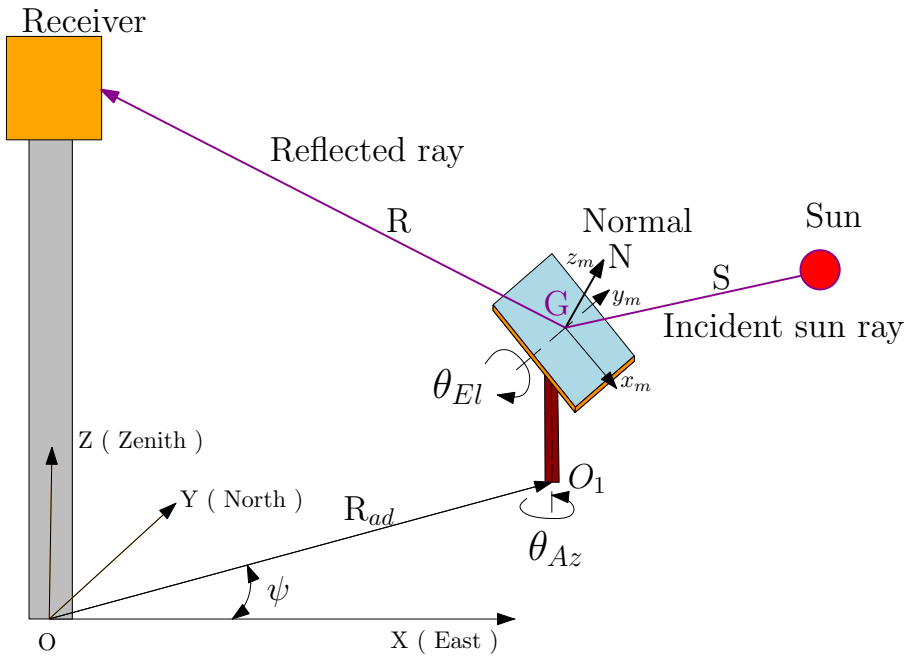

Figure 1.5: Schematic of Az-El heliostat

The Az-El Sun tracking is one of the most popular and widely used methods for CR systems. Figure 1.5 gives the schematic of the Az-El heliostat. The projection of the mirror normal ($\overrightarrow{GN}$) onto the X-Y plane makes an angle θ_{Az} with positive direction of X axis. The angle the normal makes with the X-Y plane is denoted by θ_{El}. At the start of tracking, it is assumed that the mirror co-ordinate system ($x_m - y_m - z_m$ or mirror co-ordinate system $\{M\}$) is parallel to the global coordinate system. Let the components of the normal vector $\overrightarrow{GN}$ as obtained from equation (1.4) be $[gn_x\ gn_y\ gn_z]^T$ with respect to the global co-ordinate system. Then the

actuations required can be found out as a function of time as

$$\theta_{Az} = \arctan\left(\frac{gn_y}{gn_x}\right) \tag{1.5}$$

$$\theta_{El} = \arctan\left(\frac{gn_z}{\sqrt{gn_x^2 + gn_y^2}}\right) \tag{1.6}$$

The Az-El can also be used for all other types of solar energy harvesting techniques including CR systems, parabolic troughs and dishes. Though simple and economical, the Az-El method of tracking has numerous disadvantages [22]. In order to overcome the short comings of the Az-El method, another method of tracking called the target-aligned method was proposed and is described next.

1.4.2 The Target-Aligned or Spinning-Elevation method

It was pointed out by Igel and Hughes [41] that the astigmatic aberration of the Az-El heliostats could be reduced if the heliostats are rotated about the mirror normal in addition to the azimuth and elevation rotations thus making it a three degree-of-freedom (DOF) system. This concept later led to the development of Target-Aligned or T-A heliostat [42, 43] and it overcomes certain short comings like astigmatism, hot spots etc. of the Az-El mount. Chen et al. [44], Wei et al. [45], and Guo et al. [46], derived the formulas for Sun tracking for the T-A heliostat. For completeness, the same is reproduced here.

In T-A heliostat, one of the actuator axes is collinear with the reflected ray and the other axis is perpendicular to it. Hence, the former is called spinning axis and the latter elevation axis. With reference to figure 1.6, the projection of the reflected ray (from the centre of the heliostat to the centre of the receiver) on the X-Y plane makes an angle ψ with the X axis and λ is the angle the reflected ray makes with the Z axis. For T-A heliostat also, the mirror coordinate system is assumed to be parallel with the global co-ordinate system at the start of the operation. From this, the heliostat makes two Euler rotations so that the normal to the mirror coincides with the reflected ray $\overrightarrow{GR}$. These rotations are

1. Rotation about Z by an angle ψ
2. Rotation about y_m by an angle (-λ)

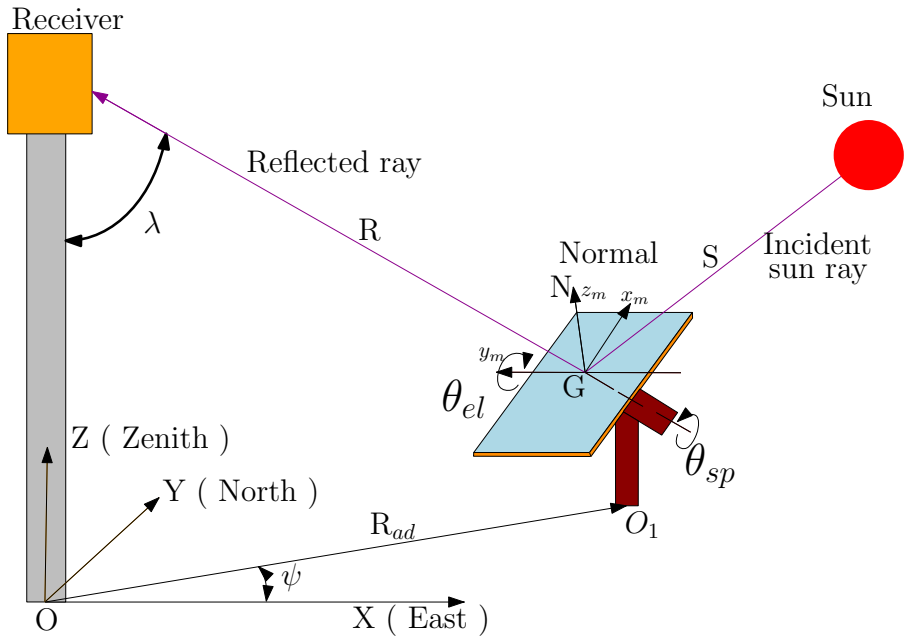

Figure 1.6: Schematic of the Target-Aligned heliostat

and the resultant rotation matrix is given by

$$R_{12} = \begin{bmatrix} \cos(\psi)\cos(\lambda) & -\sin(\psi) & -\cos(\psi)\sin(\lambda) \\ \sin(\psi)\cos(\lambda) & \cos(\psi) & -\sin(\psi)\sin(\lambda) \\ \sin(\lambda) & 0 & \cos(\lambda) \end{bmatrix} \tag{1.7}$$

After the first two rotations, the heliostat rotates about $\overrightarrow{GR}$ by an angle θ_{sp} (spinning angle) so that the the reflected ray, mirror normal ($\overrightarrow{GN}$) and the x_m axis of the mirror co-ordinate system become coplanar. Then finally, it rotates about an axis (y_m) which is perpendicular to $\overrightarrow{GR}$ in the plane of the mirror by an angle θ_{el} where θ_{el} is the half angle between the incident and reflected rays. The spinning and elevation angles can be found out as a function of time as

$$\theta_{sp} = \arctan\left(\frac{\overrightarrow{GP_0} \times (\overrightarrow{GS} \,.\, \overrightarrow{GR})}{\overrightarrow{GP_0} \,.\, \overrightarrow{GS}}\right) \tag{1.8}$$

$$\theta_{el} = 0.5 \arccos(\overrightarrow{GS} \,.\, \overrightarrow{GR}) \tag{1.9}$$

where $\overrightarrow{GP_0}$ is the vector given by the first column of the matrix R_{12}.

The T-A method is exclusively designed for CR systems. Although, the T-A was developed to overcome the short comings of the Az-El method, in a comparative study of Az-El and T-A

heliostats by Chen et al. [47], it is shown that for certain times of the day and year, Az-El performs better then T-A in terms of spillage losses and concentration.

1.4.3 Limitations of Az-El and T-A methods

As shown in figures 1.5 and 1.6, the mirrors are supported by a support frame and a pedestal which is fixed to the ground. The pedestal with the drives for the Az-El and the T-A heliostats are typically placed at the geometrical center of the mirror assembly. Due to this arrangement, the deflection of the support frame and the mirrors due to self-weight and wind load can go beyond the allowable slope error limit of 2 - 3 mrad [22] at the edges or corner of the mirror structure. In a heliostat field, the distance of the farthest mirror could be as more than 1.4 km. Thus the reflected ray from the mirror may not hit the receiver aperture. In order to tackle this problem, either the support frame has to be made more rigid or smaller sized heliostats have to be used.

To increase the concentration of incident solar radiation, the mirrors in a heliostat are typically canted – the arrangement of mirrors such that it approximate a paraboloid of revolution. There are different types of canting methods like on-axis, off-axis and parabolic canting. A comprehensive study of these methods has been made by Buck and Teufel [48]. Even though canting gives a better concentration ratio, it effectively modifies the focal point and introduces what is called the off-axis aberration as reported by Rabl [49].

The relative motion of Sun with respect to Earth is very slow – the Sun roughly goes East-West and traverses approximately 180° in about 12 hours or about 15° per hour. A simple computation shows that the rotation speed of the heliostat should be of the order of 7×10^{-5} rad/s. If typical DC electric motors, at 10 rpm, is used, it can be shown that large gear reductions (of the order of 1:15000) need to be used to track the Sun for both the Az-El and T-A methods of tracking. Gear boxes with such large reductions are expensive and typically introduce large friction and backlash errors which in turn makes Sun tracking inaccurate. To avoid large gear reductions, intermittent tracking is often used.

In order to avoid some of these difficulties, researchers have developed tracking strategies using linear actuators. An exciting tracking methodology is the pitch-roll or tip-tilt using two linear actuators. Lindberg and Maki [50] gives a detailed account of the stress analysis in presence of gravity and wind for the pitch-roll heliostat and a complete vector-based inverse kinematic solution of the pitch-roll heliostat was provided by Freeman et.al. [51]. One of the main advantages of such a system over the Az-El is that it uses less ground space. The Stellio heliostat [52, 53] uses two linear actuators in what is called a slope-drive configuration. This type of drive eliminates the high velocity required for large change in azimuth especially when

the heliostat normal reaches the vertical. Such a drive cannot be used for all heliostats in the field due to mechanical restrictions and the maximum angular distance that it can traverse is around 110°.

1.5 Errors sources and its control

There are various sources of tracking errors [54, 55] which eventually decrease the annual output of the CSP plants. They can be categorized into two main groups – optical and tracking error. The optical error can further be divided into slope and specular error. The macroscopic shape or the non-flatness of mirror due to manufacturing errors contributes to the slope error whereas the microscopic roughness causes the specular error. The tracking error occurs due to the errors in the control system. It is estimated that the sum of all these three sources of errors should be about 5 - 6 mrad for acceptable performance of a heliostat. In addition, the error from each of the sources are often apportioned as maximum optical error of less than 3 and 4 mrad [56] during calm and windy conditions respectively and maximum tracking error due to control of 2 mrad [57]. Reducing specular error is difficult and leads to increased cost. The error due to wind loading and self-weight can be reduced by appropriate design. The errors in tracking are due to reasons such as errors in modeling the motion of the Sun and inaccuracies in setting or measurement of co-ordinates of the heliostats, backlash in gears used in the drive system and errors in feedback from the joint encoders. Jones and Stone [58] analyze the tracking error sources in *Solar Two* CR system in Mojave desert, California. They have come up with a novel 'move' strategy to minimize tracking error by accurately surveying and storing in database. Various other researchers such as Stone and Kiefer [59], Malan and Gauché [60], and Kribus et al. [61] have tried to improve the tracking accuracy using open loop, model based and closed loop control strategies, respectively. Another closed loop control strategy for T-A heliostats was developed by Roos et al. [62] which ensures a tracking accuracy of 3.3 mrad. Even though closed loop tracking algorithms are available, their rather tedious task of installing CCD cameras has forced the current industrial norm to be of open loop tracking. This is achieved by a periodic calibration using a target screen situated below the receiver aperture and image processing techniques (see figure 1.7 [63]). The heliostats on the field reflect the incident Sun rays on to the calibration target one by one. There would be a camera to observe the target and a central control system which would be already fed with each heliostat parameters and the shift required to move the incident beam from the calibration target to the receiver aperture. The main disadvantage of this method is that only one heliostat could be calibrated at a time.

Figure 1.7: Calibration target for open-loop tracking

1.6 Contributions of the thesis

The focal point of this thesis is towards analysis and design of mechanisms which can help in development of low cost heliostats. The main contributions of the thesis are in the area of use of parallel manipulators for heliostats. Specifically the contributions of this work are as follows:

- Two three-DOF parallel manipulators to track the Sun. The 3-RPS parallel manipulator is shown to have less spillage losses as compared to existing Az-El and T-A mechanisms. A 3-UPU wrist manipulator which can be used in the Az-El or in the T-A configuration has also been proposed.

- The kinematic equations for the 3-RPS and the 3-UPU wrist parallel manipulators to track Sun in CR systems are developed. Extensive simulation study has been conducted to find out the actuations required, range of motion of the rotary and spherical joints used in the mechanisms and intersection of the legs with each other.

- Design of the mirror support structure for wind and gravity loading satisfying a slope error criteria of 2 mrad using finite element analysis has been carried out. It is shown that the use of the parallel manipulators can reduce the weight of the structure by 15 - 60 % for small to large heliostats, respectively.

- For the 3-RPS parallel manipulator based heliostat, extensive simulations have been done to obtain optimized design parameters. It is shown that the stroke required for the actuators is less than 700 mm for a 2 m x 2 m heliostat placed 300 m away from the receiver tower in Bangalore.

- A prototype of the 3-RPS heliostat with a mirror of dimension of 1 m x 1 m has been manufactured. The control algorithm and the developed control system is used to move the heliostat and Sun tracking is demonstrated.
- The tracking error is quantified and it is shown that the prototyped Az-El and 3-RPS based heliostats have comparable tracking errors of 20 mrad and 30 mrad respectively.

1.7 Preview

The organization of the thesis is as follows:
In chapter 2, two main aspects, viz., the existing Sun tracking using parallel manipulators and kinematics and simulation study of the proposed 3-RPS and 3-UPU wrist have been done. Chapter 3 gives a description of the finite element analysis done to find the least weight support structure. This chapter also provides an iterative approach to find certain design variables for minimizing the stroke of actuators and static and dynamic analysis of the 3-RPS heliostat. Chapter 4 provides the details regarding the prototype design, control strategy and the actual experimental validation. Finally, chapter 5 provides the conclusions and future directions of the work.

Chapter 2

Sun tracking using parallel manipulators

2.1 Introduction

The traditional Azimuth-Elevation (Az-El) and the Target-Aligned (T-A) arrangements are kinematically in a serial configuration where the actuators are placed one after the other. The mirror is also essentially mounted at a point after the two actuators used in these configuration. As in any serial configuration, the pointing or tracking error in the arrangement is the sum of the errors of the two actuators and due to the point support, the deflection in the mirror due to wind and self-weight is similar to that of a cantilever. In order to keep the pointing and tracking error within the allowable limit of 2 - 3 mrad, accurate and expensive drives with gear reduction is used and to overcome deflection due to loading, stiff and heavy supporting structures are used or smaller heliostats need to be used. Smaller heliostats implies that a large number of heliostats are required for a required power output from the solar plant with each heliostat containing two actuators with expensive drives. From the time the parallel manipulators were first introduced by Gough [64] and Stewart [65], it has been known that parallel manipulators provide high structural rigidity and more accurate positioning and orientation of the end-effector or the moving platform [66].The increased rigidity is due to the fact that the moving platform is supported at multiple points thereby the external load is shared. The increased accuracy is due to the fact that the positioning and pointing error of the end-effector is a function of the largest error in any actuator and *not* the sum of the errors as in a serial arrangement. Due to these inherent advantages, parallel manipulators have been extensively used in flight simulators, precision manufacturing, pointing devices, medical applications, and, more recently, in video games. Since precise positioning of the end-effector (mirror in our case) is one of the

advantages, use of a parallel manipulator can lead to use of low cost actuators and drives. With the increased rigidity, a heliostat can be designed with larger mirrors or for smaller mirrors, the supporting material required to withstand wind loading can be less. For a required power output from a solar plant, larger mirrors in each heliostat implies less number of heliostats and less number of actuators required in the field and less supporting material results in lowering of material and fabrication cost of a heliostat. Hence, a parallel manipulator is expected to lead to cost savings in concentrated solar power systems.

In this chapter, two 3-DOF parallel manipulators, viz., the 3-UPU wrist and 3-RPS parallel manipulator are proposed to be potential candidates for Sun tracking in central receiver systems. The 'U' denotes a two-DOF Hooke joint, the 'P' denotes single DOF a prismatic or a sliding joint, 'R' denotes a one-DOF revolute or a rotary joint and 'S' denotes a three-DOF spherical joint. In both these parallel manipulators, the 'P' joint is actuated and the other joints are not actuated or are passive. The 3-UPU wrist can be operated in both the Az-El and T-A mode by simply changing software and control strategy and *does not* require any change in the hardware. The 3-UPU wrist can thus be operated in a mode which gives the best performance in terms of spillage losses or astigmatism at a particular time of the day or a date in the year. The 3-RPS configuration has other inherent advantages when compared to the Az-El and T-A methods and these are discussed in detail in this chapter. In both the parallel configurations, linear actuators are used. The motion of the prismatic (P) joints or the stroke of the linear actuators are computed using simple inverse kinematics algorithms and adjusted with respect to time to achieve the orientation required for Sun tracking. The two parallel manipulators require three actuators as opposed to two in the Az-El and T-A configurations. However, since the support material is less or larger mirrors can be used and less expensive and less accurate linear actuators can be used, the overall cost of the plant is expected to be less.

The chapter is organized as follows: Section 2.2 gives an overview of the existing approaches for Sun tracking using parallel manipulators. In section 2.3, a detailed description of the 3-RPS parallel manipulator's geometry, inverse kinematics equations, modeling of R-P-S leg and spherical joint and simulations results are given. In section 2.4, the kinematics of the 3-UPU wrist manipulator and the simulation results and observations made during the simulation study are presented. Finally section 2.6 presents the conclusions and challenges ahead.

2.2 Overview of existing Sun tracking methods using parallel manipulators

There have been a few attempts to use parallel manipulators in Sun tracking for concentrated solar power systems. We present these attempts and their shortcomings.

2.2.1 The U-2PUS parallel manipulator and the CAPAMAN

In the work by Cammarata [67], a two degree-of-freedom parallel manipulator called the U-2PUS has been developed for photo-voltaic (PV) systems. The author claims that this manipulator is ideal for photo-voltaic systems in latitudes from 0 to 50^0. This parallel manipulator could be used for photo-voltaic systems but cannot be used for CR systems since in a field with photo-voltaic panels, all the PV panels are tracked in a similar manner. There is no reflection of the incident solar radiation and the conversion to electricity takes place in the PV panel itself. The location of the PV panels in the field do not play any part as the Sun's rays are parallel everywhere. For central receiver systems, the heliostats at different locations in the field will have different motion if the incident energy is to be reflected to a central receiver. Mathematically, it can be shown that there are more unknowns than equations available in the U-2PUS parallel manipulator system and hence it cannot be used in a CR system.

A three-degree-of-freedom parallel manipulator called CAPAMAN, containing a 17 links and 18 joints, has also been proposed for sun tracking [68]. However, to the best of our knowledge, there are no experimental results available in literature.

2.2.2 Other parallel mechanisms

A four degree-of-freedom parallel manipulator is proposed for Sun-tracking by Altuzarra et al. [69]. In his work, the collector initially is kept (before the tracking starts) high above the ground and by letting it fall in a controlled manner (using four sliders attached to it under the influence of gravity), the required orientation is achieved. This mechanism casts its own shadow on the collector. Although simulation results appear to be good, no prototype has been made and tested. To make the mechanism stiffer, some redundant bars are also used.

Google Inc. [70, 71] also developed a novel method for changing the position and orientation of the reflector (mirror). They proposed the use of an electric cable drive system which is constantly under tension. They also claim that this method will reduce the power consumption, size and cost of the actuator system. However, their light-weight frame design is susceptible to gusty winds and could be used only at places where wind velocities are very low.

Several other 2-DOF spherical mechanisms [72, 73, 74, 75] for application specific purposes

such as camera orientation, scanning spherically shaped items etc. are described in literature but none of these have been shown to be capable of tracking Sun for a central receiver systems.

Thus it is clear that the current Sun tracking approaches suffer from serious shortcomings be it large tracking errors as in the case of serial mechanisms to the inability to find the various orientations required for tracking for CR systems in parallel mechanisms. In this chapter the focus is on CR systems and we propose two potential parallel manipulators, viz., the 3-UPU wrist and the 3-RPS parallel manipulator that can be used for tracking without any of the above mentioned disadvantages. In addition, the 3-UPU can be reconfigured to be used either in Az-El or in the T-A method thus combining the advantages of both. From the next section onwards, the detailed study on the 3-RPS and the 3-UPU wrist parallel manipulators are carried out to investigate the merits of using them in CR systems.

2.3 Geometry and kinematics of a 3-RPS manipulator

Figure 2.1 shows the well known three-degree-of-freedom 3-RPS parallel manipulator. It consists of a moving top platform which is connected to a fixed base by means of three actuated prismatic(P) joints P_i, (i=1, 2, 3). At each of the connection points, S_i, $(i = 1, 2, 3)$, at the moving top platform, there is a spherical (S) joint and at each of the connection points at the fixed base, R_i, $(i = 1, 2, 3)$, there is a rotary (R) joint. The axes of the rotary joints are in the plane of the fixed platform. The mirror assembly is fixed to the top moving platform using a support structure (as shown in figure 2.2) which is designed to provide adequate stiffness such that deflections due to wind loads and self-weight are within acceptable limits. Referring to figure 2.1, the foot of the receiver tower and the origin, O, of the fixed coordinate system coincides with each other. The point O_1 is at a distance, R_d, from O and at an angle ψ with respect to the OX axis. The co-ordinate system at O_1 with axis $\{x_b, y_b, z_b\}$ (base coordinate system, $\{B\}$) is described with respect to the fixed coordinate system by a rotation γ about Z axis and a translation along $\overrightarrow{OO_1}$. The coordinate system at G is denoted with $\{x_m, y_m, z_m\}$ (mirror coordinate system $\{M\}$) and the vector $\overrightarrow{O_1G}$ is denoted by $[x_G, y_G, z_G]^T$ with respect to $\{B\}$. The variables l_1, l_2 and l_3 are the actuations at the prismatic joints and are functions of azimuth and elevation angles of Sun, heliostat location in the field, height of the receiver tower and the distance of the connection points from the centre. Even though the mirror assembly can have arbitrary shapes, for the purpose of kinematics, only the triangle formed by R_i's and S_i's need to be considered where $i = 1, 2, 3$. Without loss of generality, it is assumed that the triangle formed by the R_i's and S_i's form an equilateral triangle whose circum-radius is r_b and r_p respectively. The degrees of freedom of the manipulator can be found out by using the

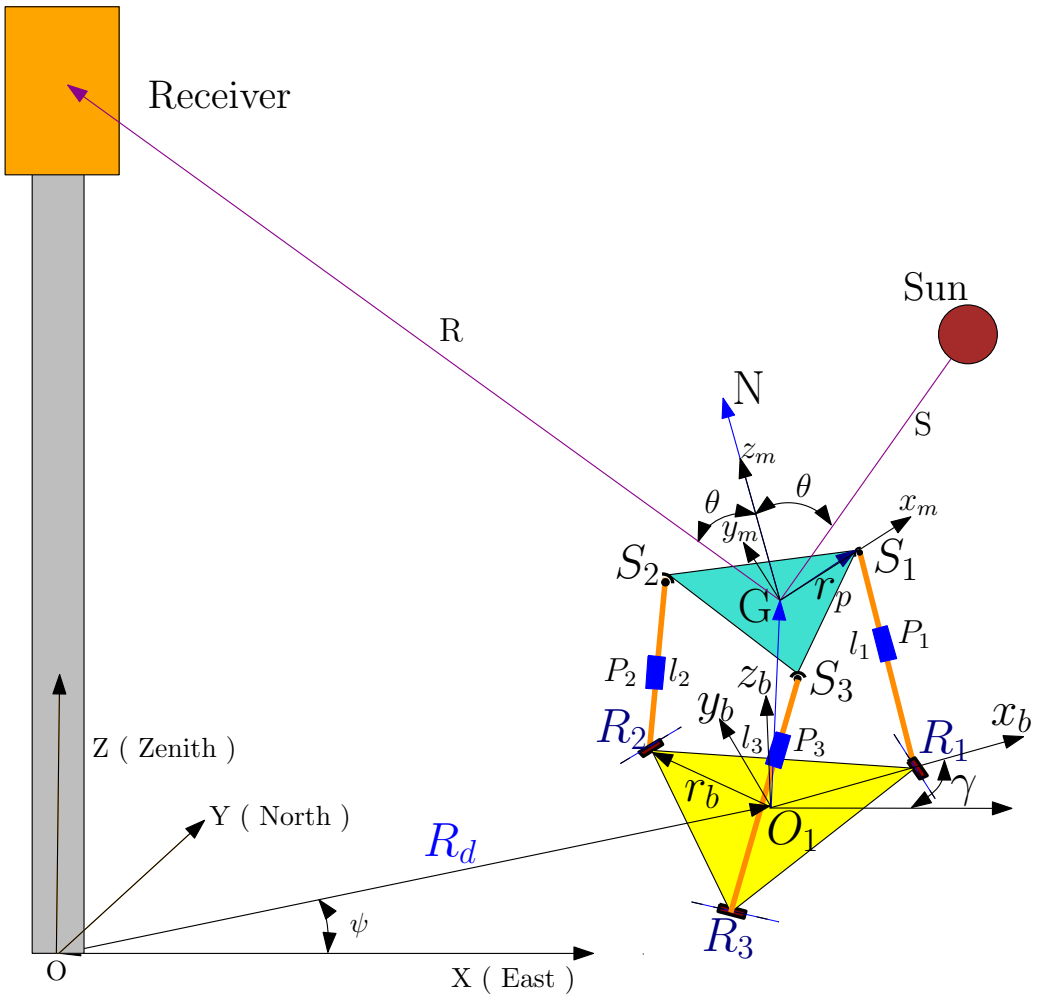

Figure 2.1: Schematic diagram of a 3-RPS manipulator

well-known Grübler - Kutzbach equation [76]:

$$DOF = \lambda(N - J - 1) + \Sigma F_i, \tag{2.1}$$

where λ is 6 for spatial and 3 for planar motion, N is the number of links including the fixed link, J is the number of joints and F_i is the degrees of freedom of i^{th} joint. For the 3-RPS manipulator, $N = 8$, $J = 9$ and $\Sigma F_i = 15$ and therefore $DOF = 3$. This implies that three actuators are required to move the top platform [76, 77]. Srivatsan et al. [78], have further shown that the three principal motions of the top moving platform are rotation about X and Y axis and a linear motion along the vertical Z axis. For tracking the Sun, only the rotation capability about the X and Y axes are used. The linear motion along the Z axis can be used to bring the mirror assembly down to a stowing position when high wind speeds are present or

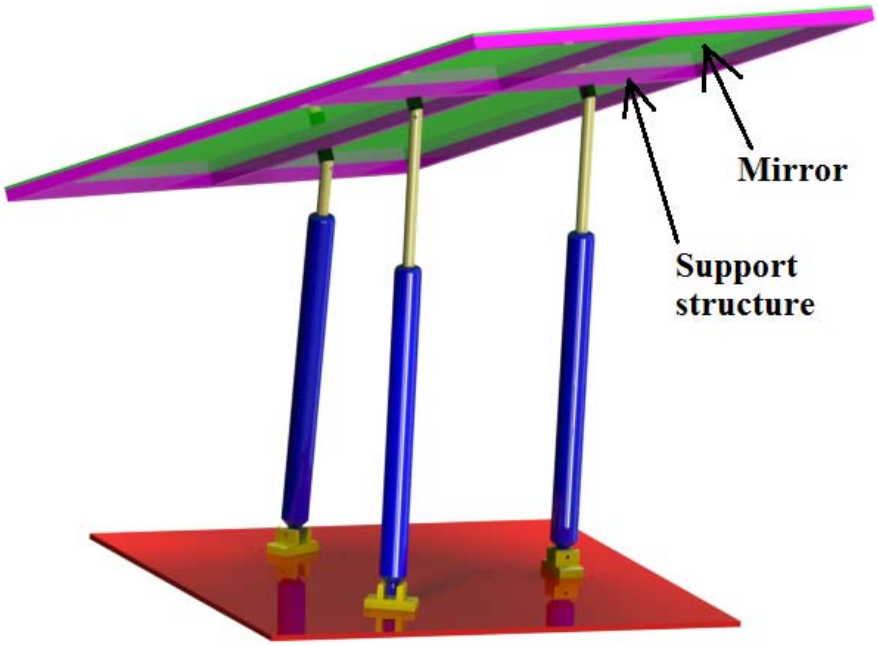

Figure 2.2: CAD model of the 3-RPS manipulator

for optimization.

The homogeneous transformation matrix $[T]$ which relates the coordinate system at O_1 and G can be described

$$[T] = \begin{bmatrix} n_1 & o_1 & a_1 & x_G \\ n_2 & o_2 & a_2 & y_G \\ n_3 & o_3 & a_3 & z_G \\ 0 & 0 & 0 & 1 \end{bmatrix} \tag{2.2}$$

where x_G, y_G and z_G are the co-ordinates of a reference point, G, on the top platform (fixed to the mirror), $(n_1, n_2, n_3)^T$, $(o_1, o_2, o_3)^T$ and $(a_1, a_2, a_3)^T$ denote the direction cosines of the x_m, y_m and normal (z_m) axes of the mirror co-ordinate system with respect to the base.

2.3.1 Kinematics of a 3-RPS manipulator

In the kinematics of a parallel manipulator, there are two well-known problems. In the direct kinematics problem, the prismatic joint variables l_1, l_2 and l_3 are known and the position vector $(\mathrm{x}_G, \mathrm{y}_G, \mathrm{z}_G)^T$ of a reference point on the moving platform, G, and the orientation of the top platform or the 4×4 homogeneous transformation matrix $[T]$ are to be found out. In the inverse kinematics problem, for a given $[T]$, the prismatic joint variables need to be obtained. For Sun tracking, we are primarily interested in the inverse kinematics of the manipulator.

In the inverse kinematics of 3-RPS manipulator, the elements of the transformation matrix, (equation (2.2)), can be computed from the knowledge of Sun vector, the location of the central receiver tower and the heliostats in a field and the three geometrical constraints of the manipulator itself. As the Sun moves in the sky, the elements of the transformation matrix change with time and at each instant the leg lengths, $l_i,\ i = 1, 2, 3$ of the manipulator need to be calculated. Since the 3-RPS manipulator has three degrees-of-freedom and the tracking of the Sun requires only two variables, there are several constraint equations relating the 12 unknowns in the transformation matrix $[T]$. As mentioned earlier, the rotation about the X and Y axis are used for orienting the top platform and one can choose the vertical motion of the top platform, z_G arbitrarily. To obtain the other constraints we proceed as follows.

As for any transformation matrix, we can write five constraint equations as

$$\begin{aligned} n_1^2 + n_2^2 + n_3^2 &= 1 \\ o_1^2 + o_2^2 + o_3^2 &= 1 \\ n_1a_1 + n_2a_2 + n_3a_3 &= 0 \\ n_1o_1 + n_2o_2 + n_3o_3 &= 0 \\ o_1a_1 + o_2a_2 + o_3a_3 &= 0 \end{aligned} \tag{2.3}$$

where $(n_1, n_2, n_3)^T$, $(o_1, o_2, o_3)^T$ and $(a_1, a_2, a_3)^T$ are from equation (2.2).

The normal to the mirror, $\overrightarrow{GN}$, is given by equation (1.4). From prior knowledge of the receiver co-ordinates, it can be found that the reflected ray $\overrightarrow{GR}$ is a function of x_G, y_G and the assumed value of z_G. Since $\overrightarrow{GS}$ is known in terms of azimuth and elevation angles of the Sun, the normal $\overrightarrow{GN}$ is also a function of the azimuth and elevation angles of the Sun and x_G, y_G and the assumed value of z_G. This implies that the direction cosines a_1, a_2 and a_3 of the normal vector $\overrightarrow{GN}$ are functions of five variables of which x_G and y_G are the unknowns.

The 3-RPS configuration introduces additional three constraints [77] given by

$$y_G + n_2r_p = 0 \tag{2.4}$$

$$n_2 = o_1 \tag{2.5}$$

$$x_G = \frac{r_p}{2}(n_1 - o_2) \tag{2.6}$$

where r_p is the circum-radius of the top equilateral triangle. Thus there are 8 equations in 8

unknowns, $\{x_G, y_G, n_1, n_2, n_3, o_1, o_2, o_3\}$. From equations (2.4) and (2.5),

$$n_2 = o_1 = \frac{-y_G}{r_p}$$

and from equation (2.6),

$$o_2 = n_1 - \frac{2x_G}{r_p}$$

Eliminating n_2, o_1 and o_2, we get

$$n_1^2 + (\frac{y_G}{r_p})^2 + n_3^2 = 1 \tag{2.7}$$

$$(\frac{y_G}{r_p})^2 + (n_1 - \frac{2x_G}{r_p})^2 + o_3^2 = 1 \tag{2.8}$$

$$n_1 a_1 - \frac{y_G}{r_p} a_2 + n_3 a_3 = 0 \tag{2.9}$$

$$-2n_1 \frac{y_G}{r} + \frac{2x_G y_G}{r_p^2} + n_3 o_3 = 0 \tag{2.10}$$

$$\frac{-y_G}{r_p} a_1 + (n_1 - \frac{2x_G}{r_p}) a_2 + o_3 a_3 = 0 \tag{2.11}$$

Thus we arrive at 5 equations in 5 unknowns, i.e., $(n_1, n_3, o_3, x_G$ and $y_G)$ which can be further reduced by substitution and using Bezout's method of elimination [79]. Finally we get two equations in x_G and y_G given in equations (2.12) and (2.13) below. Equations (2.12) and (2.13) are numerically solved for x_G and y_G in MATLAB® using the inbuilt routine *fsolve* for a given a_1, a_2 and a_3. The two equations are as follows:.

$$d_1 x_G^2 + e_1 x_G + f_1 = 0, \tag{2.12}$$

$$d_2 x_G^2 + e_2 x_G + f_2 = 0, \tag{2.13}$$

$$\begin{aligned} d_1 = &-12\,\frac{{y_G}^2 {a_2}^2}{{a_1}^2 {r_p}^4} - 4\,\frac{{y_G}^2}{{r_p}^4} - 4\,\frac{{y_G}^2 {a_2}^4}{{a_1}^4 {r_p}^4} + 4\,\frac{{a_2}^2}{{r_p}^2 {a_3}^2} - 4\,\frac{{y_G}^2 {a_2}^4}{{r_p}^4 {a_3}^2 {a_1}^2} + 4\,\frac{{a_2}^2}{{a_1}^2 {r_p}^2} - 8\,\frac{{a_3}^2 {y_G}^2 {a_2}^2}{{a_1}^4 {r_p}^4} \\ &- 4\,\frac{{y_G}^2 {a_2}^2}{{r_p}^4 {a_3}^2} - 4\,\frac{{a_3}^4 {y_G}^2}{{a_1}^4 {r_p}^4} - 8\,\frac{{a_3}^2 {y_G}^2}{{a_1}^2 {r_p}^4} \\ e_1 = &-4\,\frac{a_1 {y_G}^3 a_2}{{r_p}^4 {a_3}^2} - 4\,\frac{{a_2}^5 y_G}{{a_1}^3 {a_3}^2 {r_p}^2} + 4\,\frac{y_G {a_2}^3}{{r_p}^2 a_1 {a_3}^2} - 4\,\frac{{a_3}^2 y_G a_2}{{a_1}^3 {r_p}^2} + 4\,\frac{{y_G}^3 {a_2}^5}{{r_p}^4 {a_1}^3 {a_3}^2} - 8\,\frac{y_G {a_2}^3}{{a_1}^3 {r_p}^2} - 4\,\frac{{y_G}^3 a_2}{{r_p}^4 a_1} \\ &+ 4\,\frac{{y_G}^3 {a_2}^3}{{r_p}^4 {a_1}^3} \end{aligned}$$

$$
\begin{aligned}
f_1 = {} & \frac{{y_G}^2}{{r_p}^2} - 5\,\frac{{y_G}^4{a_2}^4}{{r_p}^4{a_1}^4} - \frac{{a_2}^2}{{a_1}^2} + \frac{{y_G}^4{a_2}^4}{{r_p}^4{a_1}^2{a_3}^2} + \frac{{a_2}^6{y_G}^2}{{a_1}^4{a_3}^2{r_p}^2} + 4\,\frac{{a_3}^4{y_G}^2}{{a_1}^4{r_p}^2} - 4\,\frac{{a_3}^4{y_G}^4}{{r_p}^4{a_1}^4} + 4\,\frac{{a_3}^2{y_G}^2}{{a_1}^2{r_p}^2} \\
& - 8\,\frac{{a_3}^2{y_G}^4}{{r_p}^4{a_1}^2} - 5\,\frac{{y_G}^4}{{r_p}^4} - \frac{{a_1}^2{y_G}^4}{{r_p}^4{a_3}^2} - 6\,\frac{{y_G}^4{a_2}^2}{{r_p}^4{a_1}^2} + 8\,\frac{{a_3}^2{y_G}^2{a_2}^2}{{a_1}^4{r_p}^2} - 8\,\frac{{y_G}^4{a_3}^2{a_2}^2}{{r_p}^4{a_1}^4} + \frac{{y_G}^4{a_2}^2}{{r_p}^4{a_3}^2} \\
& + 5\,\frac{{y_G}^2{a_2}^4}{{a_1}^4{r_p}^2} - 2\,\frac{{y_G}^2{a_2}^4}{{r_p}^2{a_1}^2{a_3}^2} + 2\,\frac{{y_G}^2{a_2}^2}{{a_1}^2{r_p}^2} + \frac{{y_G}^2{a_2}^2}{{r_p}^2{a_3}^2} - \frac{{y_G}^4{a_2}^6}{{r_p}^4{a_1}^4{a_3}^2} \\
d_2 = {} & -4\,\frac{{a_3}^4{y_G}^2}{{a_1}^4{r_p}^4} - 4\,\frac{{a_2}^4{y_G}^2}{{a_1}^4{r_p}^4} - 4\,\frac{{a_2}^4{y_G}^2}{{r_p}^4{a_3}^2{a_1}^2} + 4\,\frac{{a_2}^4}{{r_p}^2{a_1}^2{a_3}^2} - 8\,\frac{{a_3}^2{y_G}^2}{{a_1}^2{r_p}^4} + 4\,\frac{{a_2}^2}{{r_p}^2{a_1}^2} \\
& - 8\,\frac{{a_3}^2{a_2}^2{y_G}^2}{{a_1}^4{r_p}^4} - 4\,\frac{{a_2}^2{y_G}^2}{{r_p}^4{a_3}^2} - 12\,\frac{{a_2}^2{y_G}^2}{{a_1}^2{r_p}^4} - 4\,\frac{{y_G}^2}{{r_p}^4} \\
e_2 = {} & -4\,\frac{a_1{y_G}^3a_2}{{r_p}^4{a_3}^2} - 4\,\frac{{a_2}^5y_G}{{a_1}^3{a_3}^2{r_p}^2} + 4\,\frac{y_G{a_2}^3}{{r_p}^2a_1{a_3}^2} - 4\,\frac{{a_3}^2y_Ga_2}{{a_1}^3{r_p}^2} + 4\,\frac{{y_G}^3{a_2}^5}{{r_p}^4{a_1}^3{a_3}^2} - 8\,\frac{y_G{a_2}^3}{{a_1}^3{r_p}^2} \\
& - 4\,\frac{{y_G}^3a_2}{{r_p}^4a_1} + 4\,\frac{{y_G}^3{a_2}^3}{{r_p}^4{a_1}^3} \\
f_2 = {} & \frac{{y_G}^2}{{r_p}^2} - 5\,\frac{{y_G}^4{a_2}^4}{{r_p}^4{a_1}^4} - \frac{{a_2}^2}{{a_1}^2} + \frac{{y_G}^4{a_2}^4}{{r_p}^4{a_1}^2{a_3}^2} + \frac{{a_2}^6{y_G}^2}{{a_1}^4{a_3}^2{r_p}^2} + 4\,\frac{{a_3}^4{y_G}^2}{{a_1}^4{r_p}^2} - 4\,\frac{{a_3}^4{y_G}^4}{{r_p}^4{a_1}^4} + 4\,\frac{{a_3}^2{y_G}^2}{{a_1}^2{r_p}^2} \\
& - 8\,\frac{{a_3}^2{y_G}^4}{{r_p}^4{a_1}^2} - 5\,\frac{{y_G}^4}{{r_p}^4} - \frac{{a_1}^2{y_G}^4}{{r_p}^4{a_3}^2} - 6\,\frac{{y_G}^4{a_2}^2}{{r_p}^4{a_1}^2} + 8\,\frac{{a_3}^2{y_G}^2{a_2}^2}{{a_1}^4{r_p}^2} - 8\,\frac{{y_G}^4{a_3}^2{a_2}^2}{{r_p}^4{a_1}^4} + \frac{{y_G}^4{a_2}^2}{{r_p}^4{a_3}^2} \\
& + 5\,\frac{{y_G}^2{a_2}^4}{{a_1}^4{r_p}^2} - 2\,\frac{{y_G}^2{a_2}^4}{{r_p}^2{a_1}^2{a_3}^2} + 2\,\frac{{y_G}^2{a_2}^2}{{a_1}^2{r_p}^2} + \frac{{y_G}^2{a_2}^2}{{r_p}^2{a_3}^2} - \frac{{y_G}^4{a_2}^6}{{r_p}^4{a_1}^4{a_3}^2}
\end{aligned}
$$

As mentioned earlier $a_1,\ a_2$ and a_3 are the direction cosines of the vector $\overrightarrow{GN}$ and are dependent on the azimuth and elevation of the Sun (or $\overrightarrow{GS}$) and $x_G,\ y_G$ and the assumed value of z_G. The computed x_G and y_G values along with the arbitrarily chosen value for z_G give the vector $\overrightarrow{O_1G}$ and all the other unknowns in the transformation matrix can be obtained.

2.3.2 Actuations required for the 3-RPS parallel manipulator

From the geometry of the 3-RPS manipulator, the co-ordinates of the revolute joints with respect to $\{B\}$ are given by $\overrightarrow{O_1R_1} = (r_b, 0, 0)^T$, $\overrightarrow{O_1R_2} = (-\frac{1}{2}r_b, \frac{\sqrt{3}}{2}r_b, 0)^T$ and $\overrightarrow{O_1R_3} = (-\frac{1}{2}r_b, -\frac{\sqrt{3}}{2}r_b, 0)^T$ and the co-ordinates of the spherical joints with respect to $\{x, y, z\}$ are given by $\overrightarrow{GS_1} = (r_p, 0, 0)^T$, $\overrightarrow{GS_2} = (-\frac{1}{2}r_p, \frac{\sqrt{3}}{2}r_p, 0)^T$ and $\overrightarrow{GS_3} = (-\frac{1}{2}r_p, -\frac{\sqrt{3}}{2}r_p, 0)^T$. The position vector of the spherical joints with respect to the co-ordinate system $\{B\}$ is given as

$$
\begin{bmatrix} \overrightarrow{O_1S_i} \\ 1 \end{bmatrix} = \begin{bmatrix} T \end{bmatrix} \begin{bmatrix} \overrightarrow{GS_i} \\ 1 \end{bmatrix} \tag{2.14}
$$

The leg lengths or the actuation needed can be found out as [76]

$$l_i = ||\overrightarrow{O_1R_i} - \overrightarrow{O_1S_i}|| \tag{2.15}$$

where $i = 1, 2, 3$ and $||$ represents the norm of the vector. The leg lengths thus found out could be used as the inputs of an actuation system and hence used to track the Sun and orient the mirror in central receiver systems.

2.3.3 Modeling of the RPS leg

Table 2.1: D-H parameters of a R-P-S leg

i	α_{i-1}	a_{i-1}	d_i	θ_i
1	0	0	0	θ_1
2	$\frac{\pi}{2}$	0	l_1	0

An RPS leg has a rotary and a linear motion of which the latter is the actuated one. If a co-ordinate system is placed at the rotary joint with its Z axis coinciding with the axis of the rotary joint, then the Denavit-Hartenberg (D-H) [76] parameters of a R-P-S leg can be written as in table 2.1 where θ_1 is the angle the leg makes with the vertical and l_1 is the actuation required for the prismatic joint at that particular time instant. It may be noted that the three legs are 120° apart with respect to each other.

2.3.4 Modeling of spherical joint

The spherical joints can be modeled as three mutually perpendicular revolute joints intersecting at a point [76]. From the base of the leg, a set of four consecutive Euler rotations, namely rotation of the rotary joint and the Z-Y-X (or 321) rotation of the spherical joint, gives the mirror coordinate system ($x_m - y_m - z_m$). Figure 2.3 shows the co-ordinate system associated with a spherical joint and the resulting D-H table of the spherical joint is shown in table 2.2 [80].

For a given rotation matrix with elements r_{ij}, $i, j = 1, 2, 3$, the three rotations (Z-Y-X rotation) is found out by using the following algorithm:
If $r_{31} \neq \pm 1$, then

$$\theta_{s2} = \text{Atan2}[-\text{r}_{31}, \pm\sqrt{\text{r}_{32}^2 + \text{r}_{33}^2}\ ]$$
$$\theta_{s1} = \text{Atan2}[\text{r}_{21}/\cos(\theta_{s2}), \text{r}_{11}/\cos(\theta_{s2})]$$

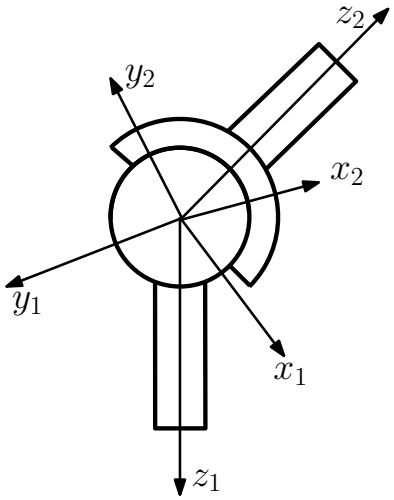

Figure 2.3: Schematic of a spherical joint

Table 2.2: DH parameters of the spherical joint

i	$\boldsymbol{\alpha_{i-1}}$	$\boldsymbol{a_{i-1}}$	$\boldsymbol{d_i}$	$\boldsymbol{\theta_i}$
1	0	0	0	θ_{s1}
2	$-\frac{\pi}{2}$	0	0	$\theta_{s2} + \frac{\pi}{2}$
3	$\frac{\pi}{2}$	0	0	$\theta_{s3} + \frac{\pi}{2}$
4	$-\frac{\pi}{2}$	0	0	$-\frac{\pi}{2}$

$$\theta_{s3} = \text{Atan2}[\text{r}_{32}/\cos(\theta_{s2}), \text{r}_{33}/\cos(\theta_{s2})]$$

If $r_{31} = 1$, then

$$\theta_{s2} = -\frac{\pi}{2}, \quad \theta_{s1} = 0, \quad \theta_{s3} = \text{Atan2}[-\text{r}_{12}, -\text{r}_{13}]$$

If $r_{31} = -1$, then

$$\theta_{s2} = \frac{\pi}{2}, \quad \theta_{s1} = 0, \quad \theta_{s3} = \text{Atan2}[\text{r}_{12}, \text{r}_{13}]$$

where Atan2 is the four quadrant inverse tangent function.

2.3.5 Simulation results for 3-RPS heliostat

To simulate the motion of the 3-RPS parallel manipulators, the kinematics equations described above were programmed in MATLAB®. The parameters for the simulation are as follow :

- The locations chosen are Bangalore and Chui, Rajastan, India (12.9716 ° N, 77.5946 ° E) and (27.0238 ° N, 74.2179 ° E) respectively.
- Simulations are done for four different days, viz., the March equinox, Summer solstice, September equinox and the Winter solstice.
- The centre co-ordinates of the receiver tower with respect to the global coordinate system is taken as $(0\ 0\ 65\ \text{m})^{\text{T}}$.
- The heliostat is placed at a radial location of 100 m from the receiver tower and at 30° from the East axis.
- Both the top and bottom platforms of the 3-RPS manipulator are assumed to be equilateral triangles of circumradius 0.50 m.
- The value assumed for z_G is 2 m from the centre of the bottom platform.
- The dimensions of mirror and the receiver aperture are considered to be 2 m × 2 m and 2.5 m × 2.5 m respectively.
- Initially, both the top and bottom platforms of the 3-RPS mechanism shown in figure 2.1 are assumed to be parallel.

Figures 2.4 and 2.5 show the simulations done for March equinox and Summer solstice for Bangalore and Rajasthan, respectively. It can be seen from these figures that the legs of the heliostat do not intersect. Extensive simulations have been done to verify this fact and found that at no instances the legs intersect.

Figures 2.6 and 2.7 give the actuation required for the 3 legs of the 3-RPS manipulator to track the Sun for equinoxes and solstices in Bangalore and Rajasthan respectively. Figures 2.8 and 2.9 give the variation of the centre of the moving platform for equinoxes and solstices in Bangalore and Rajasthan. It is clear from the plots that the variation of the centre is very small and is in the range of ±0.1 m in both X and Y axes (z is assumed constant and is equal to 2 m), i.e., the footprint of the mirror remains essentially over the base. Figures 2.10 and 2.11 gives the variation of revolute joint angles from vertical for equinoxes and solstices for Bangalore and Rajasthan, respectively. Figures 2.12 and 2.13 show the angular (Z-Y-X) motion of the spherical joint for the legs for tracking the Sun for Bangalore and Rajasthan on March equinox and summer solstice respectively. The Z rotation in a spherical joint can be between 0 and 360° and is not shown.

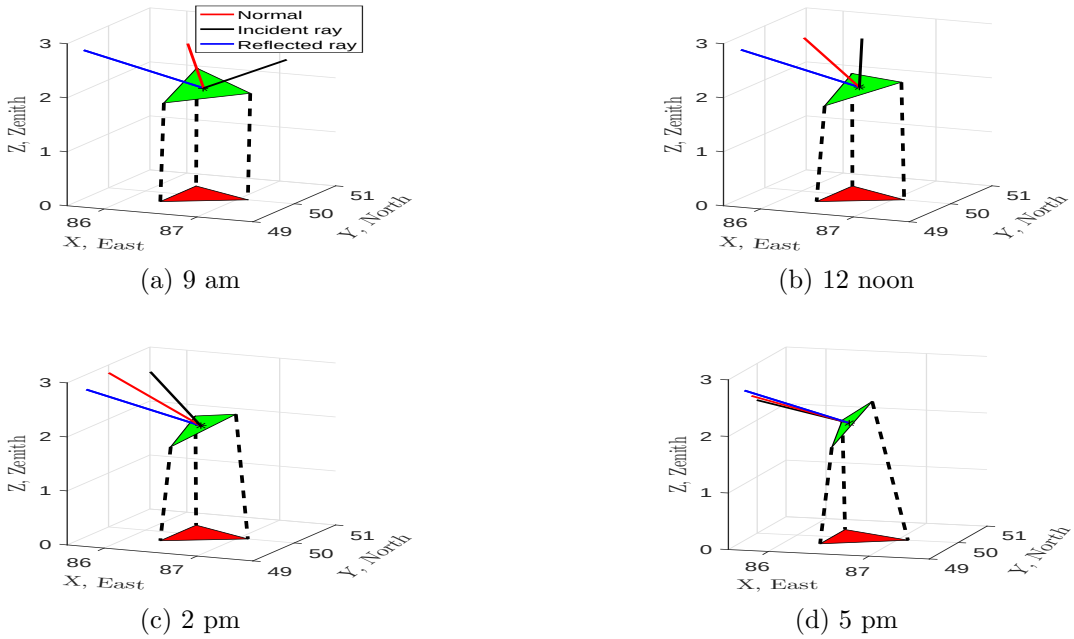

(a) 9 am (b) 12 noon

(c) 2 pm (d) 5 pm

Figure 2.4: Simulation of 3-RPS heliostat for March equinox for Bangalore

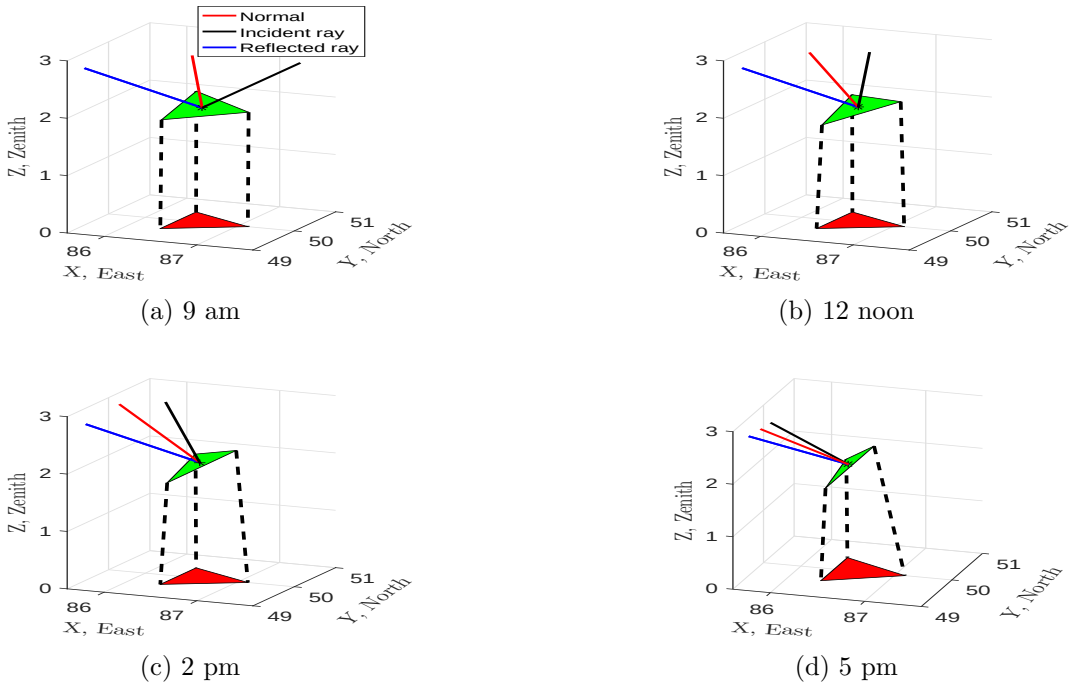

(a) 9 am (b) 12 noon

(c) 2 pm (d) 5 pm

Figure 2.5: Simulation of 3-RPS heliostat for Summer solstice for Rajasthan

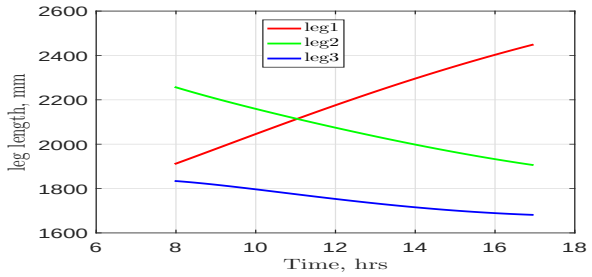

(a) March equinox

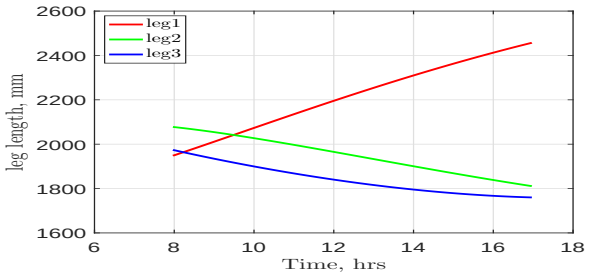

(b) Summer solstice

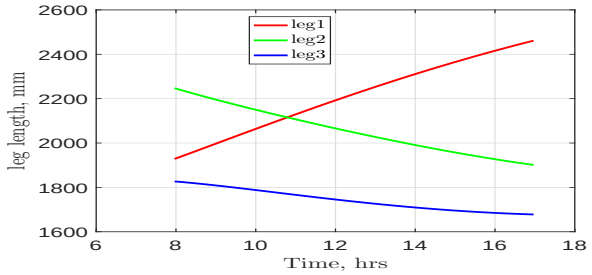

(c) September equinox

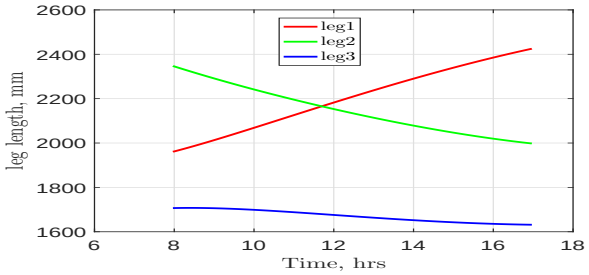

(d) Winter solstice

Figure 2.6: Actuations required for the 3-RPS heliostat in Bangalore

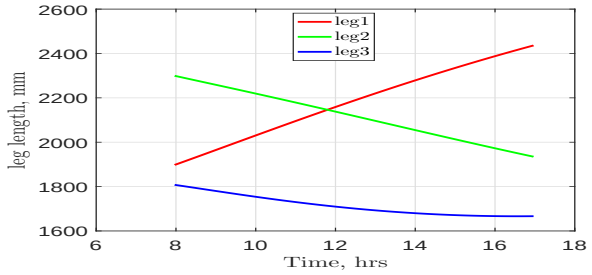

(a) March equinox

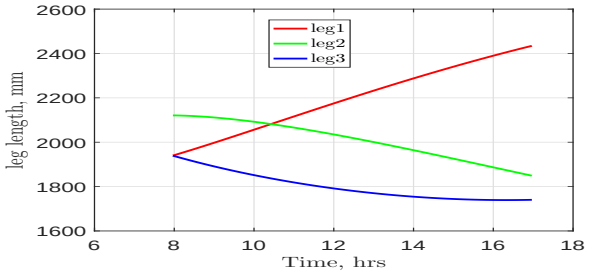

(b) Summer solstice

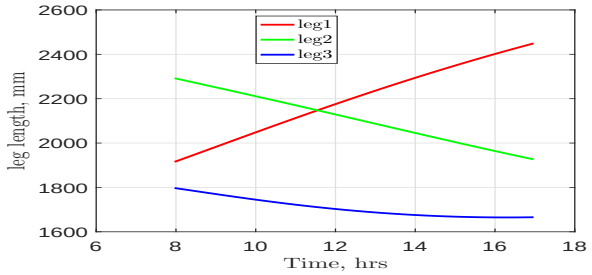

(c) September equinox

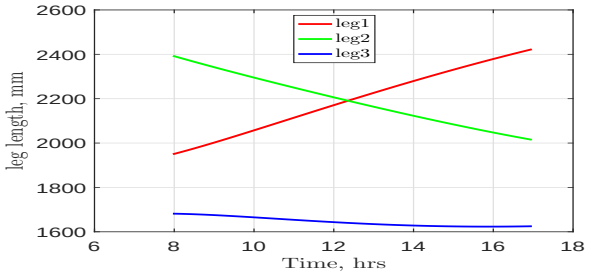

(d) Winter solstice

Figure 2.7: Actuations required for the 3-RPS heliostat in Rajasthan

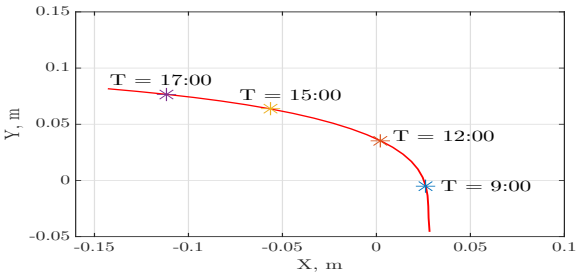

(a) March equinox

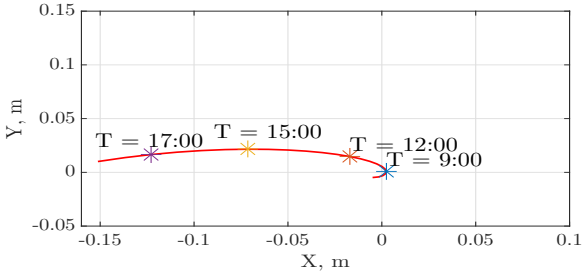

(b) Summer solstice

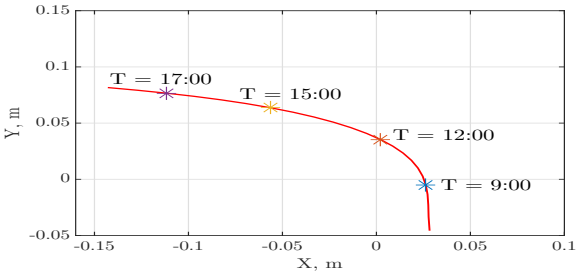

(c) September equinox

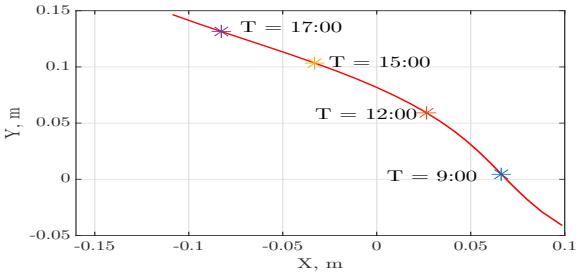

(d) Winter solstice

Figure 2.8: Variation of the centre of 3-RPS heliostat in Bangalore

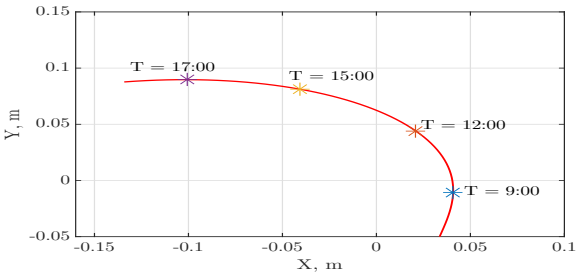

(a) March equinox

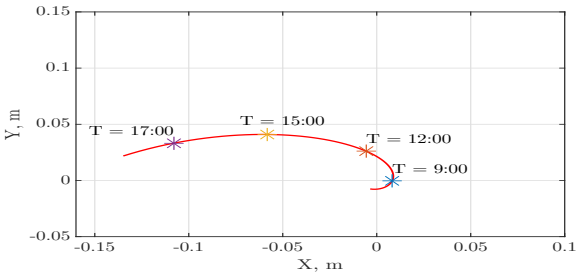

(b) Summer solstice

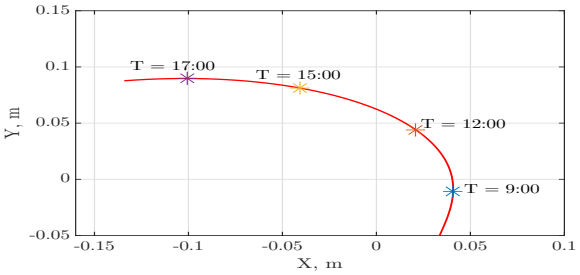

(c) September equinox

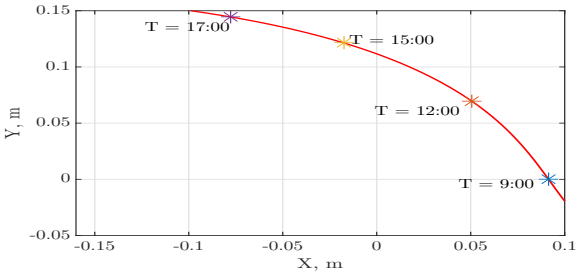

(d) Winter solstice

Figure 2.9: Variation of the centre of 3-RPS heliostat in Rajasthan

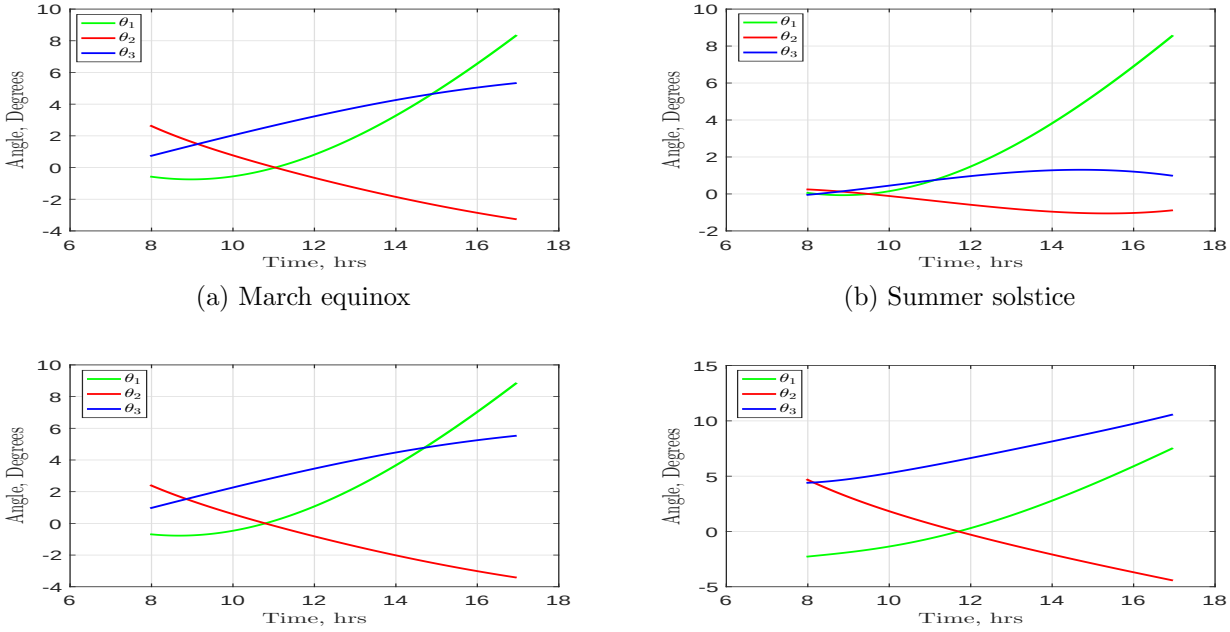

(a) March equinox

(b) Summer solstice

(c) September equinox

(d) Winter solstice

Figure 2.10: Variation of the revolute joint angles from vertical for Bangalore

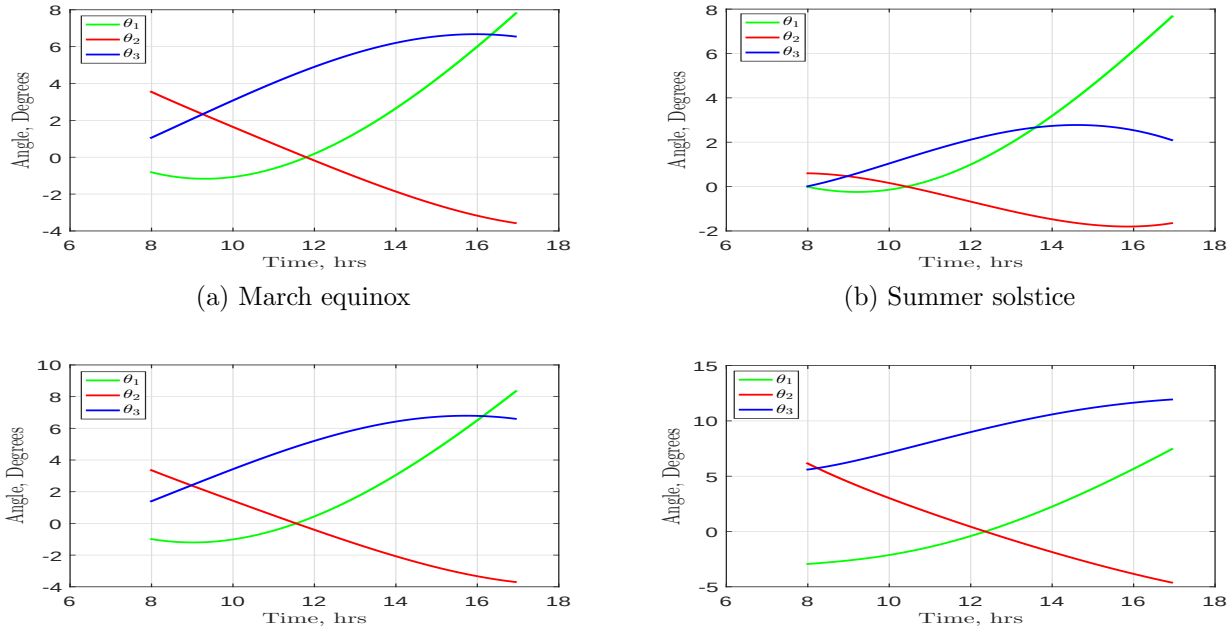

(a) March equinox

(b) Summer solstice

(c) September equinox

(d) Winter solstice

Figure 2.11: Variation of the revolute joint angles from vertical for Rajasthan

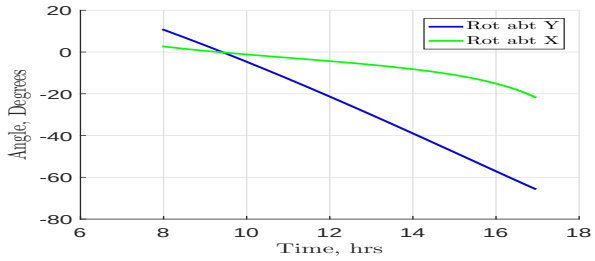

(a) Leg1

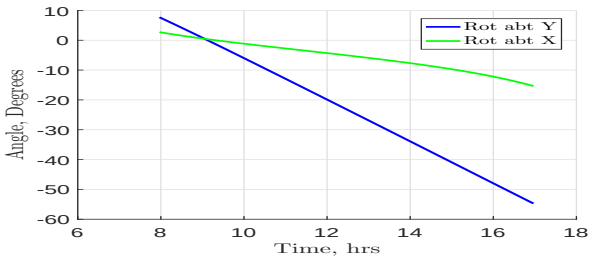

(b) Leg2

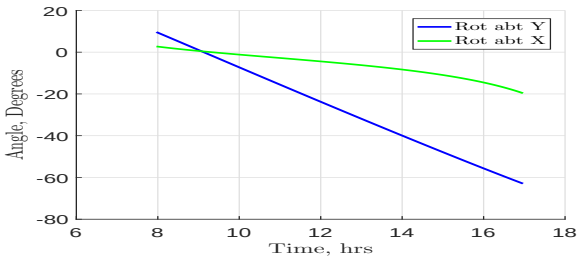

(c) Leg3

Figure 2.12: Variation of the spherical joint angles for Bangalore on March equinox

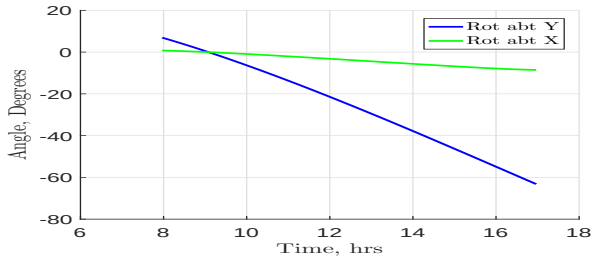

(a) Leg1

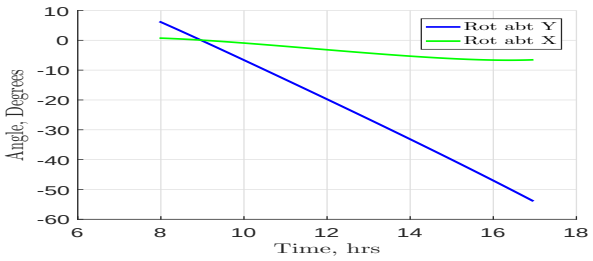

(b) Leg2

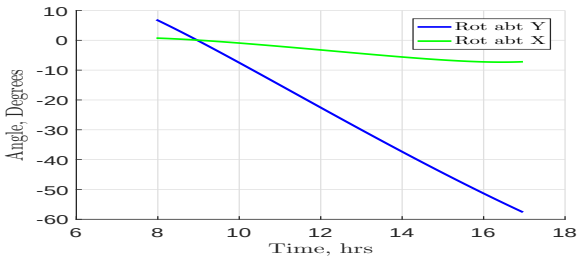

(c) Leg3

Figure 2.13: Variation of the spherical joint angles for Rajasthan on summer solstice

One can also obtain the shape of the image on the receiver. To obtain this, we assume that the ray hitting the centre of the mirror will be reflected towards the centre of the receiver aperture at every instant of time. Since the mirror is assumed to be perfectly flat and the Sun

is considered to be a point source, the parallel rays hitting the four corners of the mirror will be reflected to the receiver aperture parallel to the central ray. The points where the reflected rays from the mirror corner hit the receiver aperture are joined together to form the image polygon. This is calculated for every one minute interval from 8 a.m. to 5 p.m. In some literatures, this image area is often mentioned as spot size and the area going out of receiver aperture is called spillage loss. For the 3-RPS parallel manipulator for the chosen parameters of r_b and r_p both equal to 500 mm, the image formed on the receiver plane is shown in figure 2.14 at four instants of time. This type of analysis helps in quantifying the spillage loss when a 3-RPS heliostat is used for Sun tracking in CR systems.

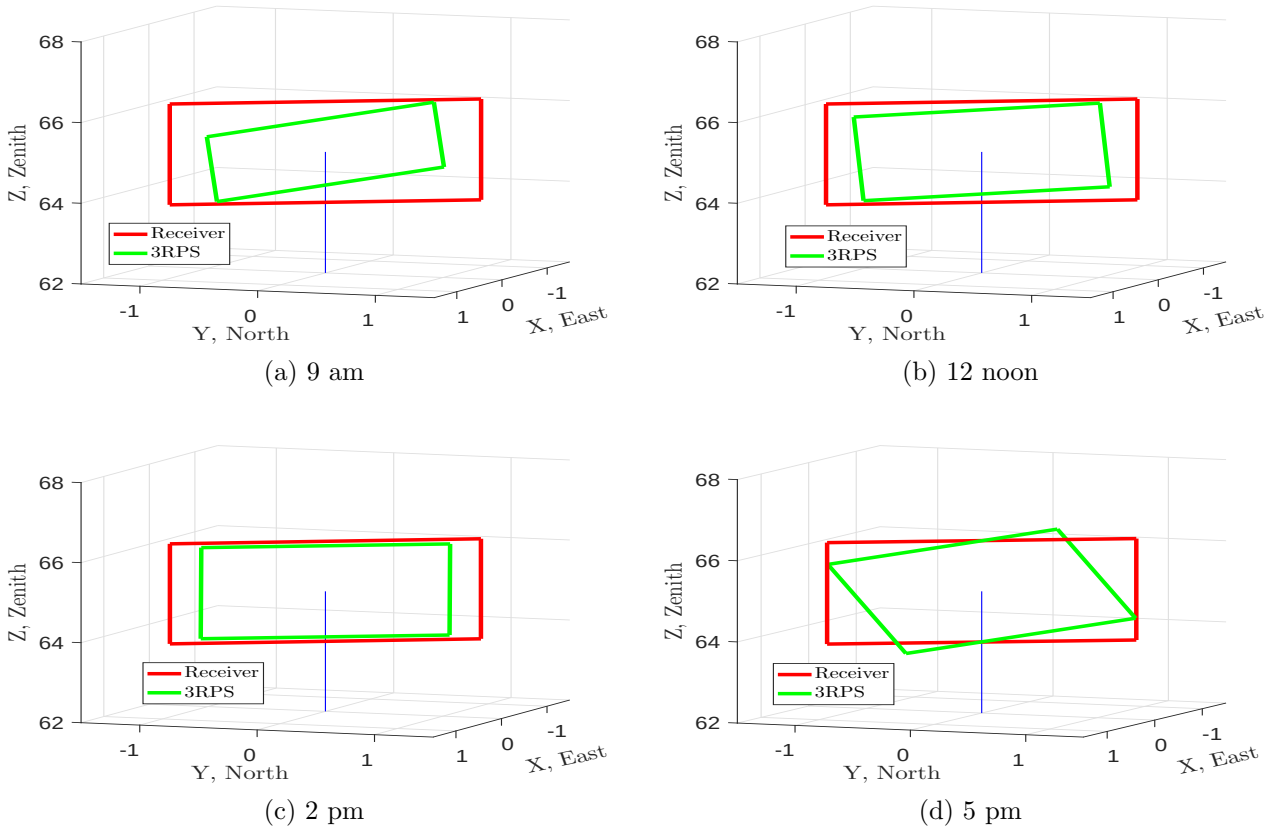

(a) 9 am (b) 12 noon

(c) 2 pm (d) 5 pm

Figure 2.14: The image on the receiver aperture at various time instants for March equinox for Bangalore

From simulations done, it is clear that the 3-RPS heliostat does not attain any singular configurations. The variation of the centre of the top platform, the revolute, prismatic and the spherical joints are within attainable limits of commercially available products. Thus the 3-RPS parallel manipulator is a promising candidate for prototyping. Further, we look at the

characteristics of a 3-UPU wrist parallel manipulator in the next section for the purpose of comparison.

2.4 Kinematics of the 3-UPU wrist manipulator

Similar to 3-RPS, the 3-UPU manipulator also has a fixed base and a moving platform connected together by three legs having joints in the order universal-prismatic-universal (UPU). The conditions which have to be satisfied for making a 3-UPU manipulator to be a wrist are listed in Karouia and Hervé [81] and the kinematics equations of the 3-UPU wrist manipulator is given by Di Gregorio [82].

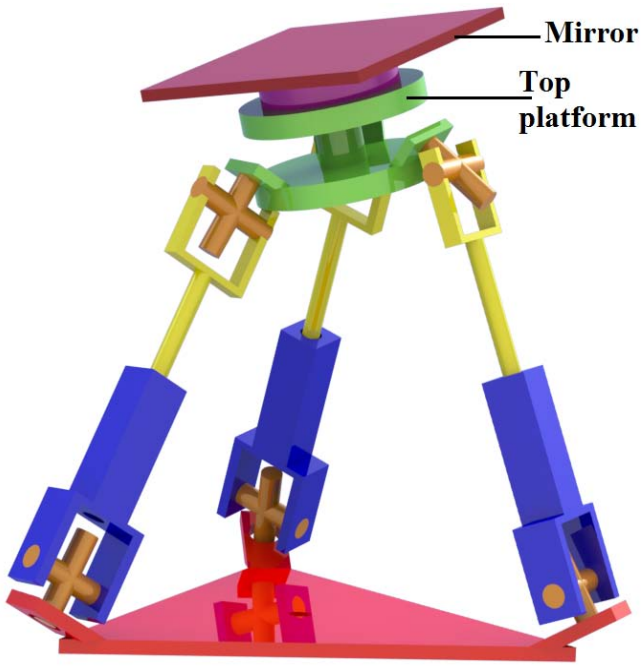

Figure 2.15: CAD model of the 3-UPU wrist

The 3-UPU wrist manipulator is not an over-constrained mechanism and is capable of performing finite spherical motions about a fixed point when the prismatic joints are actuated. For Sun tracking, the fixed point should be carefully chosen so that it falls above the moving platform at the top. As shown in figure 2.15, by using suitable attachments, the mirror centre and the fixed point are made to coincide with each other. Thus the mirror rotates about the fixed point just like in serial Az-El or T-A arrangements as one can make two consecutive Euler rotations about a point for Sun tracking.

The co-ordinate system used for 3-UPU wrist is same as that of 3-RPS manipulator. The schematic diagram of the 3-UPU wrist manipulator is shown in figure 2.16. The symbols U_{bi}

and U_{ti} $(i = 1, 2, 3)$ denote the universal joints at the base and top, respectively. Let the mirror centre or the fixed point of the 3-UPU wrist be at M. As in the 3-RPS case, the triangles formed by U_{bi} and U_{ti} are equilateral triangles whose circum-radius is r_b and r_p, respectively. The degrees of freedom of the manipulator as obtained by using equation (2.1) is 3. The calculations required to find the transformation matrix for Sun tracking in the Az-El or the T-A mode can be obtained and is described in the next section.

2.4.1 Rotation matrix for Az-El case

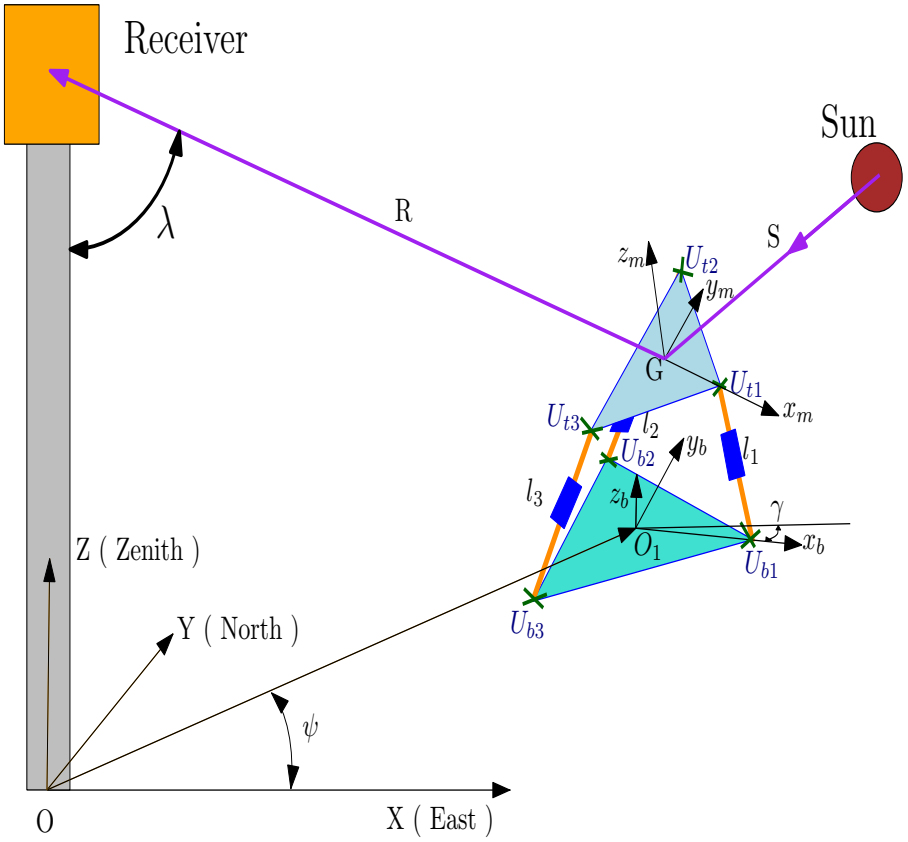

Figure 2.16: Schematic of the 3-UPU

In the home position (early morning when the tracking starts), the mirror coordinate system $(x_m - y_m - z_m)$ is kept parallel to the global coordinate system. Then for an Az-El heliostat, the two Euler rotations required to track Sun and reflect the rays to the receiver are

1. Rotation about Z by an angle θ_{Az} as given by equation (1.5).

2. Rotation about y_m by an angle $(\frac{\pi}{2} - \theta_{El})$ as given by equation (1.6)

Hence, the rotation matrix becomes

$$R_{Az-El} = \begin{bmatrix} \cos\theta_{Az}\sin\theta_{El} & -\sin\theta_{Az} & \cos\theta_{Az}\cos\theta_{El} \\ \sin\theta_{Az}\sin\theta_{El} & \cos\theta_{Az} & \sin\theta_{Az}\cos\theta_{El} \\ -\cos\theta_{El} & 0 & \sin\theta_{El} \end{bmatrix} \tag{2.16}$$

In such a rotation, the y_m axis of the mirror coordinate system would still lie on a plane parallel to the XY plane and it is verified by noting that the (3,2) element of the rotation matrix, R_{Az-El}, is zero. The third column of the rotation matrix are the direction cosines of the normal $\overrightarrow{GN}$ which is already known from equation (1.4). The other two columns of the rotation matrix are found out by carrying out suitable inverse trigonometric calculations.

The above same rotation matrix can also be found out using numerical approach. A general rotation matrix contains $(n_1, n_2, n_3)^T$, $(o_1, o_2, o_3)^T$ and $(a_1, a_2, a_3)^T$ as its first, second and third column (see equation (2.2), respectively. For Az-El rotation, we have $o_3 = 0$ and $(a_1\ a_2\ a_3)^T$ is obtained from equation (1.4). Thus we have five equations from the orthogonality of the rotation matrix and five unknowns, viz., $n_1,\ n_2,\ n_3,\ o_1$ and o_2. Using MATLAB®'s *fsolve* routine, these five equations are solved to get the values of $n_1,\ n_2,\ n_3,\ o_1$ and o_2. The actuations required is dependent on the initial conditions of the *fsolve* routine and have to be chosen carefully.

2.4.2 Rotation matrix for Target-Aligned heliostat

The initial rotation matrix required is given by equation (1.7). Then the heliostat spins about $\overrightarrow{GR}$ by θ_{sp} given by equation (1.8) and rotates about y_m by θ_{el} given by equation (1.9). The spinning and elevation rotation matrix is given by

$$R_{34} = \begin{bmatrix} \cos\theta_{sp}\cos\theta_{el} & -\sin\theta_{sp} & \cos\theta_{sp}\sin\theta_{el} \\ \sin\theta_{sp}\cos\theta_{el} & \cos\theta_{sp} & \sin\theta_{sp}\sin\theta_{el} \\ -\sin\theta_{el} & 0 & \cos\theta_{el} \end{bmatrix}$$

Thus the final rotation matrix for the T-A heliostat is given by $R_{T-A} = R_{12}R_{34} =$

$$\begin{bmatrix} c_\psi c_\lambda c_{\theta_{sp}} c_{\theta_{el}} - s_\psi s_{\theta_{sp}} c_{\theta_{el}} + c_\psi s_\lambda s_{\theta_{el}} & -c_\psi c_\lambda s_{\theta_{sp}} - s_\psi c_{\theta_{sp}} & c_\psi c_\lambda c_{\theta_{sp}} s_{\theta_{el}} - s_\psi s_{\theta_{sp}} s_{\theta_{el}} - c_\psi s_\lambda c_{\theta_{el}} \\ s_\psi c_\lambda c_{\theta_{sp}} c_{\theta_{el}} + c_\psi s_{\theta_{sp}} c_{\theta_{el}} + s_\psi s_\lambda s_{\theta_{el}} & -s_\psi c_\lambda s_{\theta_{sp}} + c_\psi c_{\theta_{sp}} & s_\psi c_\lambda c_{\theta_{sp}} s_{\theta_{el}} + c_\psi s_{\theta_{sp}} s_{\theta_{el}} - s_\psi s_\lambda c_{\theta_{el}} \\ s_\lambda c_{\theta_{sp}} c_{\theta_{el}} - c_\lambda s_{\theta_{el}} & -s_\lambda s_{\theta_{sp}} & s_\lambda c_{\theta_{sp}} s_{\theta_{el}} + c_\lambda c_{\theta_{el}} \end{bmatrix}$$

where c_z, s_z represents the cosine and sine of the respective angles given by z. Like in Az-El heliostat, the normal $\overrightarrow{GN}$ and hence the third column of R_{T-A} is known. The angles ψ and λ are known from the prior knowledge of location of heliostat in the field and centre co-ordinates of the receiver with respect to the global coordinate system. Thus the first and second columns of the rotation matrix R_{T-A} can be computed.

2.4.3 Actuations required for 3-UPU wrist

As mentioned earlier, the top-platform and the mirror are connected together using an attachment such that the orientation of both are the same with respect to the base. The only difference being the centre of the mirror remains at the fixed point even while executing finite spherical rotations whereas it is not the same for the top platform. Initially, both the top and bottom platforms are assumed to be parallel. Then the rotation which takes the mirror to the base is found out as mentioned in sections 2.4.1 and 2.4.2. The centre of the top platform will be at a constant distance from the mirror centre in its normal direction downwards. Using this information, the centre of the top platform is found out and hence the actuation required for the legs of 3-UPU wrist can be found out as follows:

Similar to 3-RPS, for the 3-UPU manipulator, the co-ordinates of the U_{bi} joints with respect to $\{B\}$ are given by $\overrightarrow{O_1U_{b1}} = (r_b, 0, 0)^T$, $\overrightarrow{O_1U_{b2}} = (-\frac{1}{2}r_b, \frac{\sqrt{3}}{2}r_b, 0)^T$ and $\overrightarrow{O_1U_{b3}} = (-\frac{1}{2}r_b, -\frac{\sqrt{3}}{2}r_b, 0)^T$ and the co-ordinates of the U_{ti} joints with respect to $\{x_m, y_m, z_m\}$ are given by $\overrightarrow{GU_{t1}} = (r_p, 0, 0)^T$, $\overrightarrow{GU_{t2}} = (-\frac{1}{2}r_p, \frac{\sqrt{3}}{2}r_p, 0)^T$ and $\overrightarrow{GU_{t3}} = (-\frac{1}{2}r_p, -\frac{\sqrt{3}}{2}r_p, 0)^T$. The position vector of the top U joints with respect to the base co-ordinate system $\{B\}$ is given as

$$\begin{bmatrix} \overrightarrow{O_1U_{ti}} \\ 1 \end{bmatrix} = \begin{bmatrix} T \end{bmatrix} \begin{bmatrix} \overrightarrow{GU_{ti}} \\ 1 \end{bmatrix}$$

The leg lengths or the actuation needed can be found out as

$$l_i = ||\overrightarrow{O_1U_{bi}} - \overrightarrow{O_1U_{ti}}||$$

where $i = 1, 2, 3$ and $||A||$ represents the norm of the vector described by A and U_{ti} and U_{bi} (i = 1,2,3,) are the universal joints at the top and base respectively as given in figure 2.16.

2.4.4 Observations

A rotation about the heliostat normal, z_m, will not affect the orientation of the mirror. Hence, the axes x_m and y_m can be chosen arbitrarily and can have infinite possibilities theoretically. Two rotations are required to track the Sun, viz., the azimuth and the elevation. Let $(\hat{k},\ \theta_1)$ and $(\hat{p},\ \theta_2)$ be the axis-angle representation of the two rotations required where $\hat{k}$ and $\hat{p}$ are unit vectors. In Az-El case, $\hat{k}$ = [0 0 1] of the fixed coordinate system, $\hat{p}$ = [0 1 0] of the moving coordinate system on the mirror, $\theta_1 = \theta_{Az}$, and $\theta_2 = \theta_{El}$ and the rotation matrix becomes as given in equation (2.16)

In T-A method, $\hat{k}$ has the direction cosines of the reflected ray and $\hat{p}$ = [0 1 0] of the moving coordinate system on the mirror and the angles θ_1 and θ_2 can be found out as in equations (1.8) and (1.9). These are called the spinning and elevation angles respectively. To summarize, the first direction of rotation, $\hat{k}$, can be chosen arbitrarily and the second rotation axis will be the y_m axis and the required angles, θ_1 and θ_2 can be found out as follows.

At the start, the mirror and global co-ordinate systems are parallel to each other. Then choose $\hat{k}$ in some arbitrary direction. Rotate the heliostat in such a way that the z_m axis must coincide with the initial chosen direction $\hat{k}$. This rotation corresponds to the initial rotations required for the heliostat. Further rotate about $\hat{k}$ by an angle θ_1 such that the $\hat{k}$ (or z_m), $\overrightarrow{GN}$ and x_m are in the same plane. Then rotate about y_m by an angle θ_2 so that the z_m axis coincide with $\overrightarrow{GN}$.

Mathematically

$$\theta_1 = \arccos(\overrightarrow{GN}_{x_m y_m z_m} \ .\ x_m)$$
$$\theta_2 = \arccos(\overrightarrow{GN} \ .\ \overrightarrow{GR})$$

where $\overrightarrow{GN}$ and $\overrightarrow{GR}$ are the unit mirror normal the unit reflected ray, respectively and the projection of $\overrightarrow{GN}$ on the heliostat plane ($x_m - y_m$ plane) is given by $\overrightarrow{GN}_{x_m y_m z_m}$.

2.4.5 Simulation results for 3-UPU wrist

The parameters used for 3-UPU simulation are same as that of 3-RPS. The fixed point of the 3-UPU wrist is at a height of 2 m from the bottom platform. The plot of the image on the receiver plane for a 3-UPU wrist working in Az-EL and T-A methods are shown in figure 2.17 Figure 2.18 shows the simulation results for various time instants for March equinox

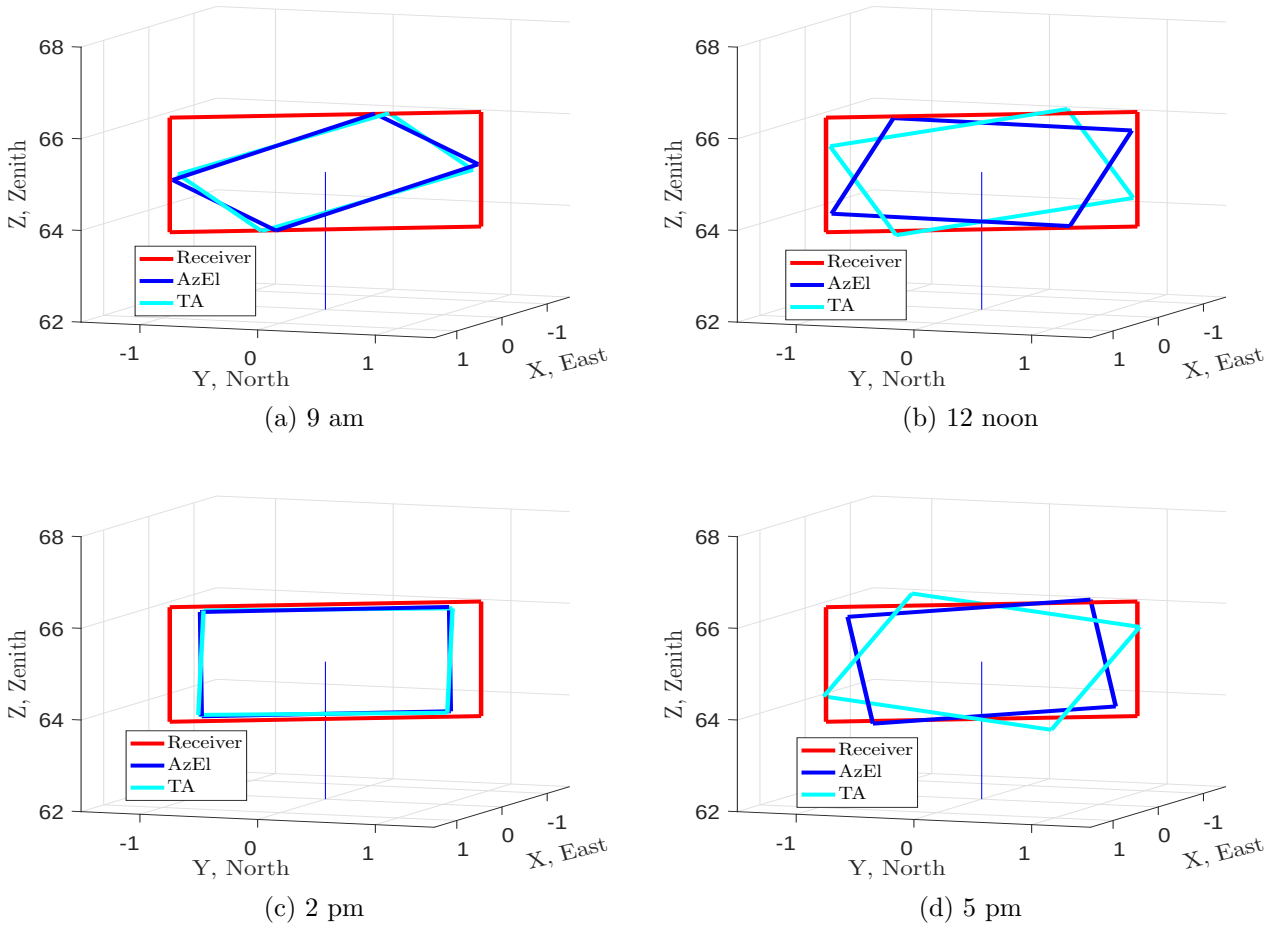

(a) 9 am (b) 12 noon

(c) 2 pm (d) 5 pm

Figure 2.17: The image on the receiver aperture at various time instants for March equinox for Bangalore

in Bangalore if the 3-UPU wrist is to be used in T-A method. It is clearly understood from figure 2.18d that the legs of the 3-UPU wrist intersect each other during the evening time. In order to prevent this, the rotation matrix obtained using T-A method can be multiplied by a rotation about the mirror normal so that the legs of the 3-UPU will not intersect. Figure 2.19 shows the modified simulation results when the T-A rotation matrix is multiplied by another rotation about mirror normal by 60°. The actuations required fpr T-A and modified T-A are

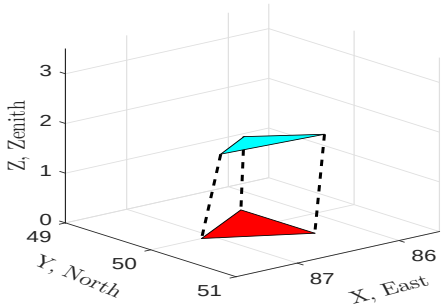

(a) 9 am

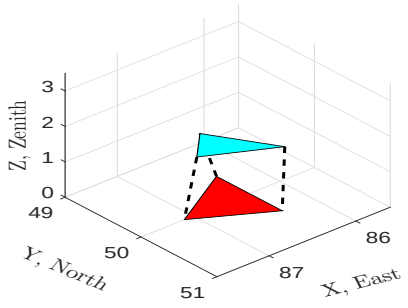

(b) 12 noon

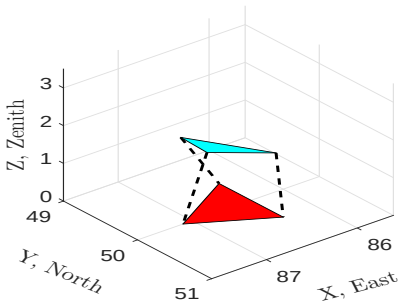

(c) 2 pm

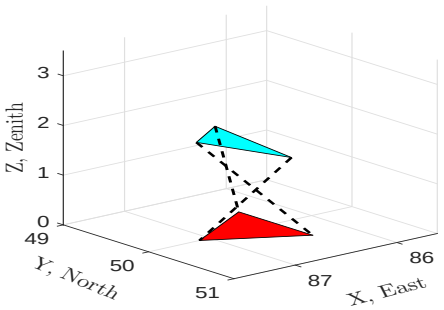

(d) 5 pm

Figure 2.18: Simulation of 3-UPU wrist for T-A mode for March equinox for Bangalore

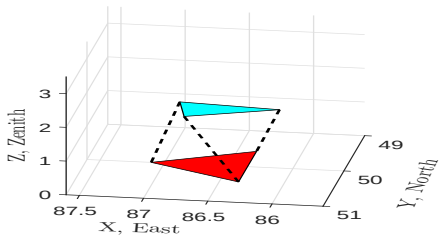

(a) 9 am

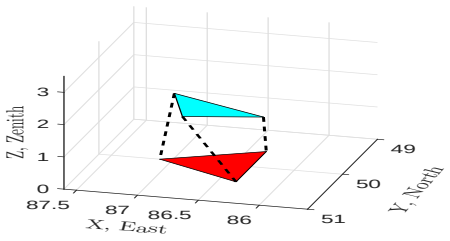

(b) 12 noon

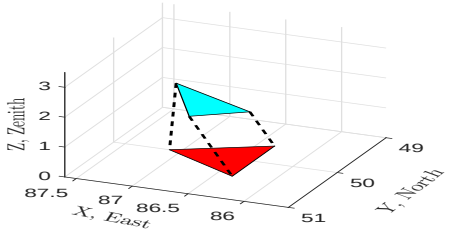

(c) 2 pm

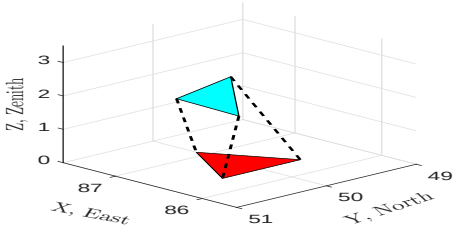

(d) 5 pm

Figure 2.19: Simulation of 3-UPU wrist for modified T-A mode for March equinox for Bangalore

given in figure 2.20. Similarly, figure 2.21 gives the simulation results obtained for modified Az-El method for summer solstice in Rajasthan. Here, the Az-El rotation matrix is multiplied with another rotation of 90° about the mirror normal to avoid intersection of the legs. Figure 2.22 gives the actuation required for the 3-UPU heliostat in Az-El method in normal operation and when modified. It is worth mentioning that for some other parameters like tower height of 20

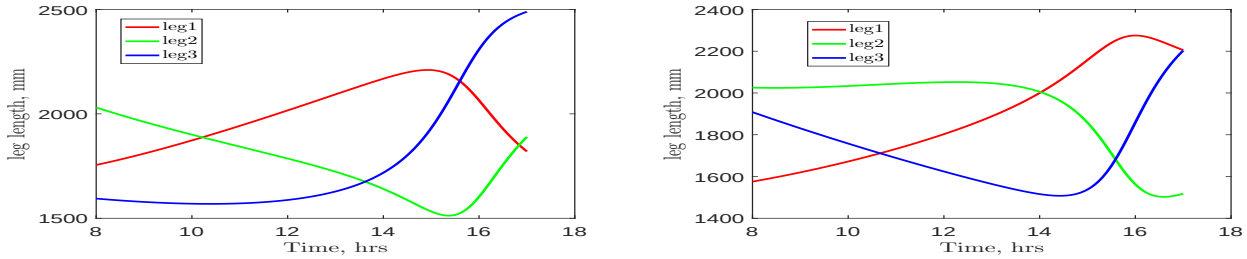

(a) T-A

(b) T-A modified

Figure 2.20: Actuations required for 3-UPU wrist for March equinox for Bangalore

(a) 9 am

(b) 12 noon

(c) 2 pm

(d) 5 pm

Figure 2.21: Simulation of 3-UPU wrist for modified Az-El mode for summer solstice for Rajasthan

m, radius of 30 m and a 30° angle from east axis, a switch from the T-A to Az-El method is totally possible without multiplying by a rotation matrix about the mirror normal.

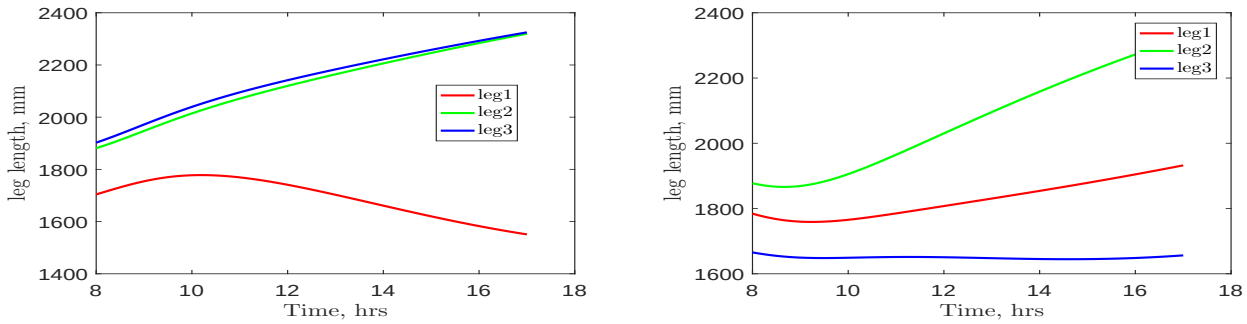

(a) Az-El (b) Az-El modified

Figure 2.22: Actuations required for 3-UPU wrist in Az-El mode for summer solstice for Rajasthan

2.5 Spillage loss for 3-RPS and 3-UPU wrist

Figure 2.23 shows the spillage loss for all the three different types of heliostat, viz., 3-UPU in Az-El and T-A and 3-RPS when kept at various angles in a 360° surround solar field in Bangalore. It has been found from the figure 2.23 that the spillage loss for 3-RPS heliostat is large for locations other than $\psi = 0$ and 180° when compared to the Az-El and T-A heliostats. The analysis assumes that the base and the global co-ordinate system are parallel to each other or the rotation matrix associated with it is identity. By changing the orientation of base with respect to global co-ordinate system (a rotation about Z axis by an angle γ as in figure 2.1), it is found that there is considerable amount of reduction in spillage loss as shown in figure 2.24. Hence, in order to reduce the spillage loss, the area under the curve in figure 2.24 has to be minimized. This area under the curve which has a dimension of m^2-hr is found out for various values of γ's and is shown in figure 2.25. It is clearly seen from figure 2.25 that the minimum occurs at four values of γ which are 90° apart. Simulations have also been carried out for various locations in the field and it has been found that the minimum spillage loss occurs at places corresponding to $\gamma = \psi,\ \psi + 90,\ \psi + 180,\ \psi + 270$. Figure 2.26 shows the spillage loss when $\gamma = \psi$ for the 3-RPS heliostat. An important point to note here is that if the initial guess to MATLAB's numerical solution routine *fsolve* changes, different results are obtained. It is clear from figure 2.27 that for this particular location (100 m and 30°) that $\gamma = \psi + 180$ gives the least actuation. It can be verified from other simulations that $\gamma = \psi$ or $\gamma = \psi + 180$ always minimize the stroke.

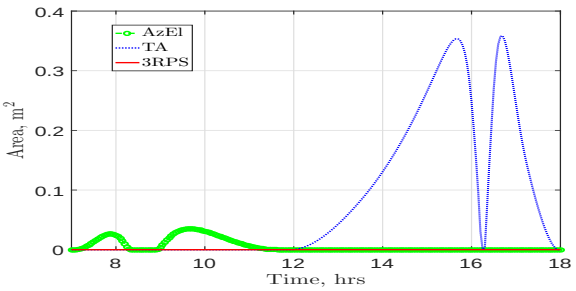

(a) $\psi = 0°$

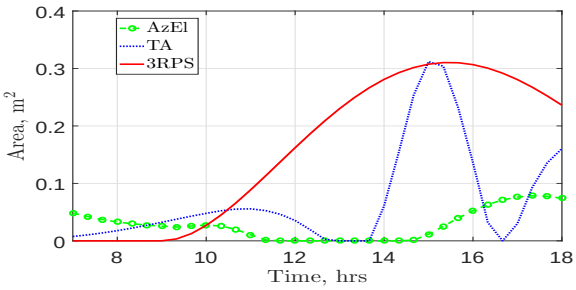

(b) $\psi = 45°$

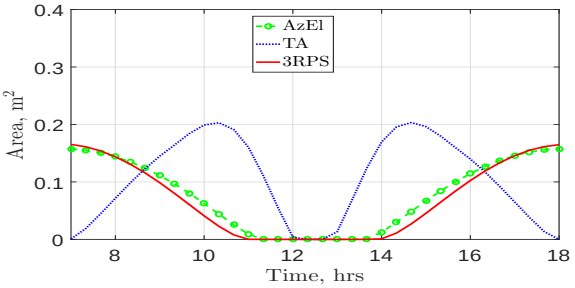

(c) $\psi = 90°$

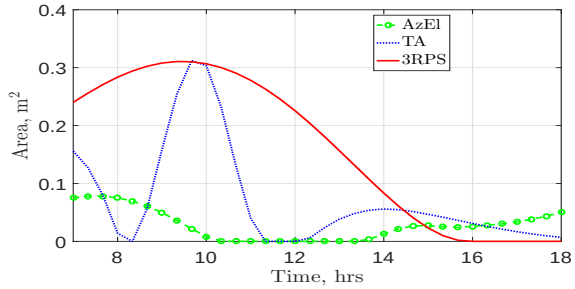

(d) $\psi = 135°$

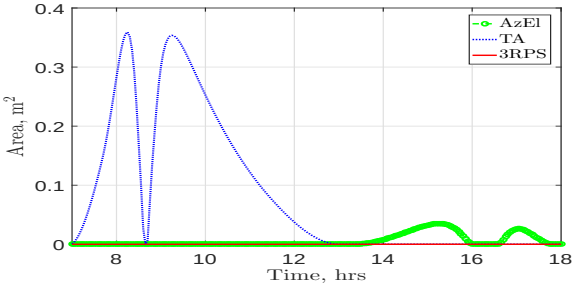

(e) $\psi = 180°$

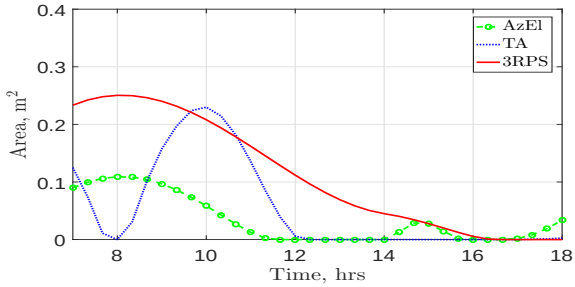

(f) $\psi = 225°$

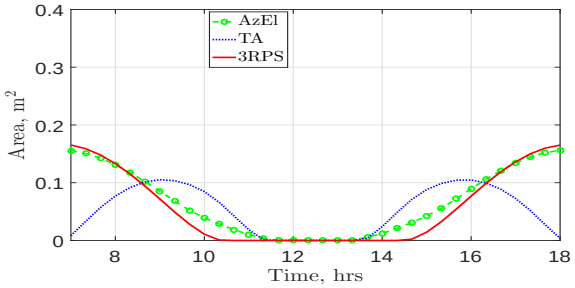

(g) $\psi = 270°$

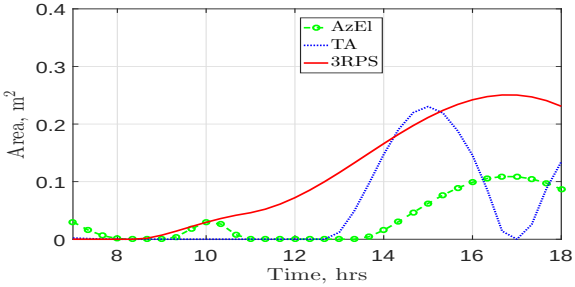

(h) $\psi = 315°$

Figure 2.23: Comparison of Az-El, T-A and 3-RPS wrt. spillage loss, March equinox, Bangalore

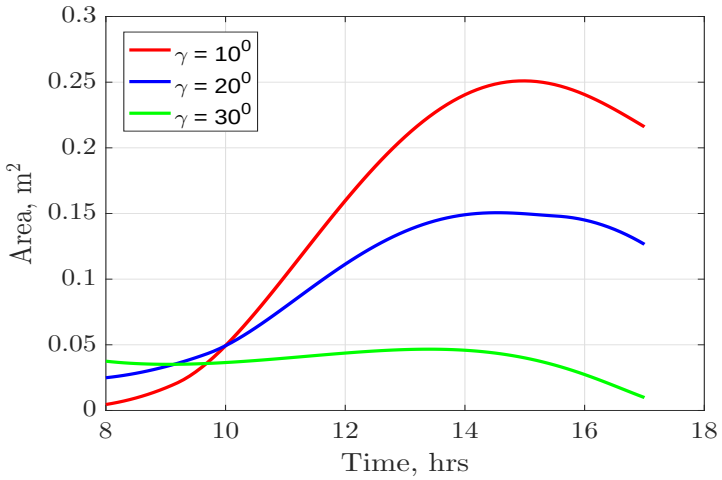

Figure 2.24: Variation of spillage loss with γ for 3-RPS for March equinox, Bangalore

2.6 Conclusions and challenges ahead

In this chapter, we have proposed two parallel manipulators which can be used for tracking the Sun. Both these have three degrees of freedom and thus require three actuators. The kinematics of the 3-RPS and the 3-UPU parallel manipulator, for Sun tracking, are developed. From the solution of the kinematics equations, the change in the lengths of the prismatic joint required to track the Sun are determined. Simulation results show that the legs of the 3-UPU wrist might intersect whereas this does not happen for 3-RPS. For 3-UPU wrist, extensive simulations are needed for locations other than Bangalore and Rajasthan to know by what amount the top-platform has to be rotated to prevent intersection of legs. For 3-RPS heliostat, the spillage loss and actuation is minimized by keeping the orientation of base platform $\gamma = \psi$ or $\gamma = \psi + 180°$.

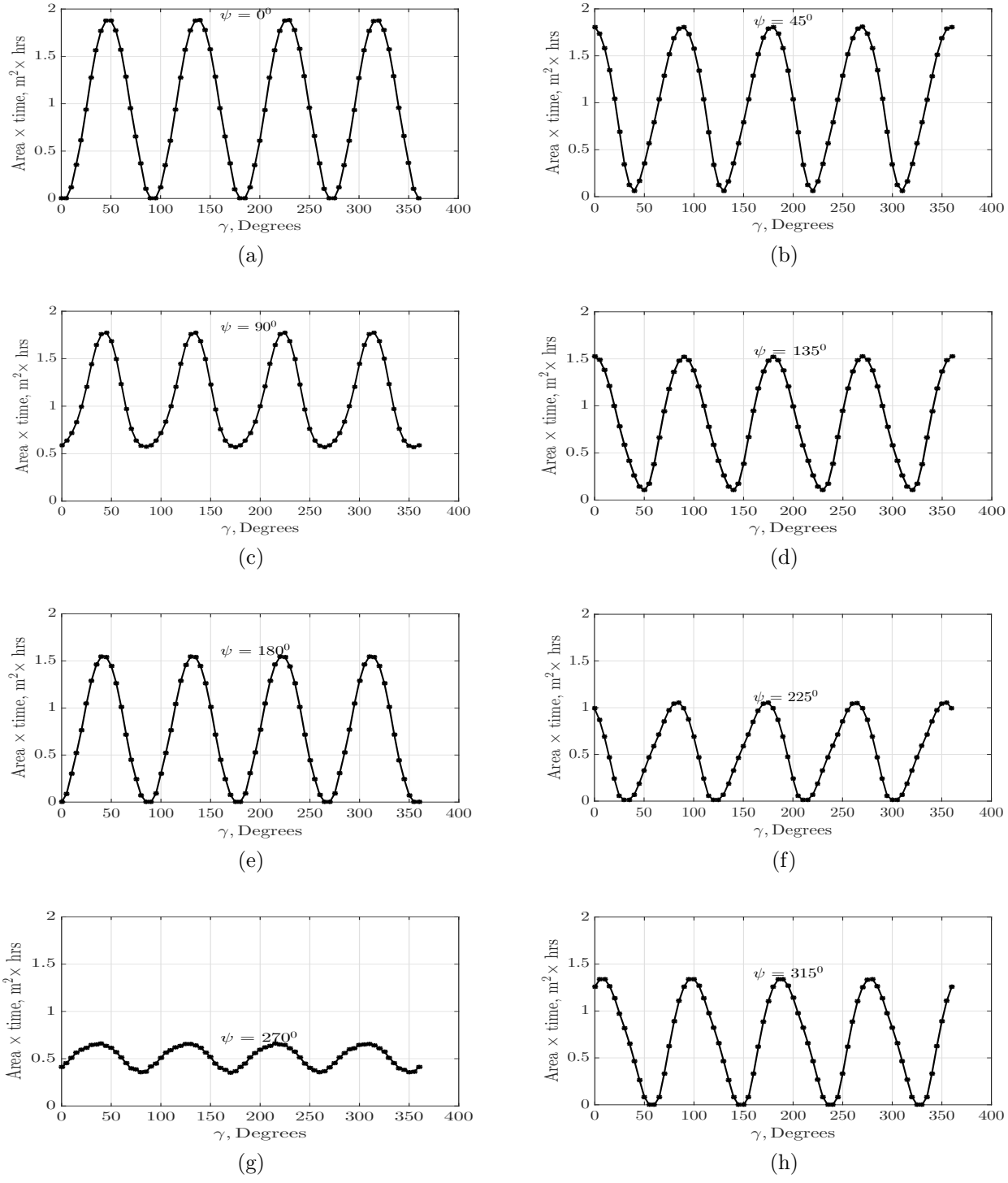

Figure 2.25: Variation of area-time with γ for March equinox, Bangalore

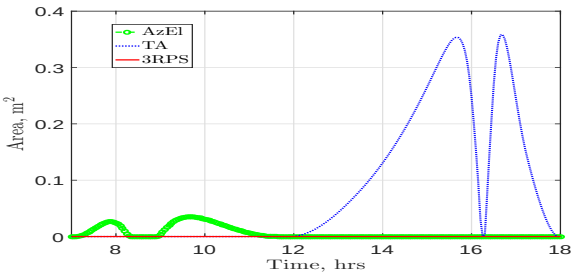

(a) $\psi = 0°$

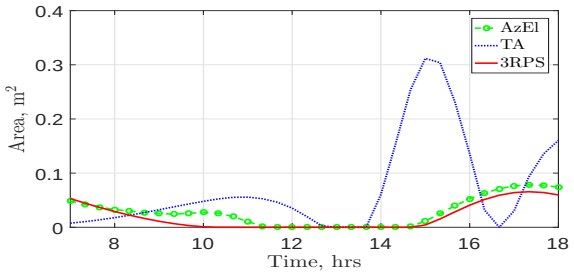

(b) $\psi = 45°$

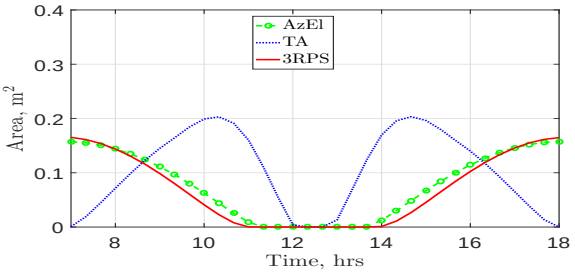

(c) $\psi = 90°$

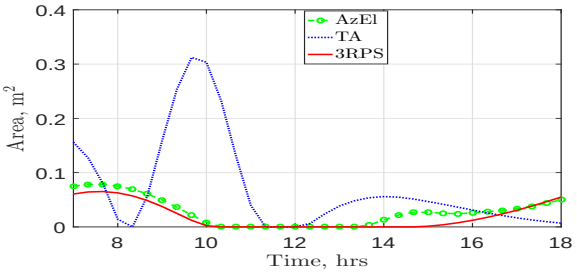

(d) $\psi = 135°$

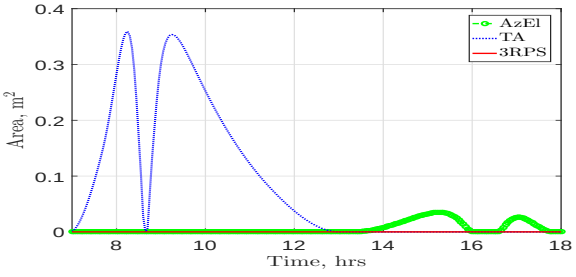

(e) $\psi = 180°$

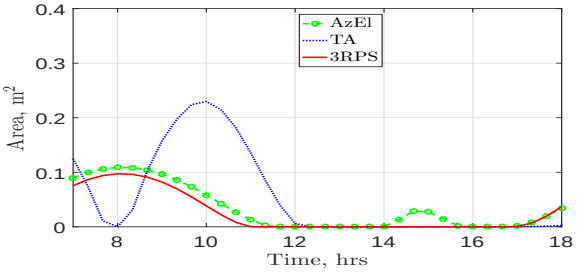

(f) $\psi = 225°$

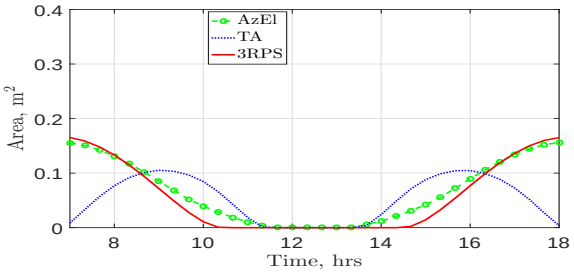

(g) $\psi = 270°$

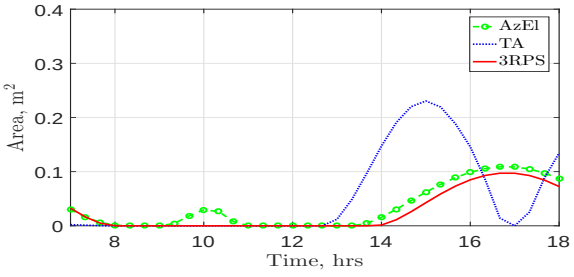

(h) $\psi = 315°$

Figure 2.26: Comparison of Az-El, T-A and 3-RPS wrt. spillage loss, $\gamma = \psi$ March equinox, Bangalore

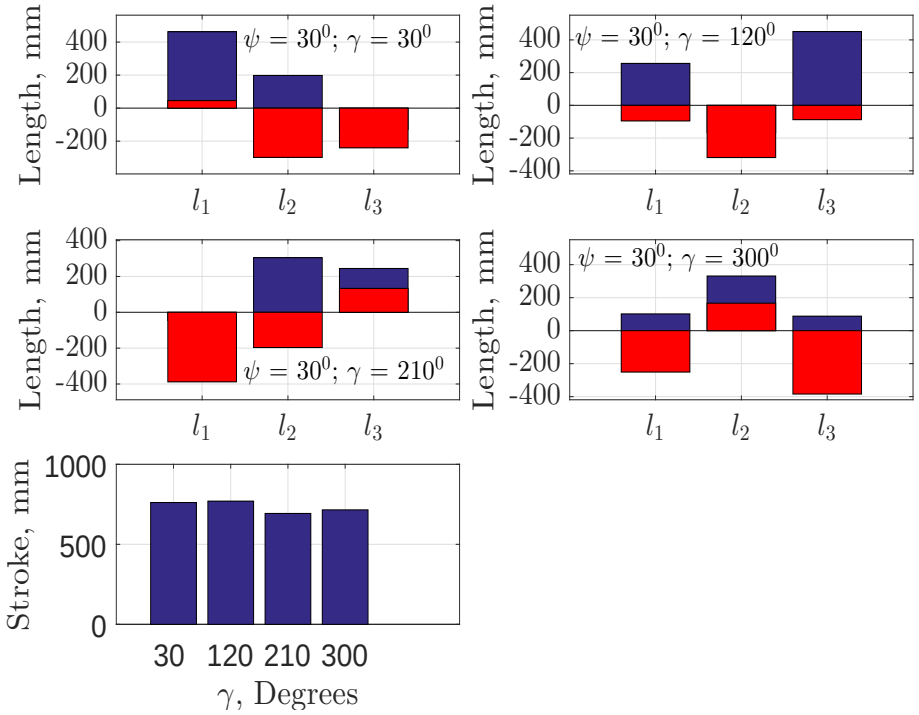

Figure 2.27: Variation of stroke with γ for March equinox, Bangalore

Chapter 3

Structural design of a 3-RPS heliostat

3.1 Introduction

In chapter 2, simulations for the 3-RPS and 3-UPU wrist manipulators for Sun tracking in central receiver systems were carried out. It was observed that the 3-UPU wrist requires precision manufacturing to get a fixed point for using it as a heliostat in CR systems. Additionally, for certain times, the kinematics resulted in the intersection of the legs. Due to these disadvantages, the 3-RPS parallel manipulator configuration was chosen for further study with a goal to design 3-RPS based heliostat for central receiver systems. In any heliostat, the design for wind loading is an important aspect as the heliostat deformation should not lead to loss in pointing accuracy and during high winds, although the heliostat would not be in use, it should not fail. This chapter mainly deals with the design of support structure against wind and gravity loading. As mentioned in previous chapter, in the 3-RPS configuration, the actuators are connected to the top and bottom platform at three points. This inherently reduces the load acting on each leg as it is shared by the three legs. Nevertheless some structural support material is required such that there is enough stiffness to withstand the wind loading and the pointing errors at the ends are limited to 2 or 3 mrad. Various frame designs were considered for single point support (Az-El and T-A) and the 3-RPS heliostats. It is shown in this chapter that for large mirrors, there is significant amount of weight reduction for the 3-RPS support structure compared to the single point supports in traditional Az-El and T-A mounts for the same required pointing accuracy. As shown in the previous chapter, a 3-RPS design has several variables such as the top platform and bottom platform circum-radii and an angle locating the first mount point. In this chapter, we perform a search based optimization to obtain optimized values of the 3-RPS design variables. We obtain designs which give the least weight of the support structure for a pre-defined wind and gravity loading and which results in least stroke in the prismatic join

actuators.

This chapter is organized as follows: In section 3.2, the various support frame considered for the design of the support structure are discussed. Section 3.3 presents the details of the finite element analysis done to find the support structure with least weight. A comparative study of 3-RPS and Az-El heliostats in terms of frame weight, deflection and stress is also shown in this section. The design variables which help in stroke minimization are found out using an iterative approach and is also presented in this section. Section 3.5 summarizes the findings described in this chapter.

3.2 Support frame topologies

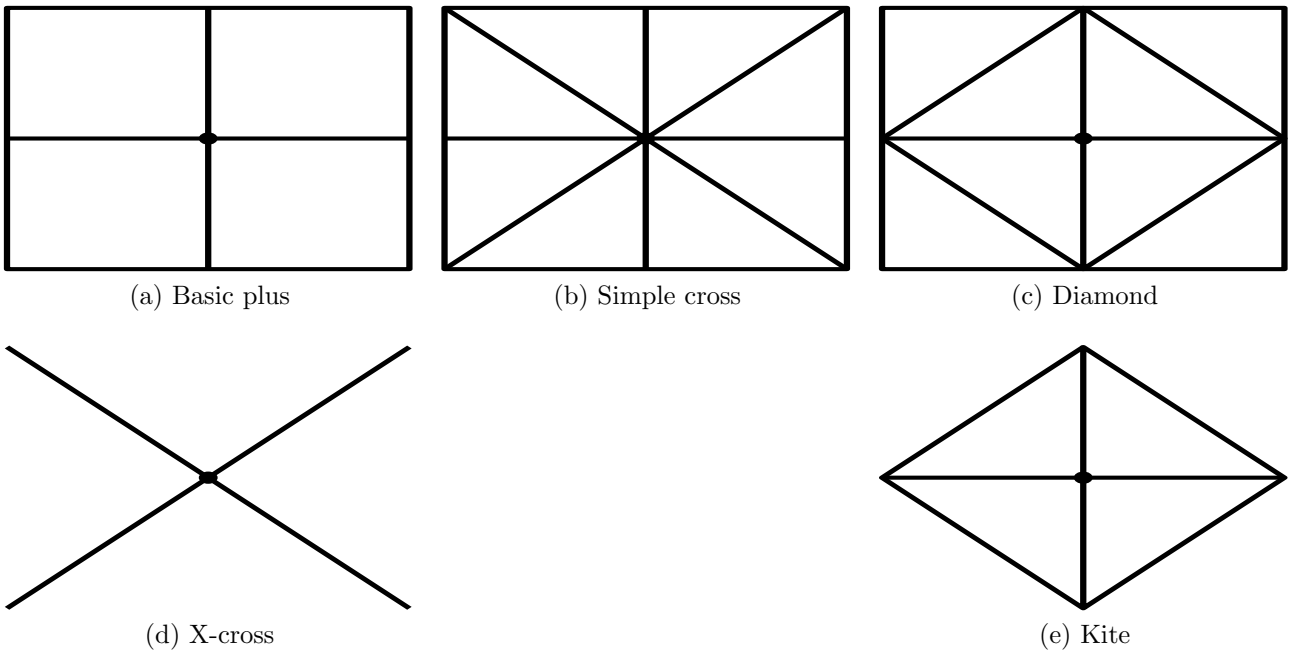

(a) Basic plus (b) Simple cross (c) Diamond

(d) X-cross (e) Kite

Figure 3.1: Various types of frame topologies considered for single point support

The various support frame topologies considered for single point support and the 3-RPS heliostats are shown in figures 3.1 and 3.2. The aim is to obtain the lightest possible support structure which satisfies the maximum pointing error due to wind loading of 2 mrad. A reduction in the amount of supporting structure material will lead to a reduction in the material cost and total cost of the heliostat. It maybe be noted that the dimensions of the support frame depends on the size of the mirror to be used and in this chapter we perform studies with mirrors with three different sizes. We use finite analysis using a commercial software tool to perform the study. This is described next.

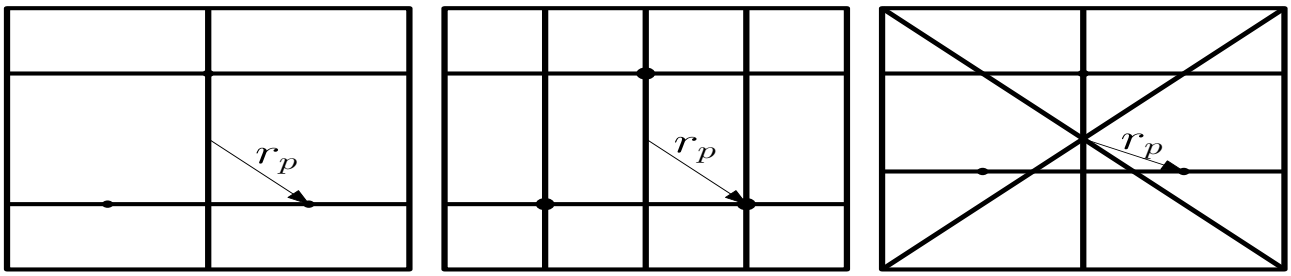

(a) (b) (c)

Figure 3.2: Various types of frame topologies considered for 3RPS heliostat

3.3 Finite element modeling of mirror and support structure

The finite element analysis of the mirror and support structure is carried out in ANSYS® Workbench [83]. The element types used are *SOLID186* and *SOLID187* with three degrees-of-freedom per node. Program controlled automatic meshing is enabled for the analysis. The mesh size is refined in each iteration until convergence is achieved.

The deformation of the mirror and support structure is found out for its self-weight and for a survival wind speed, v of 22 m/s and an operational wind speed, v of 10 m/s. It has to be noted that the wind speeds (both survival and operational) depend upon the geographic location and may not be the same value for all places. The guidelines for wind load calculation are given in [84, 85]. The structure is kept vertically and the wind pressure is assumed to be acting normal to the surface so that the worst case scenario can be simulated. The factor of safety (FoS) used for the analysis is 2.0. The uniform wind load P on the surface of the mirror is calculated by using the equation

$$P = \frac{1}{2} C_d \rho v^2 FoS$$

where $C_d = 1.18$ [86] is the drag coefficient and ρ is the density of air assumed to be 1.25 kg/m^3 (see figure 3.3). The mirror is assumed to be made of float glass weighing 10 kg/m^2 and the material chosen for support structure is plain carbon steel with density, $\rho = 7800$ kg/m^3. The CAD model of the support structure and the mirror is made in SolidWorks® [87] by parametric modeling technique which allows one to make changes in the model parameters such as length, width, height, radius of curves etc. fairly easily. Then the two are *mated* to obtain a single object and then ported to ANSYS® Workbench for finite element analysis.

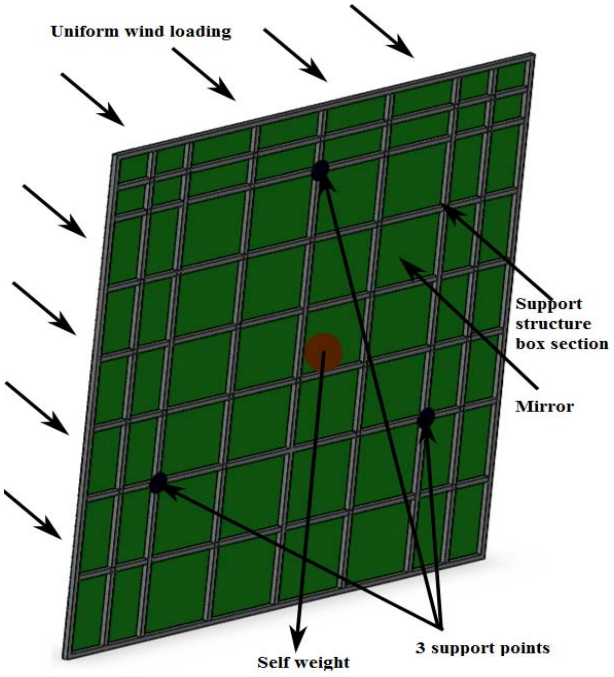

Figure 3.3: Uniform wind load acting on a 5 m x 5 m mirror

The stresses and deformation due to the wind and self-weight loading are computed by doing FEA. The parametric modeling technique also helps to identify the lightest possible support structure which could withstand the 2 mrad maximum deflection criteria. Three mirror sizes, viz., 2 m $\times$ 2 m, 3 m $\times$ 3 m and 5 m $\times$ 5 m are considered for the study to determine the support structure with least weight for each of the mirror dimensions. The goal is to obtain the lightest possible support structure, reduce stroke, satisfy the maximum deformation requirements and thus reduce material cost of the heliostat.

3.3.1 Search for r_p

With reference to the figure 2.1, the connection points at the top platform defined by the length r_p from the centre, G, has got two significant functions. As the distance of the connection points from the centre increases, the stroke required to get the same orientation also increases. The other significance is that a large value for r_p, tends to increase the deformation of the mirror at the centre due to wind and gravity loading whereas a small value corresponds to large deformation at the edges. Of the above two, the most critical criteria is on the deformation which is to be within a error limit of 2 - 3 mrad. Hence a finite element analysis is carried out to find out the deflections by varying r_p iteratively. For 2 m $\times$ 2 m, 3 m $\times$ 3 m and 5 m $\times$ 5 m mirror, the value of r_p thus obtained are 500, 900 and 1800 mm respectively. Table 3.1

shows the maximum deformation and the weight of the support structure required in each of the three mirror sizes for 3-RPS and Az-El heliostats for two different wind speed of 10 m/s and 22 m/s.

Table 3.1: Comparision of weight and deflection for Az-El and 3-RPS

Wind speed (m/s)	**Frame (m x m)**	**Az-El**			**3-RPS**		
		Max. deformation (mm)	**Stress (Pa)**	**Frame weight (kg)**	**Max. deformation (mm)**	**Stress (Pa)**	**Frame weight (kg)**
10	2 x 2	1.88	3.60E+07	20.94	1.93	4.15E+07	15
	3 x 3	2.64	3.98E+07	53.53	2.45	2.59E+07	45
	5 x 5	4.73	2.96E+07	356.97	4.90	2.88E+07	198
22	2 x 2	1.88	4.68E+07	41	1.82	5.72E+07	30
	3 x 3	2.87	4.36E+07	181.17	2.66	5.51E+07	93
	5 x 5	4.72	2.56E+07	1332.54	4.92	5.11E+07	535

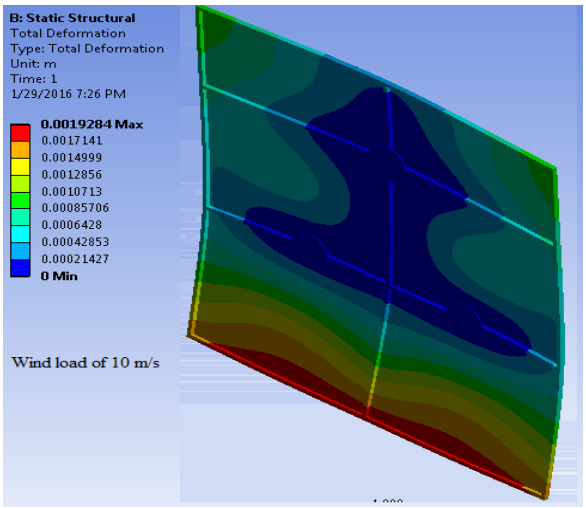

(a) Wind load of 10 m/s

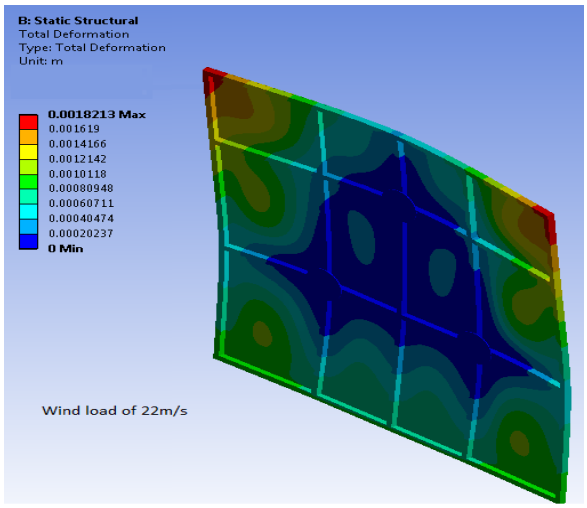

(b) Wind load of 22 m/s

Figure 3.4: Deflection of 2 m × 2 m mirror and support frame assembly for 3RPS

The corresponding deflections of the 2 m × 2 m are shown in figure 3.4. It can be seen from figure 3.5 that the two extra vertical supports on the support frame are needed to satisfy the 2 mrad deflection criteria when the wind load is 22 m/s. Figure 3.6 gives the deflection of a 2 m × 2 m mirror for Az-EL case. The FEA of the other two mirror sizes, viz., 3 m × 3 m and 5 m × 5 m for 3-RPS heliostat are shown in figure 3.7.

The details of the sections used for the finite element analysis are as follows:

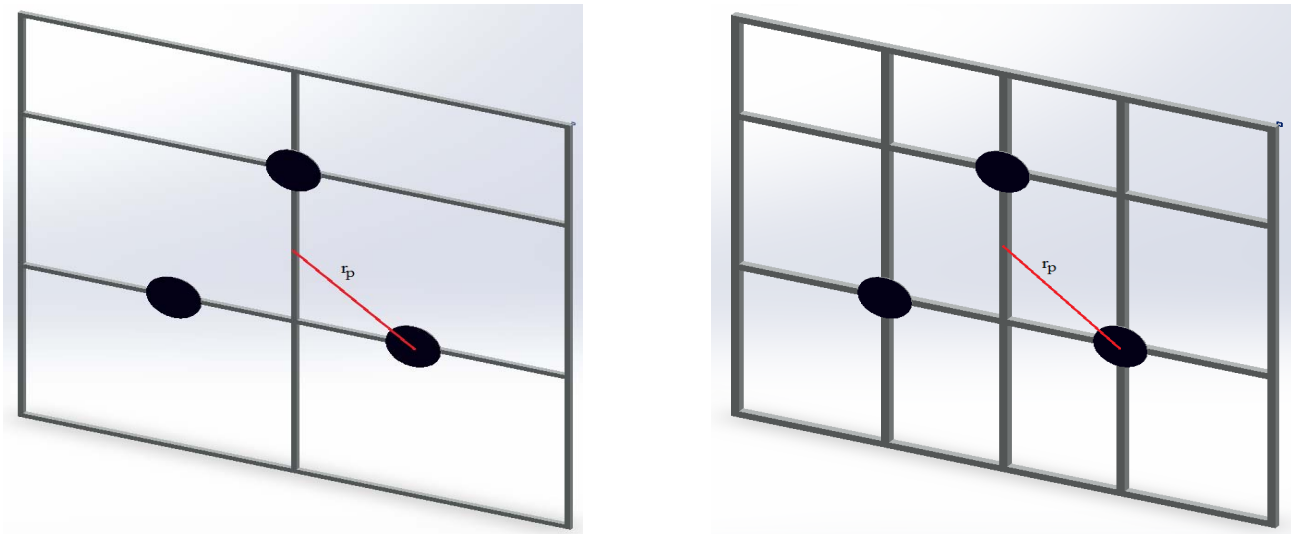

(a) Wind load of 10 m/s (b) Wind load of 22 m/s

Figure 3.5: Support frame of a 2 m × 2 m mirror for 3-RPS

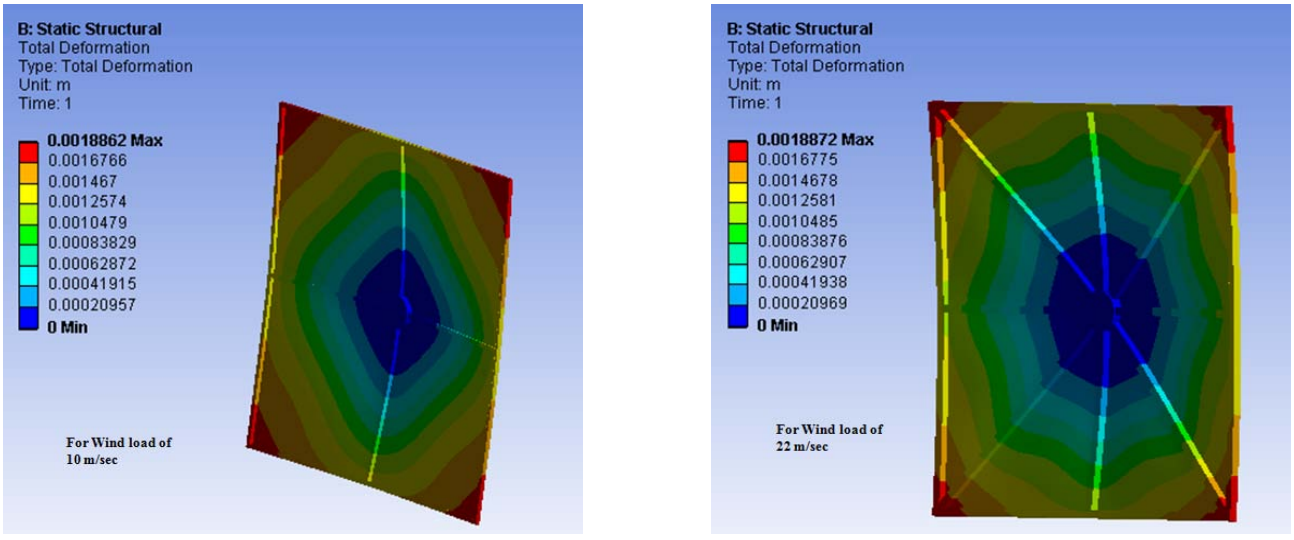

(a) Wind load of 10 m/s (b) Wind load of 22 m/s

Figure 3.6: Deflections of the 2 m × 2 m mirror for Az-El heliostat

1. Wind speed of 22 m/s

   - For 2 m × 2 m the results are for square box section of size 30 mm and wall thickness of 2 mm.
   - For 3 m × 3 m the results are for square box section of size 50 mm and wall thickness of 2 mm.

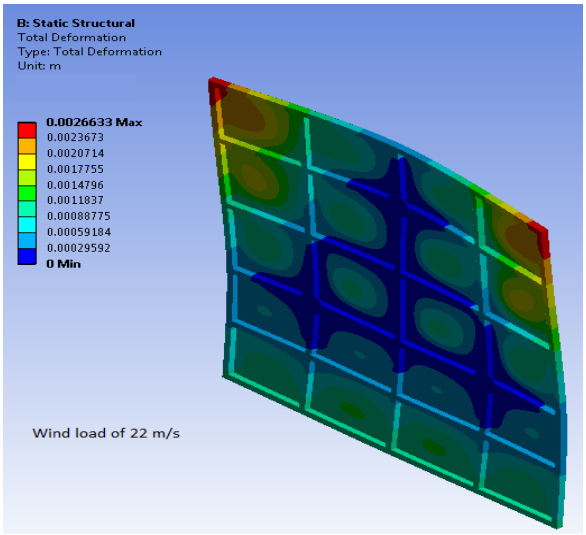

(a) 3 m × 3 m

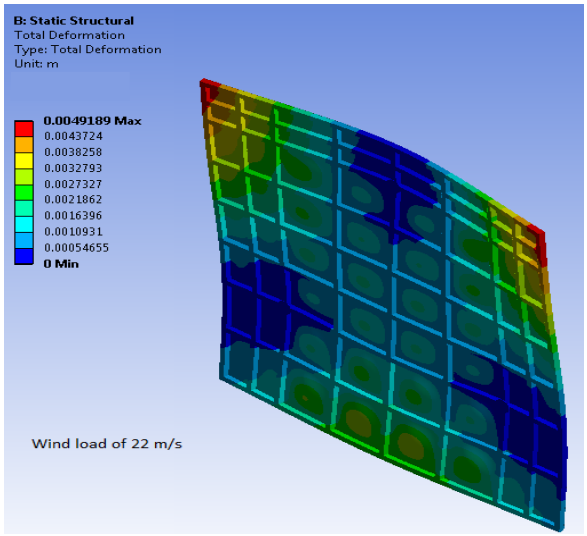

(b) 5 m× 5 m

Figure 3.7: Deflections of the 3 m × 3 m and 5 m × 5 m mirror for a wind load of 22 m/s

- For 5 m × 5 m the results are for square box section of size 70 mm and wall thickness of 3 mm.

2. Wind speed of 10 m/s

- For 2 m × 2 m the results are for square box section of size 20 mm and wall thickness of 2 mm.
- For 3 m × 3 m the results are for square box section of size 30 mm and wall thickness of 2 mm.
- For 5 m × 5 m the results are for square box section of size 50 mm and wall thickness of 2.5 mm.

The breaking stresses for solar grade mirrors (tempered glass) is very high in the order of 10^8 Pa. A stress analysis for a mirror size of 2 m × 2 m is carried out to ensure that the stresses induced are not going beyond the allowable limits. It is clear from figure 3.8 that the stresses induced by wind and gravity loading is way below the breaking stress for both Az-El and 3-RPS heliostats.

3.3.2 Search for r_b

The heliostats are assumed to be placed in a circular field with the nearest being 50 m away and the farthest 300 m in steps of 5 m. The angle ψ varies from 0 to 350° in steps of 10°.

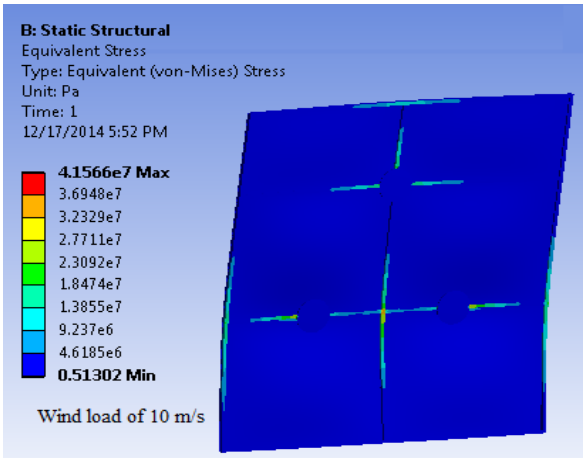

(a) 10 m/s 3-RPS

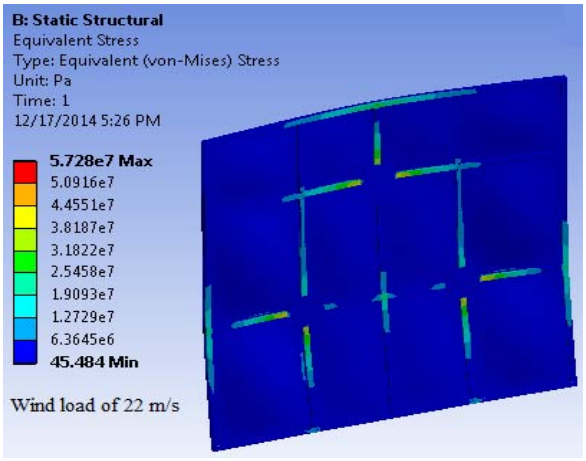

(b) 22 m/s 3-RPS

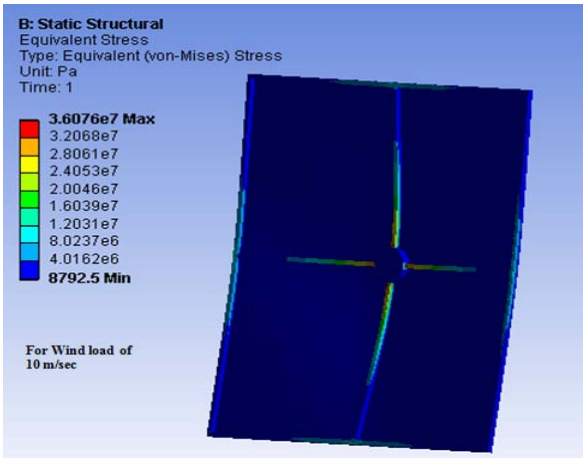

(c) 10 m/s Az-El

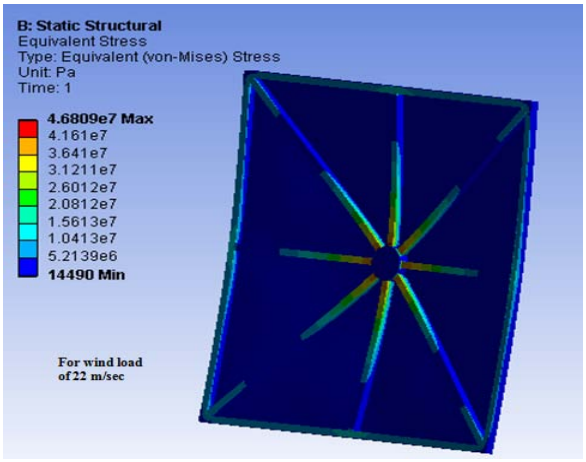

(d) 22 m/s Az-El

Figure 3.8: Stresses induced on a 2 m × 2 m

To make the analysis computationally inexpensive, only four days (the solstices and equinoxes) are considered. Depending upon the direction of incoming Sun rays, the actuation required are more for the heliostats which are nearest and farthest from the receiver tower compared to the heliostats in between. Hence the analysis is done only for an array of heliostats at radii of 50 m and 300 m. Initially, the heliostat is parallel with the ground plane and is considered to be the zero actuation position. Actuations above and below zero are considered positive and negative respectively. For any other orientation, the point on the ground where the perpendicular dropped from the connection point meets, gives the position of r_b for least actuation required. Since the heliostat is required to have several orientations to track the Sun, r_b changes with time. It is also found that for each ψ, the value of r_b which minimizes the stroke

is not a constant value. Since it is practically impossible to make different types of heliostats at different locations, the mean value of r_b is chosen as the optimal value. Thus the optimal value of r_b is found to be 487 mm, 877 mm and 1755 for a 2 m x 2 m, 3 m x 3 m and 5 m x 5 m mirror size respectively. The r_p and r_b thus obtained ensure that the stroke does not go beyond 700 mm.

3.4 Static and modal analysis of the 3-RPS heliostat

The static performance of the heliostat is dependent on the orientation of the mirror as mentioned by Zang et al. [88]. When the wind velocity is 22 m/s (survival speed), the heliostat is brought to the stow position to prevent any damage to the structure. Hence the static analysis for various mirror orientations are done for the operational wind speed of 10 m/s acting normal to the mirror plane. This will simulate the worst possible scenario. Thus the reaction forces and moments acting at the base of the leg can be determined. The co-ordinate system chosen for representing the reaction forces has origin at the base of the leg with X axis being the axis of rotation of the revolute joint and Z being the axis of the prismatic joint as shown in figure 3.9. The base co-ordinate system, as mentioned before, has its X axis towards local east and Z axis towards zenith.. Hence the transformations required to find the values of reactions forces and moments can easily be found out. Table 3.2 gives the reaction forces for a 2 m x 2 m 3-RPS heliostat at three different orientations, viz., 15°, 30° and 60° elevation. The corresponding reaction moments are shown in table 3.3. Representative results for other mirror dimension of 3 m x 3 m and 5 m x 5 m for 15° elevation are shown in tables 3.4 and 3.5.

Table 3.2: Reaction forces for a 2 m x 2 m heliostat for various orientations (in Newtons)

	leg_1				leg_2				leg_3			
	Fx	Fy	Fz	F	Fx	Fy	Fz	F	Fx	Fy	Fz	F
15^0	-6648.7	-0.93	-521.5	6669.1	82.8	-202.7	-165.9	274.7	-38.7	-310.	135.6	340.6
30^0	-9399.8	12.0	-1022.3	9455.2	75.2	-393	-274.6	485.2	-128.2	-538	34.5	554.1
60^0	-12054	29.9	2346	12281	52.1	-331.9	-233.3	409	-115.2	-831.1	216.6	866.5

Table 3.3: Reaction moments for a 2 m x 2 m heliostat for various orientations (in N-m)

	leg_1				leg_2				leg_3			
	Mx	My	Mz	M	Mx	My	Mz	M	Mx	My	Mz	M
15^0	-21.8	-60.1	-14.3	65.5	17.4	-0.006	-3.4	17.7	18	23.9	0.3	29.9
30^0	-40.5	-64.4	-26.2	80.4	30.9	-1.5	-6.9	31.7	30.9	46.7	0.4	56.1
60^0	-48.7	-49	29.1	74.9	27.4	-1.6	-5.3	27.9	50.2	67.3	-2.9	83.9

The modal analysis is done for the 3-RPS heliostat to find the natural frequencies and to obtain the effect of wind load on the heliostat. The vibration of the heliostat adversely affect

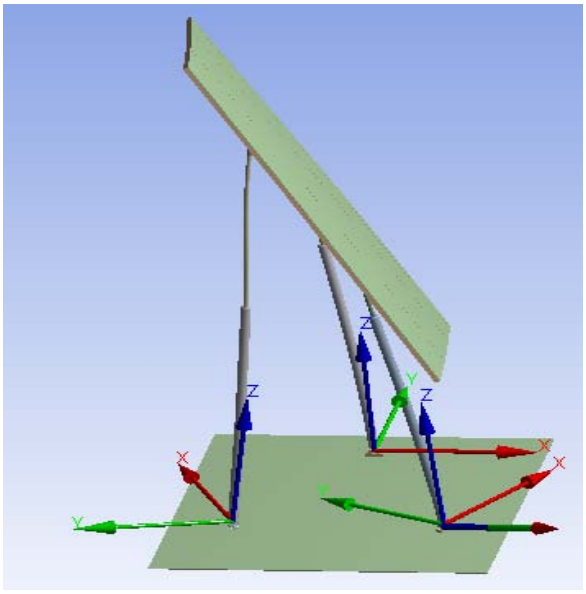

(a) 2 m x 2 m at 60^0

Figure 3.9: Co-ordinate system for reaction forces and moments

Table 3.4: Reaction forces for 3 m x 3 m and 5 m x 5 m heliostats (in N)

	leg_1				leg_2				leg_3			
	Fx	Fy	Fz	F	Fx	Fy	Fz	F	Fx	Fy	Fz	F
3 m x 3 m	-9799.6	-184.9	-1360	9895.3	345.9	-457.9	-3710.5	3754.7	1080.9	-1125	-183.9	1570.9
5 m x 5 m	10956	-150.7	3079.3	11382	887.	1830.1	-7475.6	7747.3	260.7	65.6	1917.8	1936.6

Table 3.5: Reaction moments for 3 m x 3 m and 5 m x 5 m heliostats (in N-m)

	leg_1				leg_2				leg_3			
	Mx	My	Mz	M	Mx	My	Mz	M	Mx	My	Mz	M
3 m x 3 m	67.872	-73.788	-6.2674	100.45	29.425	12.197	-9.1187	33.133	68.93	0.90115	-5.0673	69.122
5 m x 5 m	153.85	84.283	12.53	175.87	-146.2	34.172	26.494	152.46	6.3548	-167.34	6.153	167.57

the tracking accuracy. The plot of the natural modes of the three types of heliostats, viz., the 2 m x 2 m, 3 m x 3 m and 5 m x 5 m considered here are shown in figure 3.10. It is also observed during the analysis that there was very little, of the order of 10^{-2}, effect of the elevation angle on the natural frequencies.

3.5 Conclusion

This chapter dealt with the structural design of the 3-RPS heliostat against wind and gravity loading. Various frame topologies are analyzed and the lightest possible structure satisfying the

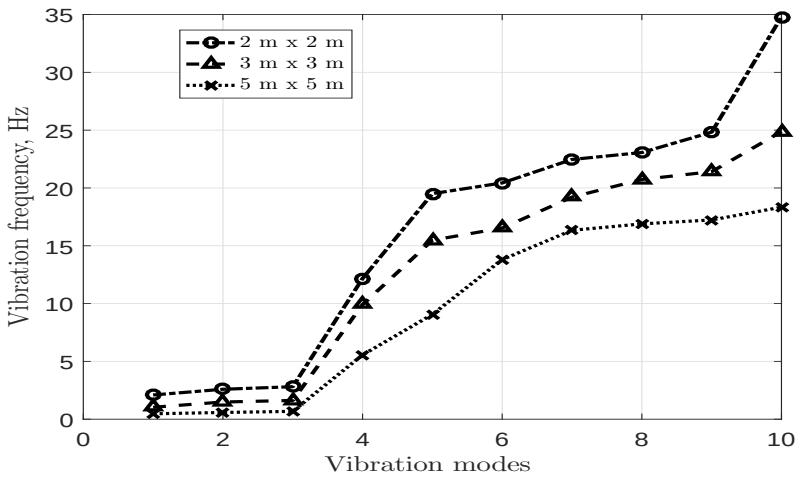

Figure 3.10: Vibration modes of the 3-RPS heliostat

deflection criteria of 2 mrad is found out. The weight reduction of the support structure for 2 m $\times$ 2 m, 3 m $\times$ 3 m and 5 m $\times$ 5 m mirror for 3-RPS heliostat are found to be 15.93 %, 48.66 % and 59.85 % respectively compared to the Az-El heliostat. Using finite element analysis and simulations done in MATLAB, the optimum value of r_p which satisfies the 2 mrad deflection criteria is calculated for various mirror dimensions. An iterative search is carried out to find the optimum value of r_b which would minimize the stroke required for the actuators. These combinations will ensure a stroke less than 700 mm when the farthest heliostat is at 300 m from the tower for Bangalore and thus help in reducing the overall cost of the system. Finally, static and modal analysis of the 3-RPS heliostat to obtain the reaction forces and moments and natural frequencies have been carried out. This would help in sizing of the actuators required for manufacturing a prototype.

Chapter 4

Fabrication and experiments with a 3-RPS heliostat

4.1 Introduction

In chapter 2, the algorithm for tracking the sun using 3-RPS heliostat was developed. Chapter 3 gives a detailed description of the structural design of heliostat for wind and gravity loading using FEA and also compares the weight reduction achieved if 3-RPS is chosen over Az-El. In this chapter we present the design and fabrication details of a 3-RPS heliostat. Experiments with the 3-RPS heliostat and the results obtained are presented. It is shown that the 3-RPS heliostat tracks the sun and can focus the incident solar radiation on to a flat wall thereby making it suitable for use in central receiver type of solar power plants. A traditional Azimuth-Elevation (Az-EL) configuration heliostat was also fabricated and it is shown that the results obtained from the 3-RPS heliostat are comparable to those obtained from the Az-El heliostat.

This chapter is organized as follows. In section 4.2, the details regarding the manufacturing of prototype 3-RPS heliostat is given. Section 4.3 gives the description of the motor driver circuit made with the help of a ATMEGA2560 micro-controller. The controller is configured for analog and digital outputs, acquiring encoder readings and sending the output to an amplifier through an opto-isolator. It also describes in detail the control strategy adopted using MATLAB-Simulink. The algorithm developed in chapter 2 to track the Sun is verified in section 4.4. The details regarding the actual Sun tracking done on the roof of ICER building in IISc., Bangalore is described in section 4.5. Section 4.6 quantifies the tracking errors observed during Sun tracking and Section 4.7 presents some of the key observations made during the study. Finally the conclusions of this chapter and scope for improvement are presented in section 4.8.

4.2 Prototype design

The prototype of the 3-RPS parallel manipulator which was fabricated is shown in figure 4.1. In chapters 2 and 3, all the analysis were done for mirror dimensions of 2 m x 2 m, 3 m x 3 m

Figure 4.1: Prototype of 3-RPS heliostat

and 5 m x 5 m but later it was found that the it would be difficult to prototype even a 2 m x 2 m due to cost, handling and space considerations. Hence, a 3-RPS heliostat with mirror dimension of 1 m x 1 m is chosen for prototyping. The mirror is enclosed in an aluminium frame at its edges having rubber beadings separating the frame and the mirror. This ensures a tight fit between the two and also avoids any scratches on the mirror. The aluminium frame is rigidly attached to the support structure using L angles. The techniques described in chapter

3 is used to find the circum-radii of the top (r_p) and bottom (r_b) platforms and are found to be 250 mm and 277 mm respectively. The base plate is made of a mild steel plate with dimensions of 1 m x 1 m x 5 mm. The bottom plate was intentionally made heavy to prevent the heliostat from toppling over in presence of gusty winds – in a real power plant the revolute joints can be fixed to the ground with concrete and no metal base plate is required. Supports are also provided at the edges for ease of handling. The support frame is made of mild steel and is shown in figure 4.2. The cross-section of the support frame has a dimensions of 20 mm x 20

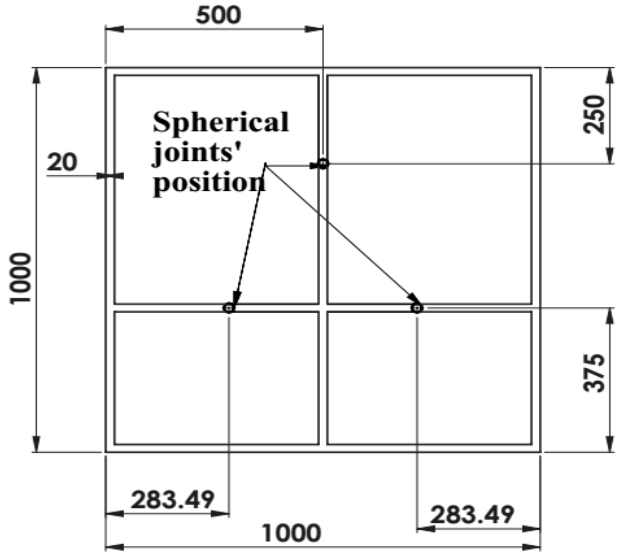

Figure 4.2: Support frame for the mirror for 2 mrad deflection

mm x 2 mm which is obtained from the finite element analysis mentioned in section 3.3. It is made such that the deflection should not exceed 2 mrad at the edges. The three different types of joints, viz., the revolute, prismatic and the spherical joints are shown in figure 4.3. The actuator consists of a DC motor, connected to a gear box and lead screw and when the motor is rotated a linear motion is obtained. The pitch of the lead screw is 2 mm. The linear actuator also contains an encoder which can measure the motor rotation and from the pitch one can estimate the linear motion of the actuator. The linear actuator is capable of carrying a load of 1500 N with a maximum stroke of 1000 mm. This linear actuator was chosen such that it can be used in a future setup where larger mirrors (2 m x 2 m or 5 m x 5 m) can be used. Two separate attachments are also made to attach the spherical joints between the support frame and the linear actuator or the prismatic joint. These attachments are connected sufficiently rigid so that no motion except the rotation of the spherical joints takes place.

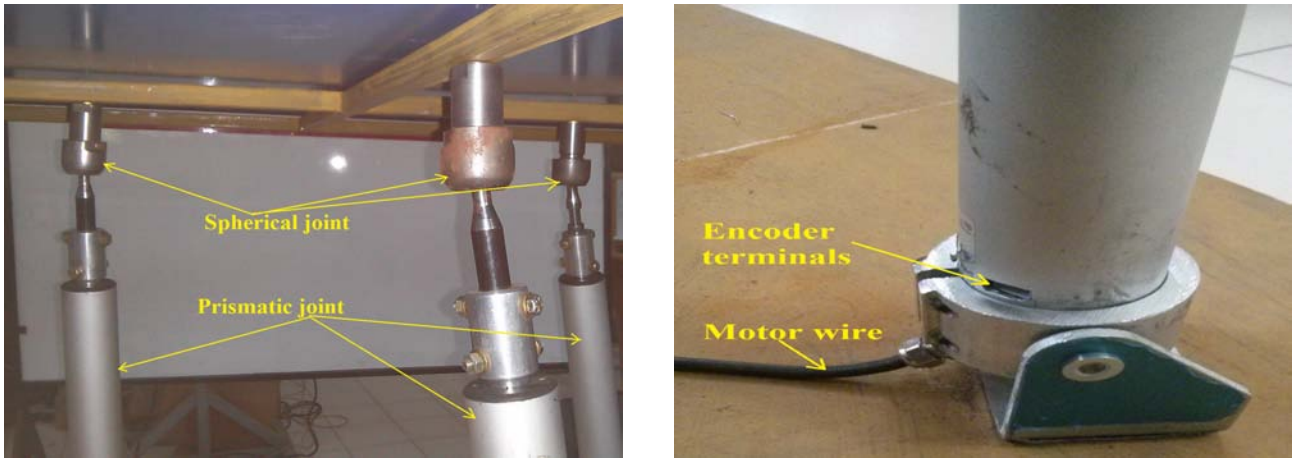

(a) Spherical and prismatic joint

(b) Revolute joint

Figure 4.3: The revolute, prismatic and spherical joints of the 3-RPS heliostat

4.3 Control strategy

The proposed control strategy for the heliostat is of intermittent tracking. In such a strategy, the heliostat is held stationary for a certain length of time denoted by t_h (idling or holding time). Referring to figure 4.4, we assume that the receiver aperture is a square, PQRS, of

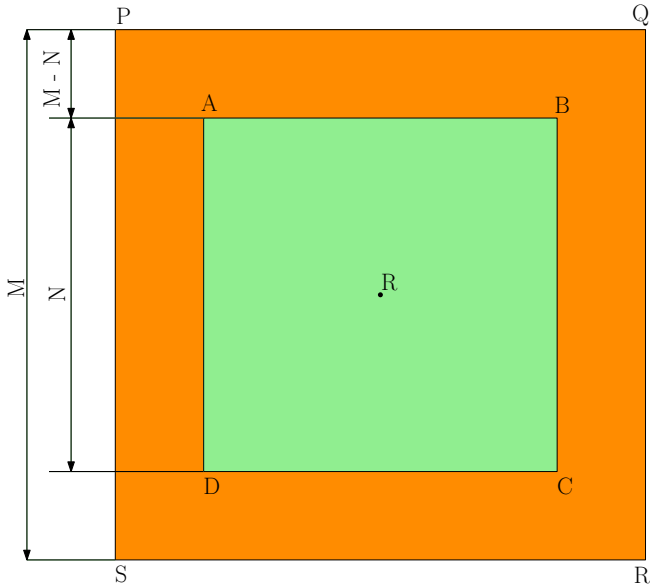

Figure 4.4: Idealised image formation on the receiver

side M. The idealized image of the reflected rays formed on the receiver will lie inside another square, ABCD, of side N. The Sun ray at the centre of the heliostat gets reflected to the centre

of the receiver at R. When the heliostat is held stationary, since the Sun moves in the sky, the point R will move on the receiver plane. One can thus hold the heliostat stationary as long as the reflected centre ray does not move out of the receiver area. From the figure 4.4, one can see that the holding time t_h will be related to the difference of M and N and this will vary with the distance of the receiver from the heliostat and on the exact motion of the Sun in the sky which is determined by the location on the Earth's surface and on the date and time of the day. The value of t_h can be found iteratively and for Bangalore, India (Latitude 12° 58' 13" N and Longitude 77° 33' 37" E) a holding time of 21 seconds is found to be acceptable when the farthest heliostat is 300 m from the receiver. Figure 4.5 shows a plot of t_h versus distance where the receiver is assumed to be of dimension 2.5 m x 2.5 m and is assumed to be 2 m x 2 m. The main advantage of using an intermittent motion is that the gear ratio can be significantly reduced and for a holding time of 21 seconds the gear ratio is approximately 1:5000 with the input at 10 rpm. It may be noted that at times the Sun moves slower than 15° per hour (for example around noon) and during such slow times, the holding time can be increased by suitable control commands to the DC motor. In our experiments, all the three actuators are

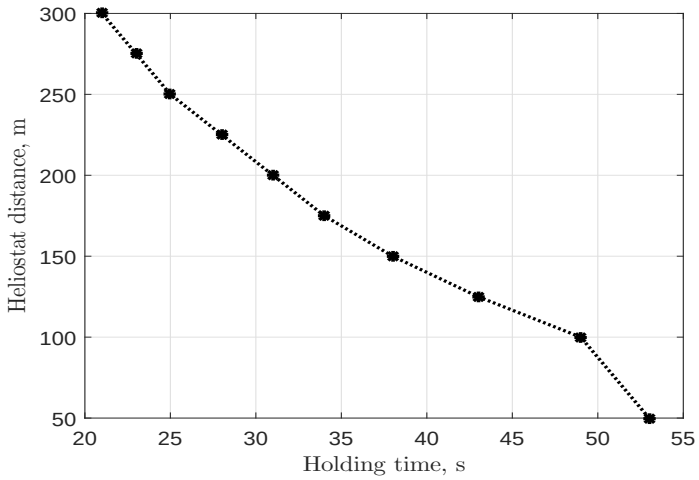

Figure 4.5: Variation of holding time with heliostat distance

kept idle for 15 minutes between any two tracking instants and after that all the actuators are simultaneously actuated to the desired position at the rated speed. The least possible velocity that the actuator can achieve is 1 mm/s. For Sun tracking, the actuators should be moved either forward or backward to get the desired orientation of the mirror. In order to facilitate the forward and backward motion of the actuators, an H-bridge circuit was designed and used.

4.3.1 H bridge

A motor driver circuit or an H-bridge is shown in figure 4.6. The H-bridge helps to drive the actuators forward and backward [89, 90]. For the H-bridge, two P type power MOSFETs

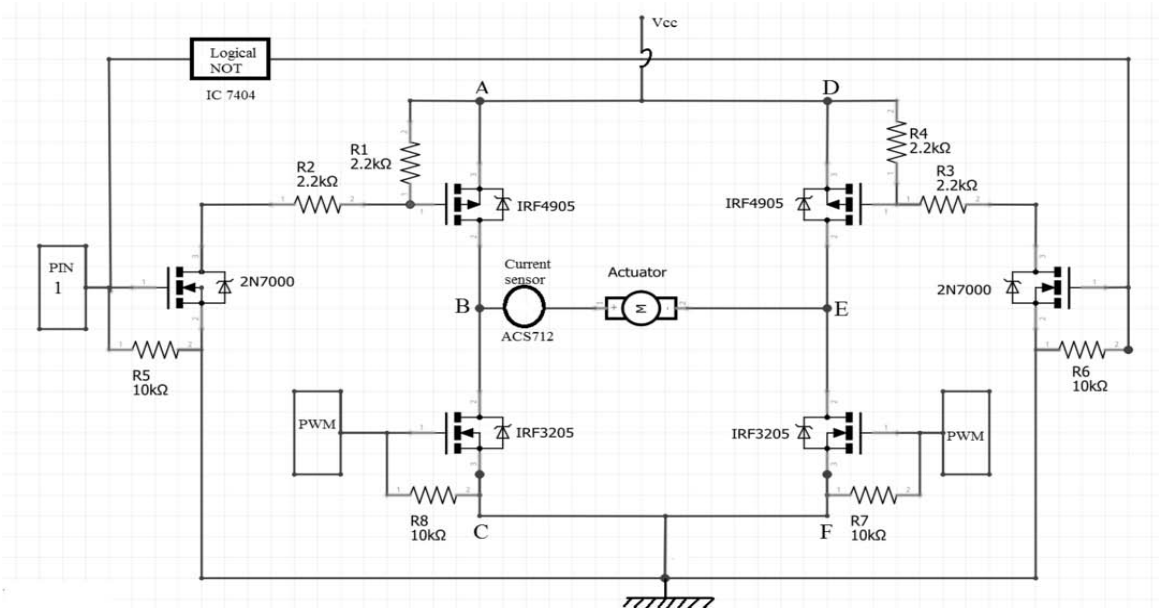

Figure 4.6: Schematic of the H-bridge circuit for an actuator

(IRF4905) and two N type power MOSFETs (IRF3205) are used. There are two Pulse Width Modulation (PWM) input ports and a digital pin to switch on the power MOSFET 2N7000. At a time, only one of the two power MOSFETs, 2N7000, will be switched on. For this to happen, a logical NOT gate, IC 7404, is connected between the two 2N7000 MOSFETs. A current sensor, ACS712, is connected in series with the motor to cut off the supply in case some excess current passes through the motor. The H-bridge implemented on a printed circuit board for all the three actuators is shown in figure 4.7. The supply voltage for the actuators is 24 V and the maximum rated current is 3.5 A.

4.3.2 The microcontroller

ATMEGA2560 micro-controller is used to provide the PWM signals, turn on digital PIN 1 and for reading the encoder output. It is an 8-bit microcontroller capable of operating at 16 MHz and is also one of the cheapest micro-controllers which could read data from all the three linear actuator encoders simultaneously. From figure 4.6, when PIN 1 is turned on using digital input from ATMEGA2560, current flows through the path ABEF and the actuator moves forward. When PIN 1 is turned off, current flows through the path DEBC and the actuator moves

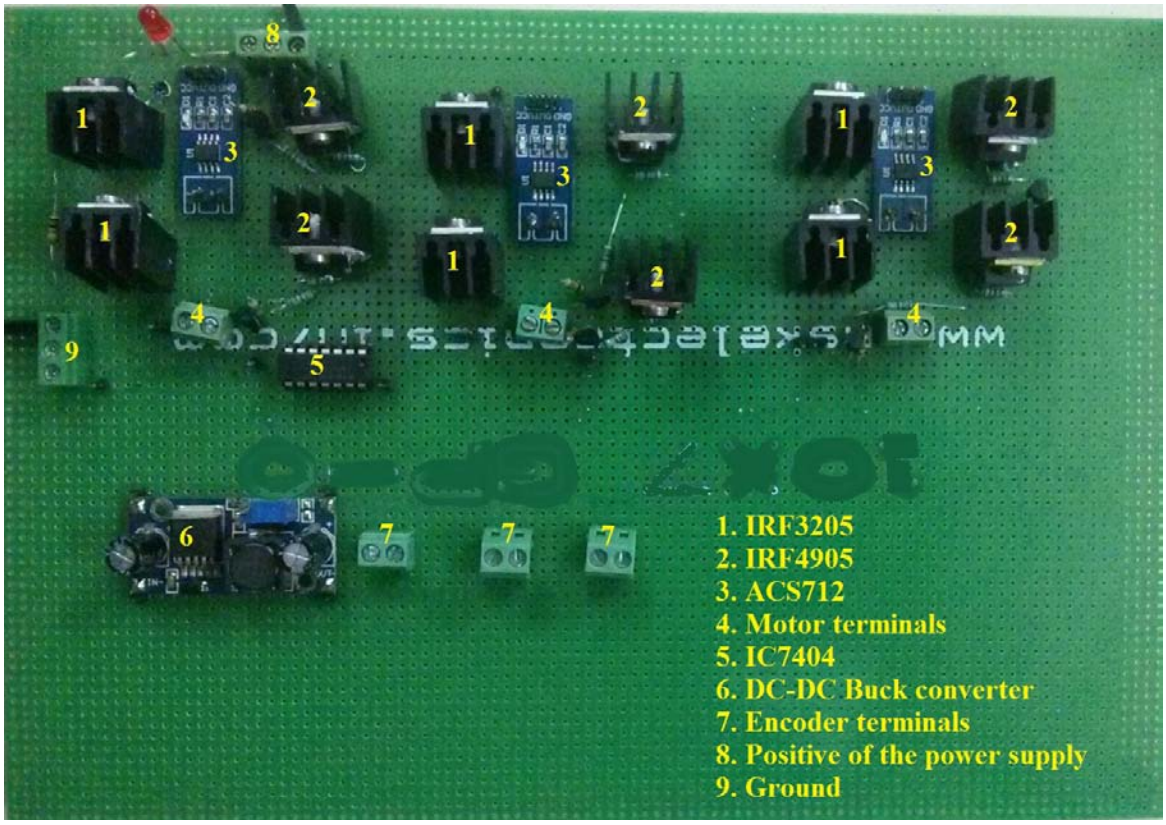

Figure 4.7: H-bridge for three actuators with a DC-DC converter for powering encoder

backward.

4.3.3 Feedback system

An quadrature type optical encoder is used for feedback. The encoder pulses can be read and converted to linear motion of the actuator by multiplying it with an appropriate gain constant having units of distance moved per count. Since the encoder is of quadrature type, by knowing the phase shift between the two output signals, the direction of motion can also be obtained. The encoder counts read by the micro-controller are sent to MATLAB through serial port communication.

4.3.4 Control using MATLAB-Simulink

The Simulink model used for control is shown in figure 4.8. The MATLAB program, given by equation (2.15), is used to compute the translation at the linear actuator (or the P joint). As the Sun moves, the translation at the P joint is computed at every instant of time. These values are stored in the variable named leg1 and is used as the reference trajectory. Thus leg1 becomes a time-series data type in the MATLAB-Simulink model. A built-in PID controller

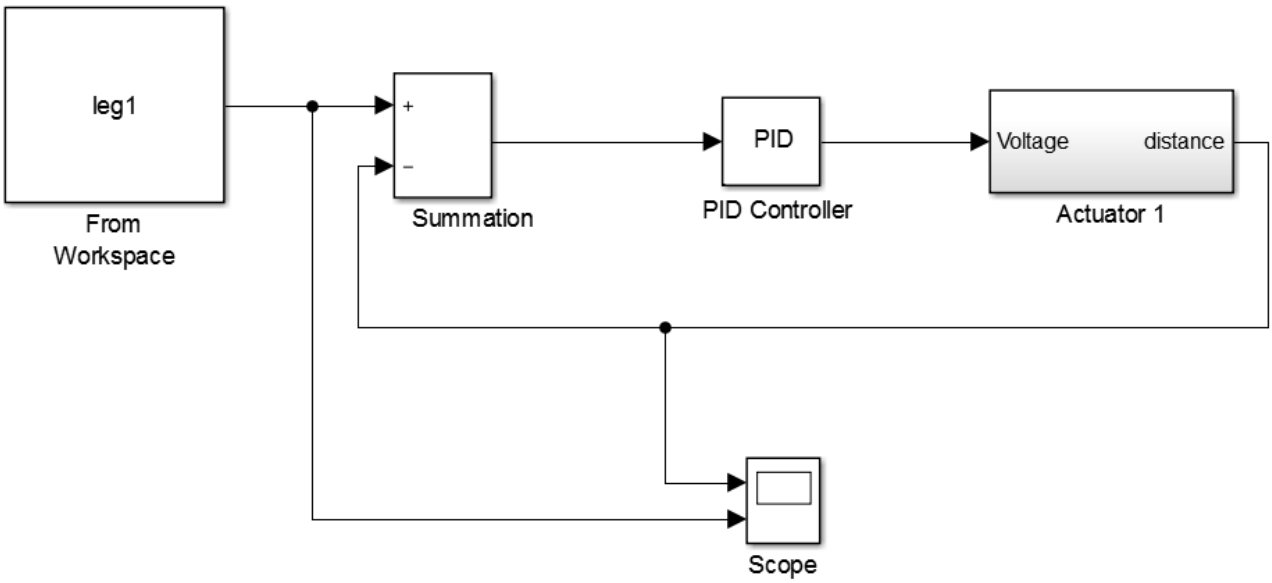

Figure 4.8: Schematic of the control strategy used

block is used and the gains, viz, the proportional gain (K_p), the integral gain (K_i) and the derivative gain (K_d) are adjusted to get the best result. From extensive experiments the values of proportional, integral and derivative gain are found to be 8, 0.7 and 0.09, respectively. The input to the PID block is the error which is the difference between the desired and actual trajectory followed. The output of the PID block is a voltage which is obtained using the PID control law given by equation (4.1).

$$V(s) = K_p + \frac{K_i}{s} + K_d \frac{N}{1 + N\frac{1}{s}} \tag{4.1}$$

where N is the filter coefficient. The voltage thus obtained is fed to the Actuator 1 subsystem as shown in figure 4.9. The Actuator 1 subsystem in Simulink consists of two parts, viz., the actuator part and the feedback/encoder part. A MATLAB function block is used to route voltage thus giving directions to the actuator for its travel. If the input to the route voltage function block is positive, it indicates that the actuator has to move forward. So PIN 1 is turned on and the outputs PWM_bwd and PWM_fwd are respectively set zero and a value 255 (8 bit representation) – as mentioned earlier, the rated voltage is 24 V and is actuated at the rated speed which corresponds to 255. If the input is to the route voltage is negative, PIN 1 is turned off and the actuator moves backward. If the input is zero, this indicates that the reference and the actual trajectory followed are exactly the same and the actuator stops

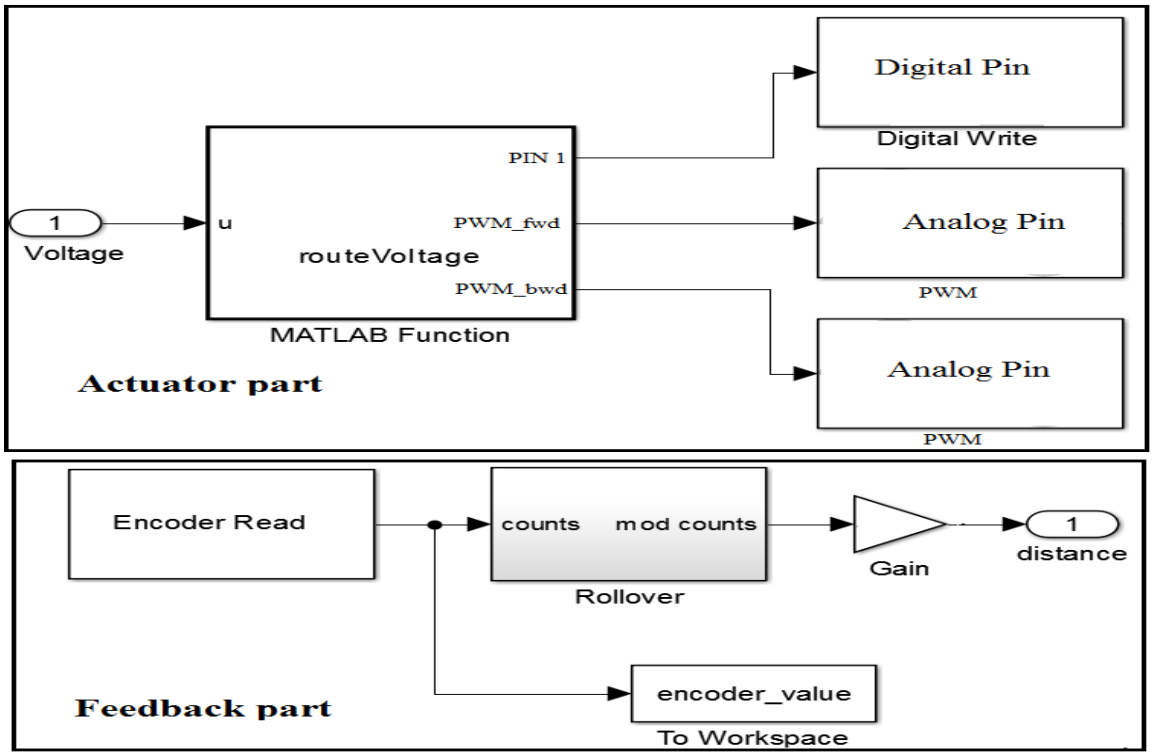

Figure 4.9: Actuator subsystem

moving. The feedback is obtained by reading the encoder pulses and the rollover subsystem is to prevent the encoder pulses from switching signs suddenly when the storage limit is attained. As mentioned before, the gain block converts the encoder pulses to the linear distance moved by the actuator.

4.3.5 Micro-controller safety

The ATMEGA2560 micro-controller can handle input voltages only up to 5V. In-order to protect the controller from the high voltage motor side, an opto-isolator is used for each of the actuators as shown in figure 4.10. The opto-isolator transfers an electrical signal from one side to the other through a short optical path. It consists of an infra red emitting diode (IRED) and a photo sensor. When an electrical signal is sent to the IRED, it picks it up and converts the electrical signal to light. This is sent across to the other side where the photo sensor picks it up again and converts the light back to electrical signal. Thus the high and low voltage sides are electrically isolated from each other. Hence by using the opto-isolator, the micro-controller is isolated from the motor side. Thus it helps in preventing any interference between the two sides and hence the safety of the micro-controller is ensured.

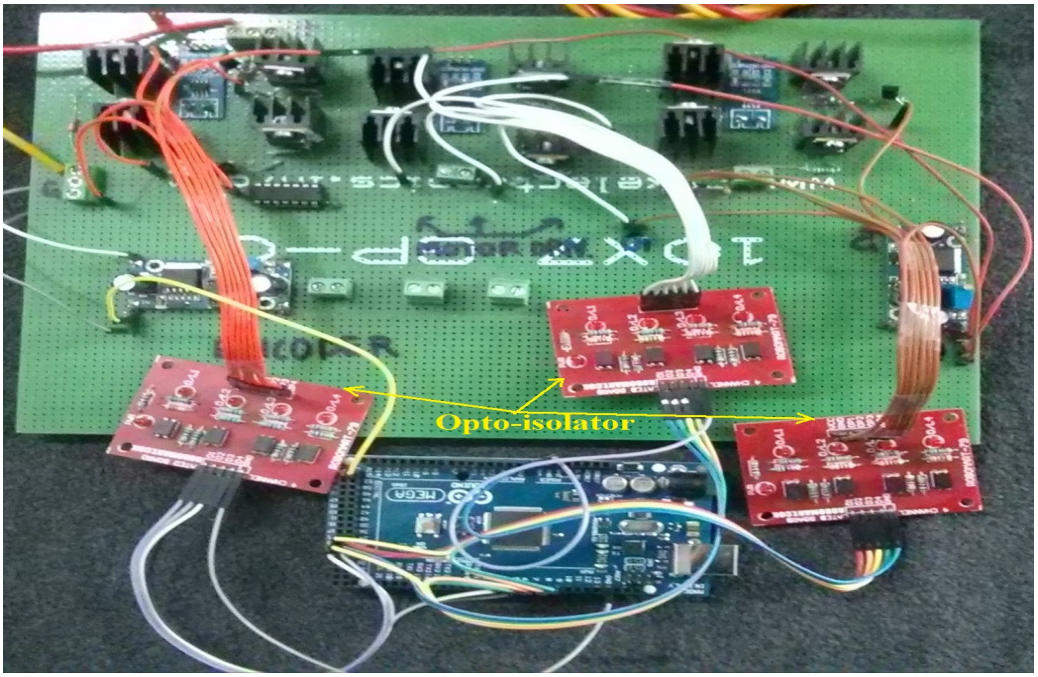

Figure 4.10: Opto-isolator coupled with the H-bridge

4.4 Verification of algorithm developed

To verify the algorithm used for tracking, the initial experiments were done indoors in the lab. The lab space is of dimension 10 m x 7 m x 4.2 m and the bottom left corner of the room is marked as the origin of the global co-ordinate system. The centre of the bottom platform of the 3-RPS heliostat is kept at co-ordinates $\overrightarrow{OO_1} = [6.55\ 3.60\ 0]^T$. A He-Ne laser placed at $[9.13\ 3.55\ 2.63]^T$ serve as the source of light. Several points (though not all) were marked on the wall which are in the direction of Sun's path on a particular day (March 20) as shown in figure 4.11. The algorithm assumes that the ray hitting the centre of the mirror will be reflected on to the centre of the receiver. Hence the laser beam is aimed at the centre of the mirror. The actuation required for the manipulator to track the points marked on the wall were found out using the algorithm developed. Using the values thus obtained, the legs of the manipulator are actuated. It can be seen from figure 4.12 that the ray reflected from the centre is going to the point marked on the wall although there is a error of about 7.1 mrad. This deviation can be explained by the fact that the centre of the 3-RPS heliostat is not at a fixed point during the tracking and other errors such as deviation in the co-ordinate system from actual East-North, variations in measurement of distances, non-ideal behavior of spherical and rotary joints etc. are not taken into account. The orientation of the heliostat at 12 noon on March 20 is also shown in figure 4.13. This matches with the MATLAB simulation given in figure 4.11.

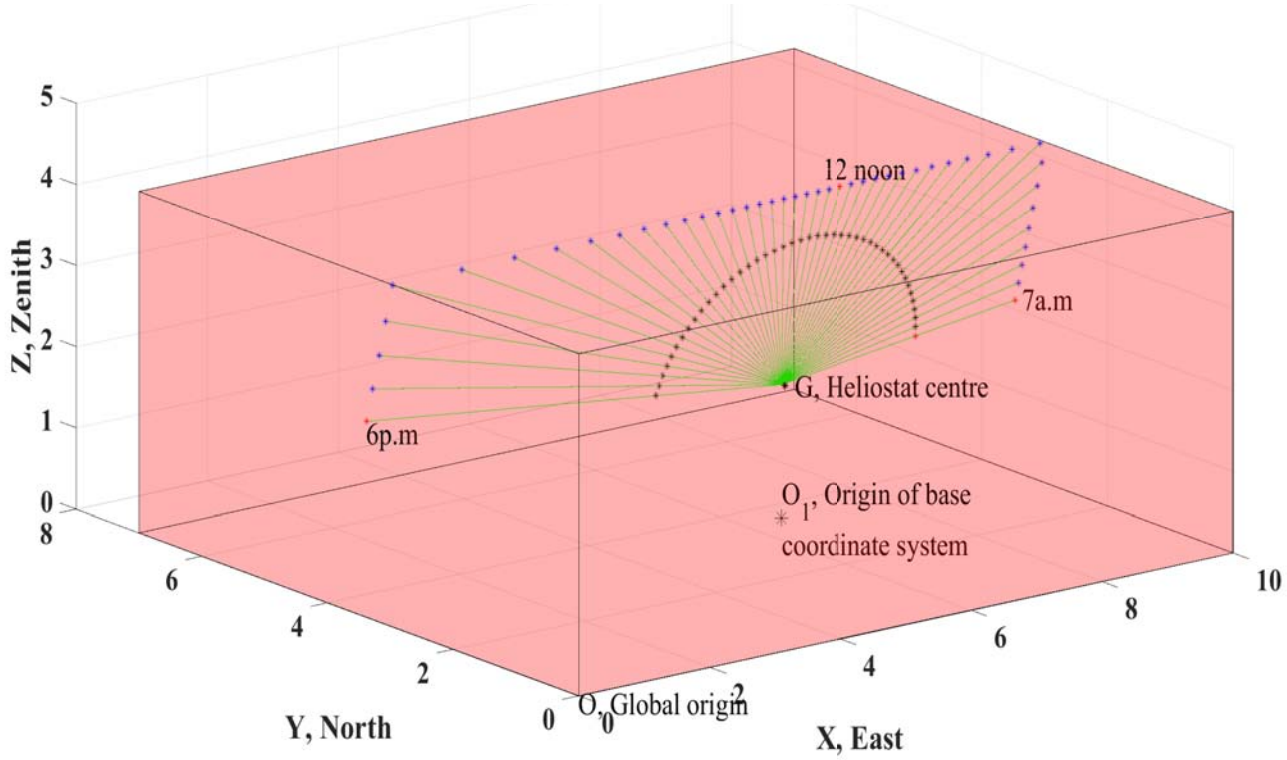

Figure 4.11: MATLAB simulation of the Sun path in lab

Figure 4.12: Algorithm verification by tracking point

Figure 4.13: The heliostat orientation at 12 noon

4.5 Actual Sun tracking

The actual Sun tracking experiment was carried out on the roof of the Interdisciplinary Centre for Energy Research (ICER) for two days, viz., October 15 and November 10, 2016. The main aim of the experiment was to test if the algorithm developed was able to reflect the incident solar radiations to the receiver screen at every tracking instant. A prototype of the Az-El heliostat having the same mirror dimension of 1 m x 1 m was also fabricated for the purpose of comparison. Table 4.1 gives the co-ordinates of the Az-El and 3-RPS heliostats with respect to global co-ordinate system (gcs). In the table, O_1, R and z_G refers to the origin of the base coordinate system, centre of the receiver and the vertical distance from O_1 to the centre of the mirror co-ordinate system (point G in figure 2.1). The images of the 3-RPS heliostat reflecting the Sun rays to the screen are shown in figure 4.14. Figure 4.15 shows the image formed on the receiver screen using an Az-El heliostat. Figure 4.16 shows the image formed on the screen when the two different types of heliostats were working together. It maybe noticed that in some images (see, for example, figure 4.14a), the Sun appears circular with a cross pattern. Ideally the image of the square mirror on the heliostat should be a square. The images on the wall where the Sun appears to be circular with a cross pattern is due to the intentional removal of some supporting material between the mirror and the supporting structure. As a result the mirror bends due to its self-weight and assumes a curved (paraboloid) shape and due to this

the Sun's image is focused. This interesting observation need to be explored further as such focusing of the Sun's image is known to be beneficial in concentrated solar power systems.

Table 4.1: Location parameters of Az-El and 3-RPS heliostats wrt gcs

	O_1 $[\mathbf{x\ y\ z}]^T$ **m**	**R** $[\mathbf{x\ y\ z}]^T$ **m**	z_G
Az-El	[-14 5.45 0]	[0 0 6.72]	1.58
3-RPS	[-14 3.45 0]	[0 0 6.72]	1.64

(a) 11.15 a.m.

(b) 12 noon

(c) Cloudy

(d) 3:30 p.m.

Figure 4.14: The image formed on the screen using 3-RPS heliostat on October 15,2016

(a) 09:30 a.m.

(b) 12 noon

(c) Cloudy

(d) 3:30 p.m.

Figure 4.15: The image formed on the screen using Az-El heliostat on October 15,2016

(a) 11:15 a.m.

(b) 12 noon

(c) Almost cloudy

(d) 3:30 p.m.

Figure 4.16: The image formed on the screen when Az-El and 3-RPS were working together on October 15,2016

4.6 Tracking errors

The tracking error as defined by King and Arvizu [91] is *the deviation of the beam centroid location from the desired aim-point on the target screen.* The tracking error sources for Az-El heliostat and various control strategies currently used to minimize it have been discussed in literature [60, 58, 92, 93]. In addition to the error sources in an Az-El configuration, in a parallel manipulator based heliostats, there will have error induced due to the non ideal behavior of the various joints. For example, the motion of the 3-RPS heliostat prototype is limited by the range of rotation of the spherical joints which caused some errors especially during morning and evening.

4.6.1 Analytical expression for error

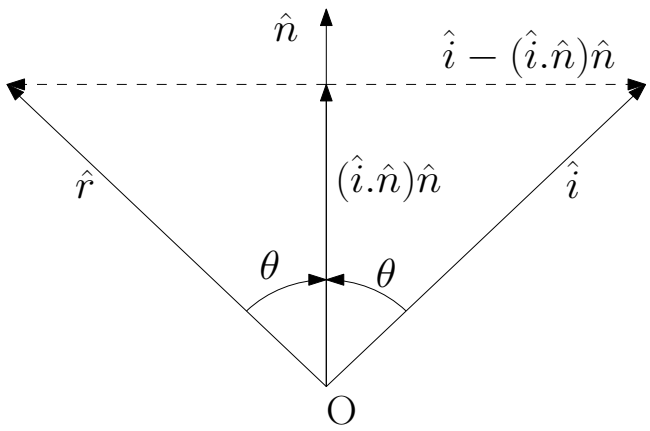

Figure 4.17: Reflection from a plane surface

Figure 4.17 shows the reflection of light from a surface where $\hat{i}$, $\hat{r}$ and $\hat{n}$ are respectively the unit incident ray, unit reflected ray and the unit normal vector to the surface. We can write

$$\begin{aligned} \hat{r} &= (\hat{i}.\hat{n})\hat{n} - (\hat{i} - (\hat{i}.\hat{n})\hat{n}) \\ &= 2(\hat{i}.\hat{n})\hat{n} - \hat{i} \end{aligned} \tag{4.2}$$

if $\hat{n}$ changes to $\hat{n_1}$ where $\hat{n_1} = \hat{n} + \delta\hat{n}$, then the change in $\hat{r}$ can be written as

$$\Delta r = 2\Big((\hat{i}.\hat{n_1})\hat{n_1} - (\hat{i}.\hat{n})\hat{n}\Big) \tag{4.3}$$

In figure 4.18, P is the centre of the receiver, P_1 is the point where the reflected ray hits the

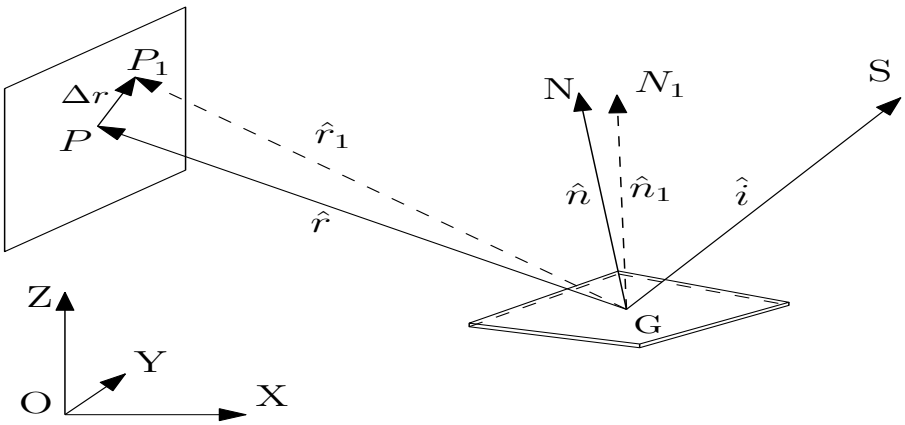

Figure 4.18: Tracking error

receiver when errors are present, G is the centre of the reflector. We can write

$$\begin{aligned} \overrightarrow{OG} + C_1\hat{r} &= \overrightarrow{OP} \\ \overrightarrow{OG} + C_1\hat{r}_1 &= \overrightarrow{OP}_1 \\ C_1\Delta r &= \overrightarrow{OP}_1 - \overrightarrow{OP} \end{aligned}$$

$$2C_1\Big((\hat{i}.\hat{n_1})\hat{n_1} - (\hat{i}.\hat{n})\hat{n}\Big) = \overrightarrow{OP}_1 - \overrightarrow{OP} = \begin{bmatrix} \Delta x \\ \Delta y \\ \Delta z \end{bmatrix} \tag{4.4}$$

where C_1 is a constant and also the errors are assumed to be small.
For Az-El method, the incident ray and normals would be

$$\hat{i} = \begin{bmatrix} \cos\alpha_s \cos\phi_s \\ \cos\alpha_s \sin\phi_s \\ \sin\alpha_s \end{bmatrix} \quad ; \quad \hat{n} = \begin{bmatrix} \cos\alpha_n \cos\phi_n \\ \cos\alpha_n \sin\phi_n \\ \sin\alpha_n \end{bmatrix} \quad ; \quad \hat{n_1} = \begin{bmatrix} \cos(\alpha_n + \Delta\alpha_n)\cos(\phi_n + \Delta\phi_n) \\ \cos(\alpha_n + \Delta\alpha_n)\sin(\phi_n + \Delta\phi_n) \\ \sin(\alpha_n + \Delta\alpha_n) \end{bmatrix}$$

where α and ϕ are the elevation (measured from ground plane) and azimuth (measured from X axis) angles of the Sun vector and normal indicated by the suffixes s and n respectively.

For the 3-RPS, in terms of the joint space variables, the coordinates of the spherical joints

with respect the base coordinate system can be written, $\{B\}$ (see figure 2.1), as

$$O_1S_1 = \begin{bmatrix} r_b - l_1\cos\theta_1 \\ 0 \\ l_1\sin\theta_1 \end{bmatrix}; O_1S_2 = \begin{bmatrix} -0.5(r_b - l_2\cos\theta_2) \\ \frac{\sqrt{3}}{2}(r_b - l_2\cos\theta_2) \\ l_2\sin\theta_2 \end{bmatrix}; O_1S_3 = \begin{bmatrix} -0.5(r_b - l_3\cos\theta_3) \\ -\frac{\sqrt{3}}{2}(r_b - l_3\cos\theta_3) \\ l_3\sin\theta_3 \end{bmatrix} \quad (4.5)$$

$$O_1S_1' = \begin{bmatrix} r_b - (l_1+\Delta l_1)\cos\theta_1 \\ 0 \\ (l_1+\Delta l_1)\sin\theta_1 \end{bmatrix}; O_1S_2' = \begin{bmatrix} -0.5(r_b - (l_2+\Delta l_2)\cos\theta_2) \\ \frac{\sqrt{3}}{2}(r_b - (l_2+\Delta l_2)\cos\theta_2) \\ (l_2+\Delta l_2)\sin\theta_2 \end{bmatrix};$$

$$O_1S_3' = \begin{bmatrix} -0.5(r_b - (l_3+\Delta l_3)\cos\theta_3) \\ -\frac{\sqrt{3}}{2}(r_b - (l_3+\Delta l_3)\cos\theta_3) \\ (l_3+\Delta l_3)\sin\theta_3 \end{bmatrix} \quad (4.6)$$

where the θ_i (i = 1, 2, 3) are the angles that the legs make with the base platform. Here, the incident ray would remain same as in equation (4.4) but the normals would be different and could be found out as

$$\hat{n} = [R]\ \frac{(O_1S_2 - O_1S_1)\times(O_1S_3 - O_1S_1)}{||(O_1S_2 - O_1S_1)\times(O_1S_3 - O_1S_1)||}$$
$$\hat{n}_1 = [R]\ \frac{(O_1S_2' - O_1S_1')\times(O_1S_3' - O_1S_1')}{||(O_1S_2' - O_1S_1')\times(O_1S_3' - O_1S_1')||} \quad (4.7)$$

where [R] is the rotation matrix which takes the base co-ordinate system to the global co-ordinate system. The same equation (4.4) could be used to find out the error. In the expressions above, Δ indicates a small change in the respective quantity. It is also assumed the motion of the centre of the 3-RPS heliostat is negligible. Figure 4.19 shows the error vector, ϵ, where R is the centre of the receiver and C_i is the centroid of the reflected image. The error vector, ϵ is resolved into its components along North and Zenith axes. The component along North axis divided by the slant height gives the horizontal error in radians. Similarly, the component along Zenith divided by slant height gives the vertical error. Figures 4.20 and 4.21 respectively give the error bar plots of 3-RPS and Az-El heliostats. It can be seen that the errors are comparable.

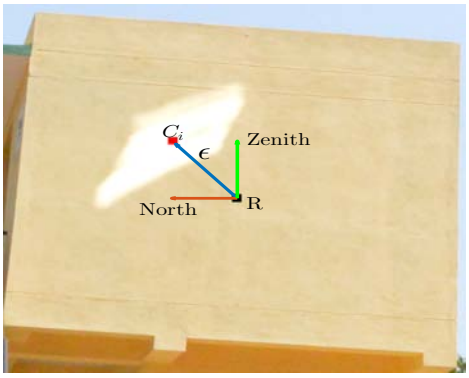

Figure 4.19: Tracking error

The errors can be made smaller with more precision and refined manufacturing and assembly.

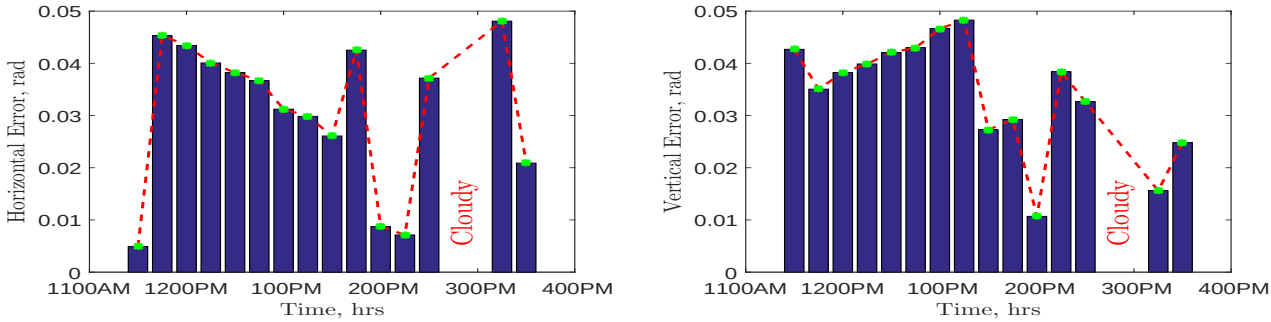

(a) Horizontal error

(b) Vertical error

Figure 4.20: Error bar plot of 3-RPS heliostat

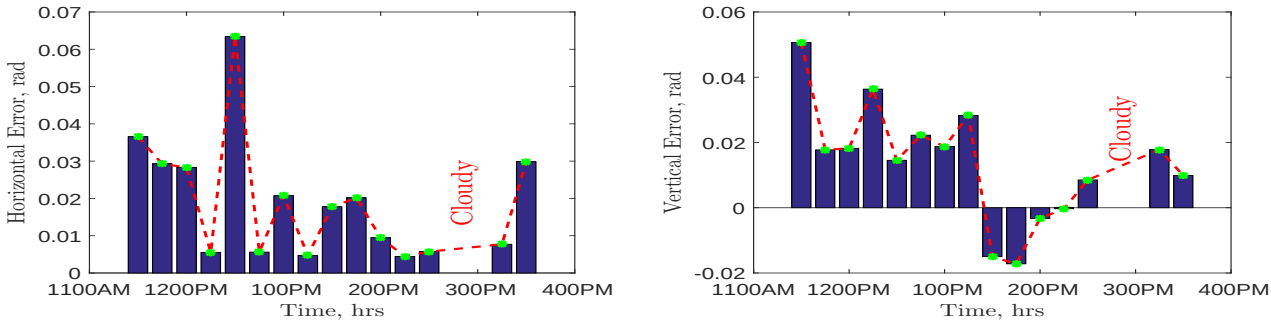

(a) Horizontal error

(b) Vertical error

Figure 4.21: Error bar plot of Az-El heliostat

4.7 Key observations made during experiments

We list some of the key observations made during the experiments with the 3-RPS and the Az-El heliostat.

- One of the observations made during the testing was that the Az-El heliostat required a torque to be always applied to hold the mirror at a particular orientation. Hence some energy is spent even while the heliostat is held stationary at one particular orientation. Such an energy loss did not happen for 3-RPS heliostat as the weight is supported at three points[1].

- The cone angle of the spherical joints used in the prototype is about $\pm$ 32°. This makes it impossible for the heliostat to track at some locations in the field especially at places where the distance between the receiver tower and the heliostat is less. A larger cone angle is required if the 3-RPS heliostat is to be used close to the receiver.

- The revolute joint of the heliostat made in the prototype is not very rigid. Ideally, the axis of the prismatic joints should meet at a point. In the prototype, there is a slight offset and hence the range of motion is limited and some bending happens when the heliostat is tracking the Sun during early morning or late evening.

- The accuracy of tracking is dependent on how precisely the coordinates of the heliostat in the field and receiver tower are found out with respect to the global coordinate system. A precise notion of the direction of East and Zenith and the Sun's path calculated using the station coordinates, day of the year and time are also required for improving the tracking accuracy.

- Since the weight of the mirror in 3-RPS heliostat is always supported by the actuator, there is no effect of backlash in the gear or drive train and thus this source of error is not present. This is an additional advantage of the 3-RPS heliostat over Az-El or T-A configurations.

4.8 Conclusions

In this chapter, fabrication and experiments done with a 3-RPS heliostat prototype has been presented. A low cost, customized motor driver circuit is designed and manufactured. A low

[1]If a linear actuator which is not back drivable is used (as in the Stellio heliostat), then no energy will be spent for maintaining the orientation.

cost controller was made using a widely available ATMEGA2560 board and a PID controller was implemented to control the orientation of the heliostat at desired instants of time. The micro-controller and the motor side are properly isolated using an opto-isolator for safety reasons. The algorithm developed for tracking the Sun in chapter 2 is verified first in the lab and then the actual Sun tracking is carried out outdoors. It is shown that 3-RPS heliostat is able to track the Sun and focus the incident solar radiation on a wall chosen as the receiver screen. It is shown that the tracking error is comparable to that obtained from a traditional Azimuth-Elevation configuration heliostat. Thus it is demonstrated that the proposed 3-RPS manipulator can indeed work as a heliostat in a CR solar thermal system.

Chapter 5

Conclusions and Future work

5.1 Summary

This thesis is an attempt to improve the current Sun tracking methods employed in concentrated solar power stations by moving from serial mechanisms to parallel mechanisms. The main reasons for such a change is the inherent advantages, such as high stiffness, large load carrying capacity, high accuracy in positioning and orienting the end effector, easy to obtain inverse kinematics and ease of real time control available in parallel mechanisms over serial mechanisms. In chapter 1, the motivation and a detailed literary survey on the approaches to harvest solar energy, existing Sun tracking methods, and sources of tracking errors are discussed. It is shown that most common heliostats used in concentrated solar power systems use a serial mechanism and they are the Azimuth-Elevation and the Target-Aligned configurations. The chapter ends with the scope and contribution of the thesis.

Chapter 2 presents the over-view of various Sun tracking approaches using parallel manipulators. The currently used parallel manipulators cannot be used in a CR system since it is difficult to find the reference point on the moving platform which is very important for the calculation of transformation matrix and to obtain motion planning algorithms. Two potential parallel manipulators, each with three actuators, are identified for replacing the serial chains used in central receiver systems. These are the 3-RPS and 3-UPU wrist manipulators. This chapter also gives a detailed account of the development of tracking algorithms using the 3-UPU wrist and 3-RPS manipulators by solving the inverse kinematics. A simulation study of the two proposed parallel manipulators is carried out and found that there are certain drawbacks, such as leg intersection and precise manufacturing required to get a fixed point, for the 3-UPU wrist.

Chapter 3 discusses the structural design of heliostats. A finite element analysis based

approach is used to model and analyze the heliostat with a goal of finding the most optimum structure of a heliostat to withstand loading due to wind and self-weight. For the operating wind load of 10 m/s and 22 m/s, an iterative search is carried out to find the optimal values of certain design parameters which would help in achieving a stroke of 700 mm for the actuators to track the Sun and to obtain the least weight of the supporting structure. It is shown that when larger mirrors, such as 5m x 5m mirrors, are used the saving in structure in the parallel 3-RPS configuration is as high as 65% when compared to the traditional serial Azimuth-Elevation and Target-Aligned configurations.

Chapter 4 deals with the detailed design and fabrication of the 3-RPS heliostat. This chapter also gives a detailed description of the motor driver circuit, the control strategy implemented using MATLAB-Simulink and ATMEGA2560 and verification of algorithm by tracking points marked on the wall. An actual Sun-tracking experiment is also carried out on the roof of a building and the tracking errors are quantified for both Az-El and 3-RPS heliostats. It is shown that the tracking errors are comparable and the 3-RPS parallel manipulator could be used as a heliostat in central receiver systems.

5.2 Scope for future work

The approach and the results reported in this work can be extended in several ways. We list some of the main ones below.

- The value of Z displacement in the 3-RPS heliostat z_G (in equation (2.2)), is chosen arbitrarily as it is a free variable. It is possible to use this redundancy to optimize the motion of the heliostat such that some objective function is minimized. We have attempted to reduce cosine losses during Sun tracking by changing z_G. However, this effect is very small as the range of z_G is limited by the maximum stroke of the linear actuators.

- Simulation study for the 3-RPS were carried out for equinoxes and solstices. There is a scope to carry out the simulation study for one whole year and see if there are any variations in the results presented in chapter 2. Rajasthan and Bangalore are the only two locations that were considered for the simulation study and it would be useful to do simulations for various other latitudes.

- A more elaborate simulation study has to be carried out for 3-UPU wrist especially to see if the legs intersect and to what angle it has to be rotated initially. The 3-UPU wrist has certain shortcomings as mentioned in section 2.6. However, it has the appealing property

of being 'software switchable' between Az-El and T-A or any other two successive rotation configuration. Hence, it would be worthwhile to design and manufacture a prototype and perform experiments with it.

- The observations made in section 4.7 have to be reworked especially related to the range of motion of the spherical joints and the prismatic joint axes. The actual Sun tracking on the roof is carried out from 11:15 am to 3:30 pm. The experiment takes a lot of time to set-up the mirror, controllers and computers. The surrounding trees also block the sunlight beyond 3:30 pm. The max slant length (distance from the mirror centre to the centre of the receiver) is less than 16 m and the relative height between the mirror centre and the receiver centre is only 5.08 m. Due to this the spherical joints try to rotate more than its allowed range and cause some bending of the actuators and noise. All these difficulties suggest more experiments with proper facilities to obtain better quantitative results in Sun tracking error and performance of the 3-RPS based heliostat.

- The first generation prototype done in this thesis could only quantify the tracking errors. The tracking errors are quite high, the average being 30 mrad for 3-RPS heliostat. This aspect needs to be reworked with more refined manufacturing and more robust control strategy. The target for the second generation 3-RPS heliostats would be to have a tracking error of less than 2 mrad. To ensure this, two methods are suggested and these are:

  1. **Self-calibrating controllers**
     This idea is from the work carried out by Baheti and Scott [54]. Here the main assumption made is that the centre of the 3-RPS heliostat(point G in figure 2.1) moves very less compared to the other dimensions. This is verified from the figures 2.8 and 2.9 in section 2.3.5 and is a reasonable assumption. From the images captured (for eg. figure 4.19), the error vector can be calculated. From this the ideal reflected ray (the ray which should have hit the centre of the receiver) and the actual reflected ray (the ray which hits the centroid of the reflected image) can be calculated. From the notion of the reflected ray, the normal to the mirror (both ideal and actual) can be determined (equation (1.4)). The error in normal, ϵ_n, would be the difference between the two and can be given as the product of a skew-symmetric matrix and a parameter matrix which is to be estimated. The elements of the skew-symmetric matrix are the direction cosines of the Sun vector. Since the skew-symmetric matrix is singular, some other approaches have to be used to evaluate the parameter matrix. One such

possibility is the use of singular value decomposition (SVD) to get an estimate of the parameters . This can be used to find the rotation matrix and hence the leg-length as described by equation (2.15). With the modern computing techniques available, a live correction using a camera and SVD can be employed to minimize the tracking error at every tracking instant.

2. **Optimization based control**
   The problem of error correction can also be posed as a distance minimization optimization problem where the distance between the centroid of reflected image and receiver centre is to be minimized. By doing so, elements of the rotation matrix which would minimize the distance, C_iR (in figure 4.19) can be found out and hence the corrections in the actuations required. This method also requires an on board computer and camera.

Appendix

A MATLAB program for calculating sun angles

```
function [elevation, azimuth]=alpha-azimuthcalc(LT,d,longitude,latitude)
  % LT=local time in seconds,        % d is the number of days since the start of the year
  % longitude of the place in degrees, East is positive and west is negative
  % latitude of the place in degrees, North is positive and south is negative
  LSTM = 15*5.5 ;% (in degrees) local standard time meridian. 5.5 is the time differance
  between local time for india and GMT
  B=60*(d-81)/365;                          % in degrees
  EOT=9.87*sind(2*B)-7.53*cosd(B)-1.5*sind(B);          % in minutes
  TC=4*(longitude-LSTM)+EOT; % Time Correction Factor (TC) in minutes
  LST=LT./3600+TC/60;          % in hours
  HRA=15*(LST-12);        % hour angle in degrees
  delta=23.45*sind(B);         % declination angle in degrees
  elevation=asind(sind(delta)*sind(latitude)+cosd(delta)*cosd(latitude).*cosd(HRA));
  a1=sind(delta)*cosd(latitude);
  a2=cosd(delta)*sind(latitude);
  a=acosd((a1-a2.*cosd(HRA))./cosd(elevation));
      for i=1:length(HRA)
            if (HRA(i)≤0 )
            azimuth(i)=a(i);
            elseif( 116 ≤ d && d ≤ 229 && HRA(i)¿0)
            azimuth(i) = -a(i);
            else
            azimuth(i) = 360-a(i);
            end          end      end
```

Bibliography

[1] NREL. *India Solar Resource*. URL: http://www.nrel.gov/international/images/india_dni_annual.jpg (cit. on p. 1).

[2] Atul Sharma. "A comprehensive study of solar power in India and World". In: *Renewable and Sustainable Energy Reviews* 15.4 (2011), pp. 1767 –1776. ISSN: 1364-0321 (cit. on p. 1).

[3] W Schiel and T Keck. "Concentrating solar power technology: Principles, developments and applications". In: *Concentrating solar power technology: principles, developments and applications*. Ed. by Keith Lovegrove and Wes Stein. Cambridge, UK: Woodhead Publishing, 2012. Chap. 9, pp. 284–322 (cit. on p. 1).

[4] K. Lovegrove and J. Pye. "Fundamental principles of concentrating solar power (CSP) systems". In: *Concentrating Solar Power Technology*. Ed. by Keith Lovegrove and Wes Stein. Woodhead Publishing Series in Energy. Woodhead Publishing, 2012, pp. 16 –67. ISBN: 978-1-84569-769-3 (cit. on p. 2).

[5] *SunShot Initiative*. URL: https://energy.gov/eere/sunshot/sunshot-initiative-goals (cit. on p. 2).

[6] Gregory J Kolb, Roger Davenport, David Gorman, Ron Lumia, Robert Thomas, and Matthew Donnelly. "Heliostat cost reduction". In: *ASME 2007 Energy Sustainability Conference*. American Society of Mechanical Engineers. 2007, pp. 1077–1084 (cit. on p. 2).

[7] Gregory J Kolb, Clifford K Ho, Thomas R Mancini, and Jesse A Gary. *Power tower technology roadmap and cost reduction plan*. Tech. rep. Sandia National Laboratories, Albuquerque, NM, 2011. URL: http://prod.sandia.gov/techlib/access-control.cgi/2011/112419.pdf (cit. on p. 2).

[8] NREL. *National Renewable Energy Labarotary*. URL: http://www.nrel.gov/csp/solarpaces/project_detail.cfm/projectID=62 (cit. on p. 2).

[9] J.B Blackmon. "Concentrating solar power technology: Principles, developments and applications". In: *Concentrating solar power technology: principles, developments and applications*. Ed. by Keith Lovegrove and Wes Stein. Cambridge, UK: Woodhead Publishing, 2012. Chap. 17, pp. 536–576 (cit. on p. 2).

[10] *PV EDUCATION*. URL: http://pveducation.org/pvcdrom/properties-of-sunlight/elevation-angle (cit. on p. 3).

[11] Ibrahim Reda and Afshin Andreas. "Solar position algorithm for solar radiation applications". In: *Solar Energy* 76.5 (2004), pp. 577–589 (cit. on p. 3).

[12] William B Stine and Michael Geyer. *Power from the Sun*. 2001. URL: http://www.powerfromthesun.net/book.html (cit. on p. 3).

[13] *NOAA Sun Position Calculator*. URL: https://www.esrl.noaa.gov/gmd/grad/solcalc/azel.html (cit. on p. 3).

[14] MATLAB. *Natick, Massachusetts,* 2012 (cit. on p. 4).

[15] *US Department of Energy*. URL: https://www1.eere.energy.gov/solar/pdfs/solar_timeline.pdf (cit. on pp. 5, 8).

[16] Zachary Alden Smith and Katrina D Taylor. *Renewable and alternative energy resources: a reference handbook*. ABC-CLIO, 2008. ISBN: 978-1-59884-089-6 (cit. on p. 5).

[17] Evangelos Bellos, Christos Tzivanidis, and Kimon A. Antonopoulos. "A detailed working fluid investigation for solar parabolic trough collectors". In: *Applied Thermal Engineering* 114 (2017), pp. 374 –386 (cit. on p. 6).

[18] L Salgado Conrado, A Rodriguez-Pulido, and G Calderón. "Thermal performance of parabolic trough solar collectors". In: *Renewable and Sustainable Energy Reviews* 67 (2017), pp. 1345–1359 (cit. on p. 6).

[19] E. Zarza Moya. "7 - Parabolic-trough concentrating solar power (CSP) systems". In: *Concentrating Solar Power Technology*. Ed. by Keith Lovegrove and Wes Stein. Woodhead Publishing Series in Energy. Woodhead Publishing, 2012, pp. 197 –239. ISBN: 978-1-84569-769-3 (cit. on p. 6).

[20] Zhongzhu Qiu, Peng Li, Chunying Li, Qunzhi Zhu, Tao Zhang, and Chengyao Wang. "A novel design concept for a reflector of parabolic trough concentrator based on pure bending and correction principle". In: *Solar Energy* 141 (2017), pp. 59–69 (cit. on p. 6).

[21] S. Meiser, S. Schneider, E. Lüpfert, B. Schiricke, and R. Pitz-Paal. "Evaluation and assessment of gravity load on mirror shape and focusing quality of parabolic trough solar mirrors using finite-element analysis". In: *Applied Energy* 185 (2017). Clean, Efficient and Affordable Energy for a Sustainable Future, pp. 1210 –1216 (cit. on p. 6).

[22] LL Vant-Hull. "Concentrating solar power technology: Principles, developments and applications". In: *Concentrating solar power technology: principles, developments and applications*. Ed. by Keith Lovegrove and Wes Stein. Cambridge, UK: Woodhead Publishing, 2012. Chap. 8, pp. 240–283 (cit. on pp. 6, 10, 12).

[23] *Roof-top solar installations for cooking*. URL: http://www.indiatimes.com/culture/food/10-facts-about-indias-mega-kitchens-that-will-leave-you-stunned-233823.html (cit. on p. 6).

[24] JJ Droher and SE Squier. *Performance of the Vanguard Solar Dish-Stirling Engine Module. Final report*. Tech. rep. Rockwell International Corp., Canoga Park, CA (USA). Energy Technology Engineering Center, 1986 (cit. on p. 6).

[25] Andrea Giostri and Ennio Macchi. "An advanced solution to boost sun-to-electricity efficiency of parabolic dish". In: *Solar Energy* 139 (2016), pp. 337–354 (cit. on p. 6).

[26] Charles E Andraka. "Dish Stirling advanced latent storage feasibility". In: *Energy Procedia* 49 (2014), pp. 684–693 (cit. on p. 7).

[27] C Lertsatitthanakorn, J Jamradloedluk, and M Rungsiyopas. "Electricity generation from a solar parabolic concentrator coupled to a thermoelectric module". In: *Energy Procedia* 52 (2014), pp. 150–158 (cit. on p. 7).

[28] USAID. *Grid-Connected Renewable Energy: Solar Electric Technologies*. URL: http://www.energytoolbox.org/gcre/mod_5/gcre_solar.pdf (cit. on p. 7).

[29] Haisheng Chen, Thang Ngoc Cong, Wei Yang, Chunqing Tan, Yongliang Li, and Yulong Ding. "Progress in electrical energy storage system: A critical review". In: *Progress in Natural Science* 19.3 (2009), pp. 291 –312. ISSN: 1002-0071 (cit. on p. 7).

[30] H. Ibrahim, A. Ilinca, and J. Perron. "Energy storage systems—Characteristics and comparisons". In: *Renewable and Sustainable Energy Reviews* 12.5 (2008), pp. 1221 –1250. ISSN: 1364-0321 (cit. on p. 7).

[31] Belen Zalba, Jose M Marin, Luisa F. Cabeza, and Harald Mehling. "Review on thermal energy storage with phase change: materials, heat transfer analysis and applications". In: *Applied Thermal Engineering* 23.3 (2003), pp. 251 –283. ISSN: 1359-4311 (cit. on p. 8).

[32] GA Lane. *Solar heat storage: Latent heat materials. Volume II. Technology*. Tech. rep. Dow Chemical Co., Midland, MI, 1986 (cit. on p. 8).

[33] A Haberle. "Concentrating solar power technology: Principles, developments and applications". In: *Concentrating solar power technology: principles, developments and applications*. Ed. by Keith Lovegrove and Wes Stein. Cambridge, UK: Woodhead Publishing, 2012. Chap. 19, pp. 602–619 (cit. on p. 8).

[34] Abbas A Akhil, Georgianne Huff, Aileen B Currier, Benjamin C Kaun, Dan M Rastler, Stella Bingqing Chen, Andrew L Cotter, Dale T Bradshaw, and William D Gauntlett. *DOE/EPRI 2013 electricity storage handbook in collaboration with NRECA*. Sandia National Laboratories Albuquerque, NM, USA, 2013 (cit. on p. 8).

[35] Michael Mendelsohn, Travis Lowder, and Brendan Canavan. *Utility-Scale Concentrating Solar Power and Photovoltaics Projects: A Technology and Market Overview*. Tech. rep. NREL Technical Report, NREL/TP-6A20-51137, 2012, pp. 275–3000. URL: https://www.nrel.gov/docs/fy12osti/51137.pdf (cit. on p. 8).

[36] A Cengel Yunus and A Boles Michael. *Thermodynamics: An engineering approach*. 2006. ISBN: 978-0073398174 (cit. on p. 8).

[37] FW Lipps and LL Vant-Hull. "A cellwise method for the optimization of large central receiver systems". In: *Solar Energy* 20.6 (1978), pp. 505–516 (cit. on p. 8).

[38] Hossein Mousazadeh, Alireza Keyhani, Arzhang Javadi, Hossein Mobli, Karen Abrinia, and Ahmad Sharifi. "A review of principle and sun-tracking methods for maximizing solar systems output". In: *Renewable and Sustainable Energy Reviews* 13.8 (2009), pp. 1800–1818 (cit. on p. 8).

[39] Chia-Yen Lee, Po-Cheng Chou, Che-Ming Chiang, and Chiu-Feng Lin. "Sun tracking systems: a review". In: *Sensors* 9.5 (2009), pp. 3875–3890 (cit. on p. 8).

[40] RB Ashith Shyam and A Ghosal. "Three-degree-of-freedom parallel manipulator to track the sun for concentrated solar power systems". In: *Chinese Journal of Mechanical Engineering* 28.4 (2015), pp. 793–800 (cit. on p. 9).

[41] Eugene A Igel and Robert Lee Hughes. "Optical analysis of solar facility heliostats". In: *Solar Energy* 22.3 (1979), pp. 283–295 (cit. on p. 10).

[42] Harald Ries and Markus Schubnell. "The optics of a two-stage solar furnace". In: *Solar Energy Materials* 21.2 (1990), pp. 213–217 (cit. on p. 10).

[43] R Zaibel, E Dagan, J Karni, and Harald Ries. "An astigmatic corrected target-aligned heliostat for high concentration". In: *Solar Energy Materials and Solar Cells* 37.2 (1995), pp. 191–202 (cit. on p. 10).

[44] YT Chen, KK Chong, TP Bligh, LC Chen, Jasmy Yunus, KS Kannan, BH Lim, CS Lim, MA Alias, Noriah Bidin, et al. "Non-imaging, focusing heliostat". In: *Solar Energy* 71.3 (2001), pp. 155–164 (cit. on p. 10).

[45] Xiudong Wei, Zhenwu Lu, Weixing Yu, Hongxin Zhang, and Zhifeng Wang. "Tracking and ray tracing equations for the target-aligned heliostat for solar tower power plants". In: *Renewable Energy* 36.10 (2011), pp. 2687–2693 (cit. on p. 10).

[46] Minghuan Guo, Zhifeng Wang, Wenfeng Liang, Xiliang Zhang, Chuncheng Zang, Zhenwu Lu, and Xiudong Wei. "Tracking formulas and strategies for a receiver oriented dual-axis tracking toroidal heliostat". In: *Solar Energy* 84.6 (2010), pp. 939–947 (cit. on p. 10).

[47] YT Chen, A Kribus, BH Lim, CS Lim, KK Chong, J Karni, R Buck, A Pfahl, and TP Bligh. "Comparison of two sun tracking methods in the application of a heliostat field". In: *Journal of Solar Energy Engineering* 126.1 (2004), pp. 638–644 (cit. on p. 12).

[48] R Buck and E Teufel. "Comparison and optimization of heliostat canting methods". In: *Journal of Solar Energy Engineering* 131.1 (2009), p. 011001 (cit. on p. 12).

[49] Ari Rabl. *Active solar collectors and their applications*. Oxford University Press, 1985 (cit. on p. 12).

[50] Victor Lindberg and Jukka Pekka Maki. "SKF dual axis solar tracker - From concept to product". MA thesis. 2010 (cit. on p. 12).

[51] Joshua Freeman, Balakrishnan Shankar, and Ganesh Sundaram. "Inverse kinematics of a dual linear actuator pitch/roll heliostat". In: *AIP Conference Proceedings*. Vol. 1850. 1. AIP Publishing. 2017, p. 030018 (cit. on p. 12).

[52] Markus Balz, Verena Gocke, Thomas Keck, Finn von Reeken, Gerhard Weinrebe, and Markus Wohrbach. "Stellio-development, construction and testing of a smart heliostat". In: *AIP Conference Proceedings*. Vol. 1734. 1. AIP Publishing. 2016, p. 020002 (cit. on p. 12).

[53] Florian Arbes, Gerhard Weinrebe, and Markus Wohrbach. "Heliostat field cost reduction by 'slope drive' optimization". In: *AIP Conference Proceedings*. Vol. 1734. 1. AIP Publishing. 2016, p. 160002 (cit. on p. 12).

[54] R Baheti and P Scott. "Design of self-calibrating controllers for heliostats in a solar power plant". In: *IEEE Transactions on Automatic Control* 25.6 (1980), pp. 1091–1097 (cit. on pp. 13, 81).

[55] M Berenguel, FR Rubio, A Valverde, PJ Lara, MR Arahal, EF Camacho, and M López. "An artificial vision-based control system for automatic heliostat positioning offset correction in a central receiver solar power plant". In: *Solar Energy* 76.5 (2004), pp. 563–575 (cit. on p. 13).

[56] *CSP Gen3 System Integration Considerations*. URL: https://energy.gov/sites/prod/files/2017/02/f34/Gen3\%20Workshop_Systems\%20Analysis_Turchi.pdf (cit. on p. 13).

[57] Jim Pearson and Bing Chen. *Assessment of heliostat control system methods*. Tech. rep. Solar Energy Research Inst., Golden, CO (USA), 1986. URL: https://www.nrel.gov/docs/legosti/old/2390.pdf (cit. on p. 13).

[58] Scott A Jones and KW Stone. *Analysis of Solar Two Heliostat Tracking Error Sources*. Tech. rep. Sandia National Laboratories, Albuquerque, NM, and Livermore, CA, 1999. URL: https://www.osti.gov/scitech/servlets/purl/3312 (cit. on pp. 13, 73).

[59] Kenneth W Stone and James A Kiefer. "Open Loop Track Alignment Methodology". In: *Solar Engineering* (1998), pp. 439–444 (cit. on p. 13).

[60] K. Malan and P. Gauché. "Model based Open-loop Correction of Heliostat Tracking Errors". In: *Energy Procedia* 49 (2014). Proceedings of the SolarPACES 2013 International Conference, pp. 2118 –2124. ISSN: 1876-6102 (cit. on pp. 13, 73).

[61] Abraham Kribus, Irina Vishnevetsky, Amnon Yogev, and Tatiana Rubinov. "Closed loop control of heliostats". In: *Energy* 29.5 (2004), pp. 905–913 (cit. on p. 13).

[62] Thomas Roos, Ndumiso Zwane, Strinivasan Perumal, Robert Cathro, et al. "A 25m2 Target-Aligned Heliostat With Closed-Loop Control". In: *Proceedings of ISES World Congress 2007 (Vol. I–Vol. V)*. Springer. 2008, pp. 1773–1781 (cit. on p. 13).

[63] M Zavodny, M Slack, R Huibregtse, and A Sonn. "Tower-based CSP Artificial Light Calibration System". In: *Energy Procedia* 69 (2015), pp. 1488–1497 (cit. on p. 13).

[64] VE Gough. "Contribution to discussion of papers on research in automobile stability, control and tyre performance". In: *Proc. Auto Div. Inst. Mech. Eng.* Vol. 171. 1956, pp. 392–394 (cit. on p. 16).

[65] Doug Stewart. "A platform with six degrees of freedom". In: *Proceedings of the institution of mechanical engineers* 180.1 (1965), pp. 371–386 (cit. on p. 16).

[66] Jean-Pierre Merlet. *Parallel robots*. Vol. 74. Springer Science & Business Media, 2012. ISBN: 978-1-4020-4133-4 (cit. on p. 16).

[67] Alessandro Cammarata. "Optimized design of a large-workspace 2-DOF parallel robot for solar tracking systems". In: *Mechanism and Machine Theory* 83 (2015), pp. 175–186 (cit. on p. 18).

[68] Jimenez E., Ceccarelli M., and Carbone G. "A dynamic analysis of the robot CAPAMAN (Cassino Parallel Manipulator) as solar tracker". In: 2011, pp. 579–594 (cit. on p. 18).

[69] Oscar Altuzarra, Erik Macho, Jokin Aginaga, and Victor Petuya. "Design of a solar tracking parallel mechanism with low energy consumption". In: *Proceedings of the Institution of Mechanical Engineers, Part C: Journal of Mechanical Engineering Science* 229.3 (2015), pp. 566–579 (cit. on p. 18).

[70] GoogleInc. *Heliostat Cable Actuation System Design*. URL: https://www.google.org/pdfs/google_heliostat_cable_actuation.pdf (cit. on p. 18).

[71] GoogleInc. *Heliostat Optical Simulation tool (Hops)*. URL: https://code.google.com/p/hops/ (cit. on p. 18).

[72] Weimin Li, Jianguang Sun, Jianjun Zhang, Kai He, and R Du. "A novel parallel 2-DOF spherical mechanism with one-to-one input-output mapping." In: *WSEAS Transactions on Systems* 5.6 (2006), pp. 1343–1348 (cit. on p. 18).

[73] Clement M Gosselin and François Caron. *Two degree-of-freedom spherical orienting device*. US Patent 5,966,991. 1999 (cit. on p. 18).

[74] M Ruggiu. "Kinematic and Dynamic Analysis of a Two-Degree-of-Freedom Spherical Wrist". In: *Journal of Mechanisms and Robotics* 2.3 (2010), pp. 031006–031015 (cit. on p. 18).

[75] Marco Carricato and Vincenzo Parenti-Castelli. "A novel fully decoupled two-degrees-of-freedom parallel wrist". In: *The International Journal of Robotics Research* 23.6 (2004), pp. 661–667 (cit. on p. 18).

[76] Ashitava Ghosal. *Robotics Fundamental Concepts and Analysis*. 5th ed. New Delhi, India: Oxford University Press, 2006. ISBN: 978-0195673913 (cit. on pp. 20, 24, 25).

[77] Kok-Meng Lee and Dharman K Shah. "Kinematic analysis of a three-degrees-of-freedom in-parallel actuated manipulator". In: *IEEE Journal of Robotics and Automation* 4.3 (1988), pp. 354–360 (cit. on pp. 20, 22).

[78] R Arun Srivatsan, Sandipan Bandyopadhyay, and Ashitava Ghosal. "Analysis of the degrees-of-freedom of spatial parallel manipulators in regular and singular configurations". In: *Mechanism and Machine Theory* 69 (2013), pp. 127–141 (cit. on p. 20).

[79] George Salmon. *Lessons introductory to the modern higher algebra*. Dublin Hodges, Foster, 1876. ISBN: 978-0828401500 (cit. on p. 23).

[80] SV Shah, SK Saha, and JK Dutt. "Denavit-Hartenberg Parameterization of Euler Angles". In: *Journal of Computational and Nonlinear Dynamics* 7.2 (2012), pp. 021006–0210015 (cit. on p. 25).

[81] M. Karouia and J. M. Hervé. "A Three-dof Tripod for Generating Spherical Rotation". In: *Advances in Robot Kinematics*. Ed. by J. Lenarčič and M. M. Stanišić. Dordrecht: Springer Netherlands, 2000, pp. 395–402 (cit. on p. 34).

[82] Raffaele Di Gregorio. "Kinematics of the 3-UPU wrist". In: *Mechanism and Machine Theory* 38.3 (2003), pp. 253–263 (cit. on p. 34).

[83] ANSYSWorkbench. *ANSYS Workbench*. 2011 (cit. on p. 50).

[84] JA Peterka, N Hosoya, B Bienkiewicz, and JE Cermak. *Wind load reduction for heliostats*. Tech. rep. Colorado State Univ., Fort Collins (USA), 1986. URL: https://www.nrel.gov/docs/legosti/old/2859.pdf (cit. on p. 50).

[85] Jon A Peterka, Z Tan, B Bienkiewicz, and JE Cermak. *Wind loads on heliostats and parabolic dish collectors*. Tech. rep. 1988, p. 22179. URL: https://www.nrel.gov/docs/legosti/old/3431.pdf (cit. on p. 50).

[86] Frank M White. *Fluid Mechanics. 5th*. 2003. ISBN: 978-0072402179 (cit. on p. 50).

[87] SolidWorks. *Solidworks*. 2013 (cit. on p. 50).

[88] Chuncheng Zang, Zhifeng Wang, Wenfeng Liang, and Xiaoyu Wang. "Structural Design and Analysis of the Toroidal Heliostat". In: *Journal of Solar Energy Engineering* 132.4 (2010), pp. 041007–041012 (cit. on p. 56).

[89] Al Williams. *Microcontroller Projects Using the Basic Stamp*. CMP Books Gilroy, CA, 2002. ISBN: 978-1578201013 (cit. on p. 64).

[90] Rik De Doncker, Duco WJ Pulle, and André Veltman. *Advanced electrical drives: analysis, modeling, control*. Springer Science & Business Media, 2010. ISBN: 978-94-007-0181-6 (cit. on p. 64).

[91] DL King and DE Arvizu. "Heliostat characterization at the central receiver test facility". In: *Journal of Solar Energy Engineering* 103.2 (1981), pp. 82–88 (cit. on p. 73).

[92] Jos M Quero, Carmen Aracil, Leopoldo G Franquelo, Jordi Ricart, Pablo R Ortega, Manuel Domínguez, Luis M Castañer, and Rafael Osuna. "Tracking control system using an incident radiation angle microsensor". In: *IEEE Transactions on Industrial Electronics* 54.2 (2007), pp. 1207–1216 (cit. on p. 73).

[93] Francisco J Delgado, José M Quero, Juan Garcia, Cristina L Tarrida, Pablo R Ortega, and Sandra Bermejo. "Accurate and wide-field-of-view MEMS-based sun sensor for industrial applications". In: *IEEE Transactions on Industrial Electronics* 59.12 (2012), pp. 4871–4880 (cit. on p. 73).